Author/s:
Jafari Harandi, Vahidreza

Title:
Muscle and joint functions during walking in individuals with transfermoral amputation

Date:
2019

Persistent Link:
https://hdl.handle.net/11343/241458

MUSCLE AND JOINT FUNCTIONS DURING WALKING IN INDIVIDUALS WITH TRANSFEMORAL AMPUTATION

Vahidreza Jafari Harandi

BSc, MSc

Submitted in total fulfilment of the requirements of the degree of Doctor of Philosophy

June 2020

Department of Biomedical Engineering

Melbourne School of Engineering

The University of Melbourne

I dedicate this work to my most beloved mother, and

to the soul of my dear father.

Abstract

Individuals with unilateral transfemoral amputation depend on compensatory muscle and joint function to generate motion of the lower limbs, which can produce gait asymmetry. Osseointegration is an alternative technique to socket-based prostheses that is used for reducing socket-skin contact problems. However, between-limb differences in joint kinematics and net joint moments may lead to abnormal hip joint contact behavior and muscle function. The aim of this dissertation is to investigate gait compensatory mechanism in individuals with transfemoral amputations fitted with socket (TFA) and bone-anchored prostheses using osseointegrated implants (BAP). In this study, two experimental and computational approaches were used to quantify the contributions of the intact and residual limb's contralateral muscles to body center of mass acceleration and hip joint contact forces during walking. In the first approach, kinematics and kinetics data were collected from 6 TFAs and 4 BAPs performing over-ground self-selected walking task. In the second approach, a processing framework was employed using OpenSim software and MATLAB API scripting for developing three-dimensional musculoskeletal models and then to predict muscle forces and muscle contribution to waling and hip joint reaction forces.

It was found that the intact limb hip muscles contributed more to body center of mass acceleration and hip contact forces than those in the residual limb. The results also suggest that osseointegrated amputees could quantify to decrease the asymmetries in the biomechanical measures between the intact and residual limbs than socket-based prosthesis amputees. The findings of this study would be useful in developing rehabilitation training programs and design of prostheses to improve gait symmetry and mitigate post-operative musculoskeletal pathology.

Declaration

This is to certify that:

i. the thesis comprises only my original work towards the PhD,

ii. due acknowledgment has been made in the text to all other material used,

iii. the thesis is less than 80,000 words in length, exclusive of tables, maps, bibliographies, appendices and footnotes.

Vahidreza Jafari Harandi *1st September 2019*

Preface

A number of published and submitted works have resulted from this thesis which are listed below and noted individually at the beginning of the relevant chapters:

Peer-reviewed journal articles (N = 3)

- **Vahidreza Jafari Harandi,** David Charles Ackland, Raneem Haddara, L. Eduardo Cofré Lizama, Mark Graf, Mary Pauline Galea, Peter Vee Sin Lee – Gait compensatory mechanism in unilateral transfemoral amputees. *Medical Engineering and Physics*, Published.
- **Vahidreza Jafari Harandi,** David Charles Ackland, Raneem Haddara, L. Eduardo Cofré Lizama, Mark Graf, Mary Pauline Galea, Peter Vee Sin Lee – Muscle contribution to hip contact forces in osseointegrated transfemoral amputees during walking. *Computer Methods in Biomechanics and Biomedical Engineering*, Accepted.

Furthermore, another article has used the results of this study as below:

- Dale Robinson, Lauren Safai, **Vahidreza Jafari Harandi**, Mark Graf, L. Eduardo Cofré Lizama, Peter Vee Sin Lee, Mary Pauline Galea, Fary Khan, Kwong Ming Tse, David Charles Ackland – Load response of an osseointegrated implant used in the treatment of unilateral transfemoral amputation: An early implant loosening case study. *Clinical Biomechanics*, Published.

Conference proceeding. P: Presentation (N=4), PO: Poster (N=1)

- **Jafari Harandi V**., D. C. Ackland, R. Haddara, P. Lee – Walking mechanics in osseointegrated transfemoral amputees via a 3D musculoskeletal modeling. ISPO congress, Kobe, Japan, 2019 [P].
- **Jafari Harandi V**., D. C. Ackland, R. Haddara, E. C. Lizama, M. P. Galea, M. Graf, P. Lee – Individual muscle contributions to propulsion in above-knee amputees with osseointegrated prosthesis during walking. ISB congress, Calgary, Canada, 2019 [P].
- **Jafari Harandi V**., D. C. Ackland, E. C. Lizama, M. P. Galea, M. Graf, P. Lee – Hip muscles forces during walking of an above-knee amputee. AOPA congress, Melbourne, Australia, 2017 [PO].
- **Jafari Harandi V**., D. C. Ackland, E. C. Lizama, M. P. Galea, M. Graf, P. Lee – A computer-based model of above-knee amputee to evaluate gait mechanics. 3DMED symposium, Austin Health, Melbourne, Australia, 2017 [P].
- **Jafari Harandi V**., D. C. Ackland, E. C. Lizama, M. P. Galea, M. Graf, P. Lee – Muscle contribution to support during walking in transfemoral amputees. Australian and New Zealand Orthopedic Research Society (ANZORS) conference, 2017 [P].

Awards and recognition

A number of travel grants and scholarships were awarded during my PhD. Travel grants in addition to supervisors' funds have provided opportunities to attend several national and international conferences. I would like to acknowledge the fund providers by listing them below:

- Melbourne Abroad Travelling **Scholarships** (MATS), July 2019, to attend ISB congress.
- Graduate Research Students **Travel Bursary**, The University of Melbourne, December 2017.
- **Travel grant** Biomedical Engineering symposium, Beihang University, China, November 2018.
- Graduate Research Students **Travel Bursary**, The University of Melbourne, December 2017.
- **Travel grant** Australian and New Zealand Orthopedic Research Society, October 2017.
- Melbourne International Fee Remission **Scholarship** (MIFRS), 2015-19.
- Melbourne International Research **Scholarship** (MIRS), 2015.
- Endeavor International Postgraduate Research **Scholarship** (IPRS), 2016.
- **Relocation grant**, The University of Melbourne, 2015.

Signed ()

Vahidreza Jafari Harandi

Peter VS. Lee

Vijay Rajagopal

David C. Ackland

Acknowledgments

Firstly, I am deeply thankful to my advisors, Prof. Peter Lee and A/Prof. David Ackland for their support, advice and enthusiasm throughout my entire PhD journey. Peter kindly introduced me to begin and continue research in a wonderful area of amputees walking biomechanics. David also has been an encouraging supervisor, who patiently supported me with constructive and helpful feedback. I also thank Drs. Eduardo Cofre Lizama and Mark Graf and Prof. Mary Galea from Royal Melbourne Hospital for their help during data collection and providing subjects for my experimental study.

I sincerely thank my Advisory Committee Chair, Dr. Vijay Rajagopal for his insightful and inspiring discussion and guidance.

I would like to express my gratitude to all my peers, friends, and colleagues in the Biomechanical Engineering research group, both past and present. I am especially indebted to Dr. Yi-Chung Lin, Dr. Fatemeh Malekipour, Dr. Azadeh Kian, Dr. Dale Robinson and Mrs. Raneem Haddara for their invaluable, knowledgeable, and encouraging discussion and comments on my work.

On a more personal level and even though far away from me, I profoundly thank my family. I am eternally indebted to the love and support of my lovely mother which have always been with me during life. My appreciation is also extended for my late father who instilled a love of learning in engineering in me from childhood to perform at the best of my ability.

Contents

List of Tables

List of Figures

Chapter 1.   Introduction

1.1 Motivation for studying muscle behavior in individuals with transfemoral amputation during gait

Transfemoral amputation is associated with substantial functional limitations, which affect daily activities and social life (Hammarlund et al., 2011, MPhty, 2012). Secondary diseases, which involve musculoskeletal disorders such as the intact limb hip and knee joints osteoarthritis (OA) and low back pain, often occur over time in transfemoral amputees (Struyf et al., 2009, Morgenroth et al., 2012). Thus, understanding muscle function to help avoid OA and low back pain is important.

Previous gait analyses in patients with transfemoral amputation have focused on spatiotemporal parameters, joint kinematics and kinetics, muscle electromyography (EMG) and consequently asymmetry and changes to the amputee's walking patterns compared to non-amputees (Jaegers et al., 1995b, Jaegers et al., 1995a, Jaegers et al., 1996, Kaufman et al., 2007, Kaufman et al., 2012). Although new socket designs have improved walking, skin problems are still a major concern (Van de Meent et al., 2013). As a result, osseointegrated prosthesis have been sought as a way to combat these problems and have been recognized as the better alternative in some cases (Branemark et al., 2001, Al Muderis et al., 2018). On the other hand, more recent studies have shown that lower extremity muscles such as ankle plantarflexors and knee extensors are responsible to generate motion in non-amputees (Liu et al., 2006, Pandy and Andriacchi, 2010, Lin et al., 2015). In transfemoral amputees with socket and osseointegrated implants, these muscles are absent and thus other intact and residual limb muscles must compensate the lost muscles role to perform a movement. Investigation of muscle forces is required for understanding the compensatory mechanism employed by amputees.

An overarching aim of this dissertation is to investigate the individual lower limb muscle function during walking in transfemoral amputees. Post-amputation rehabilitation is a prominent procedure trying to maximize the amputee's capabilities to walking and prevent injuries. While transfemoral amputees use compensatory mechanism to generate a movement, they may confront musculoskeletal disorders due to amputation more than non-amputees (Struyf et al., 2009, Morgenroth et al., 2012). Understanding the walking strategies among both TFAs and BAPs is also crucial to devise new training programs and improve prosthesis designs with the aim of increase in activities performance and prevention or postponement the subsequent musculoskeletal diseases.

1.2 Rationale for use of computer-based musculoskeletal modeling and simulation

The intact limb lower-extremity joint injuries in unilateral transfemoral amputees occur when large mechanical loads are applied to the joint. Thus, knowledge of the forces that joint sustains is of importance for understanding the criteria that affect joint loadings. Also, the most fundamental way to explain muscle recruitment strategies during walking in transfemoral amputees is understood by how much force each muscle generates to move body center of mass forward, upward and sideway. Direct measurement of muscle forces in vivo through non-invasive way is not feasible. However, some studies have reported muscle forces in human using invasive methods such as strain-gauge transducers for a limited number of muscles (Komi et al., 1987, Fukashiro et al., 1995). In other words, such methods are not able to calculate the forces of multiple muscles at time (Komi et al., 1987).

In a computer-based simulation, a number of muscle significant parameters such as a time history of musculotendon length during movements can be estimated using computer models. The time history is of particular relevance in the scope of injuries related to muscle strain. Years of using musculoskeletal models have shown development in the accuracy of anatomy and anthropometry of the individual during dynamics locomotion in non-amputees (Delp and Loan, 1995, Anderson and Pandy, 1999, Liu et al., 2006, Chumanov et al., 2011). Thus, understanding human movement biomechanics and motor control have been achieved using musculoskeletal simulations. Musculoskeletal models provide a quantitative prediction of the loads produced by individual muscles. Computational musculoskeletal simulations have enabled researchers to investigate the role of muscles in walking in healthy and amputee groups (Liu et al., 2008, Pandy and Andriacchi, 2010, Silverman and Neptune, 2010, Dorn et al., 2012b, Silverman and Neptune, 2012).

OpenSim, an open-source musculoskeletal modeling platform (Delp et al., 2007) and MATLAB API scripting were used as primary computational tools in this dissertation. The OpenSim models are comprised of solid segments, joints, muscle model, musculotendon parameters and physiological force-length-velocity properties of muscle, which all are integrated to create musculoskeletal models. The OpenSim community has developed different models for non-amputees; however, creating and developing musculoskeletal models for transfemoral amputees is required to analyze and investigate the role of lower limb muscles during daily activities.

1.3 Contributions of the dissertation and specific aims

The overall aims of this dissertation were to provide a better comprehension of the mechanism that transfemoral amputees employ during walking. This was achieved using experimental data recorded from transfemoral amputees walking at their self-selected speed and computational musculoskeletal modeling to simulate and analyze walking. The findings of this dissertation will not only contribute to areas such as biomechanical engineering and rehabilitation engineering but also advance the use of human-motion computer-based modeling. Thereafter, the key contributions of this dissertation are as follows:

1. **Developed a 3D musculoskeletal model for transfemoral amputees fitted with socket and osseointegrated prosthesis.**

   Decades of laboratory-based studies have shed light on differences in biomechanical criteria during walking in transfemoral amputees. Spatiotemporal parameters, joints kinematics, kinetics, and EMG-based studies were reviewed and summarized to depict the asymmetries associated with transfemoral amputees fitted with socket and osseointegration prosthesis. Although these studies provide valuable information on walking strategies, the perception of the dynamical role of muscles to generate motion is vital to understand how transfemoral amputees employ compensatory mechanisms. In chapter 3, experimental and computational approaches including data collection protocol, musculoskeletal model development, and mathematical procedures were presented to represent transfemoral amputee.

2. **Evaluated the functional behavior of lower extremity muscles during self-selected over-ground walking of transfemoral amputee groups with socket and osseointegrated implants.**

   Previous studies have mostly used EMG to study the role of lower-extremity muscles, in particular, proprioception and muscle activation, during walking in transfemoral amputees. However, these parameters do not illustrate the forces produced by muscles. Given that the muscles play a critical role in propel, support and control of the body, quantifying lower limb muscle function may extend the current knowledge about walking mechanisms in both amputees with socket and osseointegration prosthesis. Since osseointegration has introduced new way to combat socket-skin difficulties, it is more important to investigate its effect on walking mechanism. In chapter 4, the muscle forces and muscle contribution to walking were calculated using experimental data and developed computational musculoskeletal models.

3. **Quantified the intact and residual limb hip joint contact forces and then identified and determined major muscle groups that contribute to the hip contact forces.**

   Walking asymmetries have been illustrated to increase the risk of hip OA in transfemoral amputees. To numerically assess hip joint forces, chapter 5 quantified the resultant hip contact forces in the intact and residual limb of amputees. Using experimental data and musculoskeletal model as well as the results of muscle contribution to walking calculated in chapter 4, the muscle contribution to hip contact forces were computed for both amputees wearing socket and osseointegration prosthesis to evaluate how muscles generate hip forces during walking.

1.4 Outline of the thesis

- **Chapter 2** describes the comprehensive literature review relevant to the objectives of this dissertation. The following topics will be discussed in this chapter: Biomechanical parameters in transfemoral amputees walking, Muscle behavior in walking of transfemoral amputees, Muscle contribution to walking, Muscle contribution to hip contact force during walking, Musculoskeletal modeling and challenges.

- **Chapter 3** presents a detailed overview of musculoskeletal modeling development for transfemoral amputees.
- **Chapter 4** focuses on individual muscle behavior in walking of transfemoral amputees with socket and osseointegration prosthesis.
- **Chapter 5** investigates individual muscle contribution to joint contact forces during walking of transfemoral amputees.
- **Chapter 6** presents a conclusion and future work associated with the discussion and limitations of this dissertation.

Chapter 2. Background and literature

This chapter provides a comprehensive review of the walking biomechanics literature in people with unilateral transfemoral amputation. It begins with a definition of transfemoral amputation, after which a literature review of the gait parameters associated with unilateral transfemoral amputee walking is described, discussing kinematics, kinetics, muscle electromyography (EMG) and muscle forces. Thereafter, a computational perspective is taken, discussing the outcome delivered by simulation and modeling is emphasized. The chapter concludes with the specific questions addressed by this thesis.

2.1 An overview of transfemoral amputation

Transfemoral or above-knee amputation is a surgical procedure that removes a lower extremity from the body at or above the knee joint (Berke et al., 2008), to remain as many healthy bones, muscles, and vessels (Figure 2.1). Amputations are notably caused by peripheral vascular disease, diabetes, infection, trauma, and cancer. However, the leading cause of amputation has been reported to be due to severe vascular and diabetic disease (Gottschalk, 1999). The risk of lower extremity amputation has been estimated to increase up to fifteen times in diabetic people (Nelson et al., 1988). In addition, the annual financial burden of the lower limb amputation had been reported to be between £50 and £75 million in the UK at the period of 2003-2008 (Moxey et al., 2010).

Figure 2.1- An individual with unilateral transfemoral amputee (Ottobock).

In total, each year over 150,000 people undergo amputation surgery due to vascular disease or diabetes around the world (Dillingham et al., 2005). The number of individuals with lower limb amputation has increased over the past decade in Australia (Dillon et al., 2017). In Australia, the most common reason for lower limb is diabetes, which accounts for 85% of cases (AIHWb, 2014). Approximately, 222,000 transfemoral amputees were living in the US by the year 2008, which is 20% of the total amputees' population (Berke et al., 2008). It is also predicted that the number of lower extremity amputees will double by 2050 (Ziegler-Graham et al., 2008).

Based on the level of amputation, some muscles, which mostly span the knee joint, will be removed and some bi-articular muscles spanning the hip and knee joints will be re-anchored. The re-anchorage strategy usually depends on what muscle stabilization technique is used, myoplasty or myodesis. In the traditional method, myoplasty, both agonist and antagonist muscles such as *hamstrings*, *rectus femoris*, and *adductor magnus* will be sutured over the end of stump without preserving muscle tension (Gottschalk, 2004). The muscle tension is not preserved through myoplasty. Thus, another surgical procedure which is known myodesis have been recommended for the hip adductors and *medial hamstring* to be directly re-inserted to the end of femur under tension (Gottschalk, 2004, Tintle et al., 2010). As a result, the capacity of these muscles to generate forces and moments about the hip has been improved (Ranz et al., 2017).

Transfemoral amputees replace a part of the leg, which is lost because of amputation, with prosthesis enabling most of them to perform daily activities. One conventional method to fix the prosthesis to the body is by employing a custom-designed socket (Figure 2.2). Of those conventional socket transfemoral amputees, one third experiences severe skin pain and discomforts related to the socket-skin interface (Rommers et al., 1996, Hagberg and Brånemark, 2001b, Meulenbelt et al., 2009, Butler et al., 2014), which has resulted in low quality of life and doing daily activities (Pezzin et al., 2000, Demet et al., 2003, Pezzin et al., 2004a). Although new socket designs have improved walking, socket-stump interface problems including dermatitis, acne, pressure sores as well as inappropriate control for support and propel the body are still major concerns (Hagberg and Brånemark, 2001b, Dudek et al., 2005, Meulenbelt et al., 2011, Van de Meent et al., 2013). As a result, osseointegrated prosthesis have been sought as a way to alleviate these problems and have been recognized as a suitable alternative in many cases (Branemark et al., 2001, Al Muderis et al., 2018). This bone-anchored approach has been utilized as an intervention to mitigate skin problems and improve quality of life (Branemark et al., 2001). In this method, the prosthesis is directly attached to the bone through a percutaneous implant system (Branemark et al., 2001, Brånemark et al., 2014) (Figure 2.3). This type of surgery has been depicted additional benefits to the amputees including walking ability improvement (Frossard et al., 2010, Hagberg et al., 2014), energy cost reduction (Van de Meent et al., 2013), awareness improvement through osseoperception (Jacobs et al., 2000, Haggstrom et al., 2013), good alignment of femur and hip range of motion (Frossard et al., 2013, Frossard, 2019, Frossard et al., 2019).

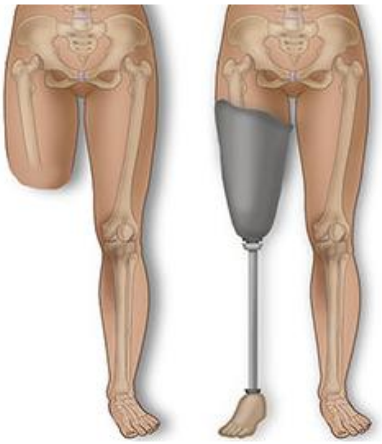

Figure 2.2- A socket-type prosthesis. (Moveforwarddpt)

Figure 2.3- An osseointegrated transfemoral amputee. (Kennon)

Individuals with unilateral transfemoral amputation have shown musculoskeletal disorders when compared to able-bodied people. For example, a greater prevalence of the hip and knee osteoarthritis (OA) in the intact limb with 14% than non-amputees, has been evidenced in their population (Morgenroth et al., 2012, Welke et al., 2019). The greater risk of developing the knee OA of the intact limb in transfemoral amputees than non-amputees has been depicted in previous studies (Hungerford and Cockin, 1975, Kulkarni et al., 1998, Melzer et al., 2001). For instance, approximately two-third of transfemoral amputees fitted with socket have exhibited knee degeneration in the intact limb, compared with one-fifth of a matched control group (Hungerford and Cockin, 1975). Norvell et al have indicated that the symptomatic knee OA in the intact limb of lower limb amputees was greater than the non-amputees, even when the subjects with a knee trauma history were excluded from the study (Norvell et al., 2005). In another study, 27% of individuals with lower extremity amputation has been reported to be indicative of the intact limb knee OA in comparison with 2% of non-amputees (Struyf et al., 2009).

There is a strong relation between joint conditions and mechanical loading and joint OA development. The loading abnormality of the articular cartilage lends evidence to the incident of OA (Radin et al., 1991, Felson et al., 1992). The body weight effect on joint degeneration is an important factor in the OA pathogenesis (Felson et al., 1992, Messier et al., 2005). It also has been confirmed that an increase in GRFs may be directly associated to a high possibility of lower limb joints OA in healthy subjects (Lemaire and Fisher, 1994, Robbins et al., 2001). Hence, greater GRFs in the intact limb than that of the residual limb of transfemoral amputees may contribute to joint loading abnormalities and degeneration.

Transfemoral amputees also have been reported to exhibit a higher risk of low back pain (Kulkarni et al., 2005, Morgenroth et al., 2009, Morgenroth et al., 2010, Matsumoto et al., 2018). These secondary musculoskeletal disorders have mostly resulted from disability in mobility, which affect their quality of life and physical activity such as walking and running (Hagberg and Brånemark, 2001b, Hagberg et al., 2004, Van de Meent et al., 2013).

2.2 Biomechanical parameters in transfemoral amputees during walking

This section reviews previous studies on spatiotemporal parameters, kinematics, kinetics, EMG and muscle forces in transfemoral amputees.

2.2.1 Spatiotemporal, kinematics and kinetics

Gait deviations in transfemoral amputees fitted with socket prosthesis have been extensively investigated in previous studies, including reduction in walking speed and increase in metabolic cost of energy compared to able-bodied people (Vaughan et al., 1992, Jaegers et al., 1995b, Boonstra et al., 1996, Genin et al., 2008). Transfemoral amputees have shown longer stance phase and stride length as well as wider stride width in the intact limb in comparison with their residual limb and non-amputees (Jaegers et al., 1995b, Mattes et al., 2000, Segal et al., 2006, Hof et al., 2007, Goujon-Pillet et al., 2008, Highsmith et al., 2010, Pinard and Frossard, 2012, Wentink et al., 2013). Furthermore, the higher hip joint range of motion and ground reaction forces (GRFs) in the intact limb than those of the residual limb have been found in previous experimental studies (Sjödahl et al., 2002, Sjödahl et al., 2003, Goujon-Pillet et al., 2008, Schaarschmidt et al., 2012, de Cerqueira et al., 2013). Reduced hip, knee and ankle moments, works and powers have been observed in the residual limb relative to those of the intact limb during walking (Seroussi et al., 1996, Segal et al., 2006, Prinsen et al., 2011, Okita et al., 2018).

However, a few studies have considered biomechanical parameters in individuals with osseointegrated prosthesis during gait. Previous studies have observed increased self-selected walking speed, shorter walking time and quicker cadence in the osseointegrated amputees in comparison to socket amputees as well as slower cadence and larger walking duration compared to non-amputees (Hagberg et al., 2005, Frossard et al., 2010, Tranberg et al., 2011, Pinard and Frossard, 2012, Van de Meent et al., 2013, Leijendekkers et al., 2017, Robinson et al., 2020).

2.2.2 EMG and muscle forces in transfemoral amputees

Muscle behaviors in transfemoral socket amputees have primarily been focused on studies associated with EMG. A greater level of muscle activation and longer duration have been observed in transfemoral amputees compared to non-amputees (Jaegers et al., 1996, Bae et al., 2009, de Cerqueira et al., 2013, Wentink et al., 2013). Wentink showed longer activity in most of the upper leg muscles of the residual limb in late-stance in contrast to non-amputees, which may be due to increase in socket fitting by lifting the prosthesis in the swing phase (Hong and Mun, 2005, Wentink et al., 2013). In addition, the prolonged activity of the lower limb in the intact limb (Wentink et al., 2013), including *soleus* and *tibialis anterior,* may be related to an increase in ankle plantarflexors' work in pre-swing to push the body forward and also assist foot clearance (Seroussi et al., 1996, Nolan and Lees, 2000). In another study, the activation of *gastrocnemius* and the coactivation of the upper leg intact limb's muscles were shown to be greater in amputees than a control group, which may correspond to excessive ankle power of the intact limb relative to the residual limb (Bae et al., 2009). In osseointegrated transfemoral amputees, the similarity was found in the function of the residual limb's hip muscles activities compared to those in able-bodied people (Pantall and Ewins, 2013).

2.3 Musculoskeletal modeling and challenges

This section explains challenges in human locomotion modeling and muscle force prediction. These challenges are resulted from the experimental data collection process. Therefore, the limitations of the results of muscle forces must be taken into account. Besides the simulation' challenges, the merits of computational and simulation-based approaches are discussed. Finally, the muscle forces' validation during walking will briefly be reviewed, which can be evidence to justify some of the challenges.

Only few studies have used simulation and modeling to investigate gait in transfemoral amputees. Burkett et al. developed a simple two-dimensional model, using a forward dynamics approach, to simulate the swing phase of the residual limb to optimize knee position (Burkett et al., 2004). In other simulation studies, 2D dynamic models of the residual limb were developed to optimize knee motion controller with the focus on gait biomechanical measures, including spatiotemporal parameters, joint kinematics, and kinetics (Pejhan et al., 2008, Shandiz et al., 2013). Also, a 2D musculoskeletal model was constructed to minimize muscles metabolic cost of energy with the purpose of optimizing knee joint friction of the residual limb (Suzuki, 2010). Collectively, a comprehensive three-dimensional musculoskeletal simulation should be utilized to indicate well the role of muscles and act more realistic to human walking.

Bae et al. calculated muscles forces using dynamic simulation and found that the forces generated by the hip abductors and extensors and knee extensors of the intact leg were greater than those in the residual limb, which is because of inadequate hip joint torque in the residual limb relative to the intact limb (Bae et al., 2007). A muscle-driven simulation technique was utilized to examine differences in muscle forces to minimize the period of swing phase (Suzuki, 2010). Furthermore, Ranz et al. investigated the effect of amputation techniques on muscle load during walking. The musculoskeletal model results showed that the balance and capacity of muscles were greater when myodesis stabilization was considered (Ranz et al., 2017). However, the latter observation concluded hip adduction moment and moment arm, the lack of reporting individual muscles forces still exists. Thus, variations in muscles forces in transfemoral amputees should be well illuminated to distinguish the role of muscles in walking. Ranz' model also used data from one non-amputee which does not reflect the real behavior of amputees. Also, Ranz' study did not consider prosthesis properties such as mass, center of mass and moment of inertia.

2.3.1 Computational frameworks in muscle forces prediction during walking

The method of muscle forces and activations' calculation has been a debatable topic. It is impossible to directly and non-invasively measure muscle forces. Nonetheless, some invasive techniques such as strain-gauge transducers have been applied to measure muscle forces (Komi et al., 1987, Fukashiro et al., 1995, Komi et al., 1996, Komi, 2000). Ethical considerations do not encourage the in vivo regular use due to many known disadvantages such as indistinguishable between muscles and between muscle and tendon components. In addition, such methods are capable of measuring a single muscle force and then cannot be included the coordination of multiple muscles at a time.

Musculoskeletal models and simulation frameworks have widely been used to understanding muscle behaviors during daily activities due to unfeasibility of invasive measurements of the biomechanical parameters such as muscle forces (Zajac et al., 2002, Zajac et al., 2003). These frameworks mathematically represent human body and include skeleton, which is a series of rigid bodies, that connects by varying degrees of freedom of joints. The skeleton joints are then actuated by muscles (Delp et al., 1990, Ward et al., 2009). A human body, which uses the same principles of a multi-body dynamics to simulate robots and machines, is actuated by the muscles and GRFs to produce locomotion (Erdemir et al., 2007). On the other hand, the lack of suitable muscle model and geometry, then physical muscle properties as well as a large number of muscles have been recognized as major challenges in human motion simulation (Erdemir et al., 2007, Fregly et al., 2012). For instance, opposed to large number of muscles, limited number of equilibrium equations exist to predict the muscle forces. Thus, this inherent property ideally propelled researchers in using optimization-based approaches. To calculate muscle forces, a musculoskeletal model needs to consider the muscle lines of action and moment arms, the force-generation muscle properties and an optimization technique. Each of these features will be discussed below.

2.3.1.1 Muscle lines of action and moment arms

Each muscle crossing the joints is determined by unique origin and insertion points. The muscle paths, however, are often represented as curves around joints. A muscle line of action is defined as the direction of the resultant generated force at each point of attachment. The moment arm is referred to the perpendicular distance between the joint center of rotation and the muscles line of action. The joint torque is estimated as a product of the muscle force and the moment arm. A biarticular muscle spanning two joints produces different torques of joint. The greater joint torque occurs at the joint with a larger moment arm. A muscle moment arm needs an accurate estimation for the calculation of the joint torque to drive human motion (Delp and Loan, 1995).

2.3.1.2 Muscle model: Force-generation properties

A muscle, which is responsible for body posture and locomotion, is excited and activated by a neural signal and then produces force and power. Muscles are connected to the skeleton's bones through tendons. The properties of muscle force generation configure the principles of producing force and movement. The magnitude of a muscle force depends on the length-velocity relationship of the muscle fibers (Hill, 1953, Bahler, 1968). As shown in Figure 2.4, the relationship between the force and the length of a muscle describes the amount of force generated at different muscle lengths. The percentage of muscle excitation is determined by the shape of the force-length graph. Also, the force-velocity curve depicts that increasing velocity of concentric (shortening) contractions will rapidly generates less force and greater force will be because of increasing velocity of eccentric (lengthening) contractions.

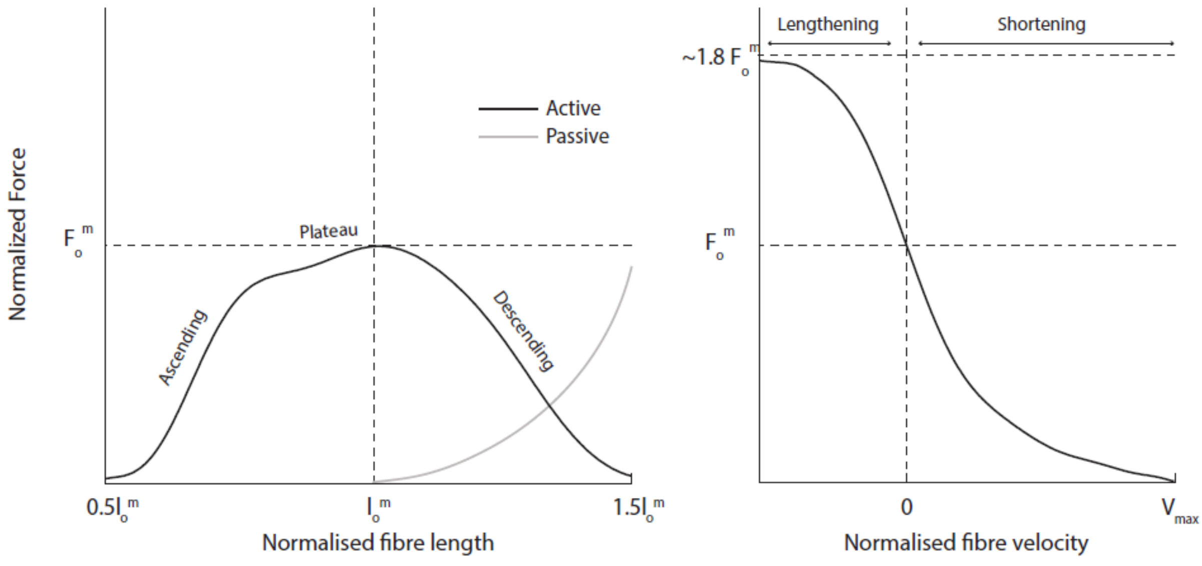

Figure 2.4. The maximum isometric force (F_o^m) describes the force in the muscle under maximum (100%) isometric contraction. As seen in the active force-length curve (left), peak force is produced when the muscle is at its resting length (l_o^m). When a muscle is shortened below or above its resting length (i.e. a muscle operating on the ascending or descending region, respectively), it produces less force output. Passive force is produced when the muscle is lengthening but not active. The force-velocity curve (right) shows that under isometric conditions, the muscle is neither shortening or lengthening. A muscle produces no force when it reaches its maximum shortening velocity (V_{max}).

Hill-type muscle-tendon actuator is mostly used to model a muscle which is connected in series with an elastic tendon (Hill, 1938, Zajac and Gordon, 1989). Based on this model, a muscle comprises active and passive elements acting in parallel. The inherent parameters of the Hill-type model, which are due to a great number of cadaver studies (Delp et al., 1990, Ward et al., 2009), are a maximum isometric force, pennation angle, muscle fiber length and tendon slack length (Thelen et al., 2003).

2.3.1.3 Methods of muscle force estimation

To estimate muscle forces, various optimization means as described in this subsection may be used.

Inverse dynamics methods only require the joints position and GRFs as external forces to calculate the forces of muscles spanning the joints. Forward dynamics techniques try to use muscle excitation/activation to generate the desired motion. These two methods are based on optimization; however, forward dynamics uses one optimization problem during a complete gait cycle and is a more computationally expensive approach. In inverse dynamics-based methods such as static optimization, an objective function is applied to iteratively compute and update muscle forces at each time step. In forward dynamics, the tracking error between experimental data and kinematics predicted by the model is minimized to iteratively estimate muscle excitations.

Static optimization strategies have been applied to various daily activities of healthy and pathological subjects such as walking (Anderson and Pandy, 2001b, Pandy and Andriacchi, 2010, Lim et al., 2013), running (Edwards et al., 2010, Dorn et al., 2012b) and landing (Mokhtarzadeh et al., 2013, Ewing et al., 2016). This approach is sensitive to the selected objective functions including the sum of squared muscle stress, instantaneous muscle power, and minimizing total muscle activations (Crowninshield and Brand, 1981, Collins, 1995, Rasmussen et al., 2001, Cleather and Bull, 2011). A major limitation associated with static optimization theory is its inability to accurately predict co-activation of agonist-antagonist muscles (Lin et al., 2011). In a mathematical model, the two-joint antagonistic muscles such as the contraction of *rectus femoris* and *hamstrings* during cycling have been demonstrated to be simultaneously activated as they are shortening (Ait-Haddou et al., 2000). Multiple degrees-of-freedom (DOF) systems have been shown to produce incompatible forces when considered with fewer DOFs (Jinha et al., 2006). However, static optimization approach has been proven to predict muscle contraction in a system with one and three DOF knee joint during a landing motion (Mokhtarzadeh et al., 2014).

Forward dynamics method includes excitation-contraction dynamics which acts differently than static optimization. An objective function along with a constraint that limits excitation between 0 and 1 is utilized. Regarding the time limitations of numerous integrations of the model state equations performance, simplifications such as the reduction in the number of muscles (Davy and Audu, 1987) and grouping excitation patterns (Neptune and Hull, 1998) are applied. In 2003, computed muscle control algorithm (CMC) was introduced which requires one integration of the state equations and includes many muscles to produce a muscle-actuated forward simulation (Thelen et al., 2003). CMC thrived to diminish the computational cost evolved from dynamic optimization by including both static optimization and feedback control theory. Notably, CMC has been used to predict muscle forces during walking (Anderson and Pandy, 2003), running (Lin et al., 2012) and landing (Mokhtarzadeh et al., 2014).

In addition to the optimization techniques explained above, a neuromusculoskeletal tracking (NMT) can be applied to dynamically resolve muscle redundancy problem (Seth and

Pandy, 2007). NMT considers forward dynamics and an additional time-dependent objective function. In all optimization techniques, the selection of objective function is controvertible. Although Pandy has shown that different objective function would result in similar muscle forces (Pandy et al., 1995), it has been found producing realistic gait requires fatigue-like cost functions (Ackermann and Van den Bogert, 2010).

EMG-driven forward dynamics model is another technique to predict muscle forces. The EMG data is used to prescribe muscle activations into the model (Hof and Van den Berg, 1981). The requirement of this method is the isometric EMG and joint torque relationship obtained through maximal isometric trials to measure maximum voluntary contractions (MVCs). An EMG-to-activation model was utilized in a broad range of tasks to represent muscle activation to estimate the joint moments calculated by inverse dynamics (Lloyd and Besier, 2003, Shao et al., 2009, Sartori et al., 2012). To represent physiological parameters, EMG-driven models need a time-consuming calibration process. Furthermore, muscle forces are calculated by multiplying maximum isometric force and EMG activation normalized by MVC in EMG-to-force models. The predicted muscle forces of ankle plantarflexors have been depicted good correlation to those estimated using static optimization, however, the forces generated by knee muscles have shown less correlation (Bogey et al., 2005, Heintz and Gutierrez-Farewik, 2007). Finally, a measured MVC is mostly subjective and depends on the subject motivation to contract a muscle to a maximum level.

In general, measuring EMG signals depends on many factors (De Luca, 1997); some controllable factors are called extrinsic factors such as electrode placement and type of signal measurement device, while some intrinsic factors related to the inherent properties of the muscle such as fiber density, diameter, and depth. The EMG signals can also be contaminated by noises caused by skin artefact and cross-talk from nearby muscles. Thus, the measured signals of reliability are influenced. Moreover, suitable signal processing methods should be selected. Regarding the limitations of EMG data recording and interpreting, these models must be used carefully.

2.3.2 Challenges in modeling

Experimental measurements must be used to validate musculoskeletal modeling (Zajac et al., 2002). One potential challenge relates to experimental errors (e.g. GRF, EMG and kinematics) and model errors when joint kinematics and marker trajectories and inertial characteristics of prosthesis are computed (Dumas et al., 2016). These unavoidable and common errors in biomechanics, which affect the accuracy of the muscle forces, could be reduced through filtration of data (Kristianslund et al., 2012, Kristianslund et al., 2013). Another inherent challenge in human locomotion simulation and muscle force estimation is the effect of changes in the musculotendon properties. Although the Hill-type model is one of the widely-used muscle models in computer-based simulations, some of its parameters (e.g. fiber and tendon slack length) may have intrinsic errors evolved from medical images during determining some anatomical variables (Wretenberg et al., 1996, Tsaopoulos et al., 2007). Moreover, maximum isometric forces measurements obtained from cadavers may be controversial, in which they may not represent the exact behavior of muscles during daily activities of humans. However, experimental measures only in gait are standardized. The maximum isometric force must be varied for each muscle to ensure the generated muscle forces are enough to balance the forces and moments around joints with the net joint torques (Dorn et al., 2012b).

Another issue concerning simulation is that major lower extremity muscles are more sensitive in the prediction of muscle forces through changes in the muscle moment arm and tendon slack length (Ackland et al., 2012). However, the sensitivity of muscle-tendon slack length to muscle function has been indicated to be greater than that of muscle moment arm (Ackland et al., 2012). Although the above-mentioned challenges in the simulation may affect the accuracy of the results, the biomechanical areas take advantage of musculoskeletal modeling due to its superior to invasive procedures (Fregly et al., 2012).

2.4 Induced acceleration analysis of human locomotion: state of the art

In a dynamic system, the effects of individual forces to generate coordinated motion are identified using induced acceleration analyses. In fact, accelerations caused or induced by individual forces are computed using this method. For instance, individual actuators (e.g. muscles and devices) function in producing human motion are often determined by these analyses (Zajac et al., 2002, Zajac et al., 2003). Induced acceleration analyses have been shown as powerful techniques to identify targeted muscles for surgical procedures such as muscle lengthening and tendon transfer or exercise training and rehabilitation programs. The development and design of prostheses, orthoses, and exoskeletons can also be influenced by identifying muscle behaviors.

As described in section 2.3, muscle forces can be calculated using musculoskeletal modeling. Thereafter, induced acceleration analyses are capable to interpret how each force contribute to generating the simulated movement, which cannot be achieved by another method. These state-of-the-art analyses, particularly, determine the role of individual muscles to either accelerate or decelerate body center of mass and joint. In the application to human movements, these techniques have been used to identify muscles adaptation to walking (Neptune et al., 2001, Anderson and Pandy, 2003, Neptune et al., 2004, Liu et al., 2006, Lim et al., 2013, Lin et al., 2015), running (Dorn et al., 2012b, Hamner and Delp, 2013, Debaere et al., 2015), turning (Ventura et al., 2015), pathologic gait (Peterson et al., 2010, Steele et al., 2010, Silverman and Neptune, 2012), stair walking (Lin et al., 2015), upslope/ downslope walking (Pickle et al., 2016), and other tasks.

Induced acceleration analyses have been assessed pathological gait to explain that how altered movement patterns may be evolved from differences in individual muscles functions. For example, crouch gait in children with cerebral palsy is characterized by excessive hip and knee flexion. This analytical method has revealed that greater crouched postures are provided by an increase in the uniarticular knee extensor demand. Because, a reduction in the efficacy of body support from a straighter leg posture increases the contribution of muscles to skeletal support (Steele et al., 2010). In people with stroke, the higher functional walking status has been depicted to associate with the hip abductors and ankle plantarflexors’ contributions to body propulsion (Hall et al., 2011).

In below-knee amputees, the residual limb’s body propulsion is reduced due to the lack of ankle plantarflexor muscles function. This reduction is correlated with a decrease in the ipsilateral knee extensors forces to maintain constant walking speed by slowing down of the body center of mass (Silverman and Neptune, 2012). The approach of induced acceleration methods has demonstrated that the reduced knee extensors’ contributions to body support and backward propulsion (breaking) in patients with total knee arthroplasty may be related to the movement patterns of quadriceps avoidance. As an adaptation strategy, trunk muscles provided greater contributions to supporting and breaking the body by forward leaning of the trunk (Li et al., 2013).

Induced acceleration analysis approaches can also be applied to determine how muscles contribute to joint contact forces. In people with transfemoral amputation, the intact limb hip and knee joint has been proven to be in a high risk of OA (Struyf et al., 2009, Morgenroth et al., 2012). Similarly, identifying muscle behaviors in joint loads are of importance in rehabilitation training to prevent osteoarthritis progression and joint pain. Obviously, the results of induced acceleration analyses have delivered valuable information in understanding pathological gait patterns with many potential applications for clinical translation.

2.5 Muscle contributions to walking

The muscles' coordination act as actuators to enable the body operating over ground walking, running and up-down stairs walking (Zajac, 2002, Zajac et al., 2002, Pandy and Andriacchi, 2010). Each muscle accelerates joints via generating a torque about that joint, which is defined by multiplying muscle moment arm (i.e. the distance from the joint center) and muscle force, to initiate movement (Zajac et al., 2002). In addition, non-crossing joint muscles have been shown to accelerate that joint via the dynamic coupling mechanism. In this regard, an individual muscle contribution to center of mass (COM) acceleration is calculated, consequently using Newton's Third Law, its contribution to the forces and moments generated by the foot-ground interaction is computed (Pandy et al., 2010, Dorn et al., 2012a, Lim et al., 2013, Lin et al., 2015). The individual muscle contribution to the gravity, inertia and foot-ground interaction is in good agreement with the laboratory-collected GRF patterns (Anderson and Pandy, 2003). As the GRF is the main external force acting on the foot, in which by applying the Newton's Second Law, necessitates behaving as the primary responsible for the body COM acceleration (Winter, 2009). In addition, transfemoral amputees are unique population because inverse dynamics can be validated with direct measurements (Dumas et al., 2016).

Previous studies on able-bodied subjects have extensively investigated the role of lower limb muscles in the fore-aft, vertical and mediolateral COM acceleration which represent forward progression (accelerate or decelerate the body), body support against gravity and mediolateral balance, respectively (Neptune et al., 2001, Anderson and Pandy, 2003, Neptune et al., 2004, Liu et al., 2006, McGowan et al., 2009, Pandy et al., 2010). These studies have mentioned that the *vasti* and *gluteus maximus* contributed to braking in early stance, while *soleus* and *gastrocnemius* were the major contributors in the late stance (Zajac et al., 2003, Neptune et al., 2004, Lim et al., 2013, Lin et al., 2015). Body support was mostly provided by the *vasti*, *gluteus maximus* and *gluteus medius* in the first half of stance and the ankle plantarflexors contributed to vertical COM acceleration in the second half of stance (Liu et al., 2006, Pandy and Andriacchi, 2010, Lim et al., 2013). Individual muscle contribution to mediolateral COM acceleration has also been considered during walking. The hip adductors and *hamstrings* have been shown to be important contributors to lateral COM acceleration during early stance to maintain body balance (Pandy et al., 2010, Silverman and Neptune, 2012). *Soleus* and *gastrocnemius* were responsible for providing lateral acceleration during late stance (Allen and Neptune, 2012, Silverman and Neptune, 2012). The medial balance was notably provided by *gluteus medius* throughout stance (Pandy et al., 2010, Lim et al., 2013), whereas tensor fascia latae contributed medially in mid-stance (Allen and Neptune, 2012, Silverman and Neptune, 2012). The *vasti* acted to accelerate the body laterally in early stance (Pandy et al., 2010, Lim et al., 2013). However, one study has found the medial contribution of the *vasti* to COM acceleration (Allen and Neptune, 2012).

In lower limb amputees, either the role of some missed muscles such as *soleus*, *gastrocnemius* and the *vasti* or the re-anchored muscles of the residual limb such as *hamstrings* may influence ambulation and result in gait compensatory mechanism. There is only one study investigated muscle contribution to GRF impulse in transfemoral amputees using optimization through a forward dynamics technique (Ranz, 2016). Ranz found that intact limb's body support was primarily provided by *tibialis anterior*, *gluteus maximus*, *gluteus medius*, and *hamstrings* in the first half of stance. The major contributors to support during the second half of stance of the intact limb were *soleus* and *gastrocnemius*, followed by *tibialis anterior*, the *vasti* and iliacus and psoas. *Hamstrings* and *gluteal* muscles of the residual limb were the great contributors to support during the first half of stance, while *gluteus medius* produced a major contribution to vertical GRF impulse in the second half of stance. Furthermore, the intact limb *hamstrings* contributed more to forward propulsion in the first half of stance, whereas tibialis anterior and iliacus and psoas were the important contributors to braking. During the second half of stance, *soleus* and *gastrocnemius* contributed anteriorly, while *iliacus* and *psoas* contributed posteriorly. Of the residual limb, *hamstrings* and both *iliacus* and *psoas* contributed more to the fore-aft GRF impulse, respectively. Moreover, the intact limb balance was mostly provided by the contribution of the *gluteal* muscles to lateral GRF impulse. In the residual limb, *gluteal* muscles were the major contributors to medial GRF impulse, followed by *hamstrings*. Also, the prosthesis was found to functioning similar to the *vasti* and ankle plantarflexors of the intact limb (Ranz, 2016).

Although this study has depicted muscle contribution to walking, it has not shown the muscle behavior throughout the whole stance, specifically in major gait events such as heel-strike and toe-off in both intact and residual limbs. Ranz' study has not investigated muscle behavior in transfemoral amputees with the osseointegrated prosthesis or active knee socket prosthesis. In addition, the kinematic data applied in Ranz' study was from an able-bodied person, not an amputee. Another limitation of that study was lack of the inertial properties of the prosthesis (e.g. mass, center of mass and moment of inertia) in the musculoskeletal modeling. That study has also used a muscle-driven method to obtain muscle forces. The results of forward dynamics algorithms have been depicted to be less robust and efficient than those which are calculated based on the static optimization method (Lin et al., 2012). Since some muscles are absent in amputees, the functional behavior of other muscles and prosthesis would be different from non-amputees which needs to be considered.

2.6 Muscle contribution to hip contact forces

The lower extremity joints are susceptible to structural degeneration and injury over time due to their functional roles to withstand high contact forces during daily activities. For instance, an increase in joint loadings has been associated with the progression of OA (Felson, 2004, Lafeber et al., 2006). Previous *in vivo* studies have reported hip contact force during walking using instrumented implants in non-amputees (Rydell, 1966, Davy et al., 1988, Kotzar et al., 1991, Bergmann et al., 1993, Read and Nigg, 1999, Bergmann et al., 2001, Damm et al., 2013). This costly and invasive approach, however, is restricted to patients who mostly have undergone hip joint replacement surgery and cannot be applied for healthy able-bodied people and amputees (Read and Nigg, 1999). Computer-based simulation frameworks have been demonstrated as an alternative approach for obtaining reasonable estimates of hip contact forces during walking in non-amputees (Brand et al., 1994, Heller et al., 2001, Stansfield et al., 2003). The results of simulation have been compared, then validated and concluded to be in good agreement with the *in vivo* experiments (Heller et al., 2001).

Lower limb muscles act as primary contributors to the joints' mechanical loading (Herzog et al., 2003). One study has found a correlation between the atrophy of hip muscles, as a reduction in muscles strength (Gottschalk, 1999), and hip OA (Amaro et al., 2007). The role of hip abductors is related to maintain joint stability and prevent overloading in the musculoskeletal system during walking (Amaro et al., 2007). The weakness in *gluteus medius* in the stance limb will unstable pelvis with an excessive drop towards the swinging limb, which has been depicted in patients with hip OA and total hip replacement (Madsen et al., 2004, Beaulieu et al., 2010). In non-amputees, however, few studies have investigated the individual muscle contribution to hip contact forces during daily activities of non-amputees (Correa et al., 2010, Pandy and Andriacchi, 2010, Schache et al., 2018). All experimental data were collected during walking at 1.4m/s and evaluated using musculoskeletal modeling. *Gluteus maximus*, *gluteus medius*, and iliopsoas were shown to be major contributors during stance, while the largest contribution to hip contact forces were generated by iliopsoas and *gluteus maximus* during swing (Correa et al., 2010, Pandy and Andriacchi, 2010, Schache et al., 2018). *Gluteus medius*, *gluteus maximus*, and *rectus femoris* were the main contributors to the first peak of hip contact forces at contralateral toe-off, whereas the second hip contact forces peak was mostly generated by *gluteus medius*, *iliopsoas* and *rectus femoris* at contralateral heel-strike. It was also visible a smaller peak in the hip contact forces around heel-strike, which may arise from *hamstrings* action (Pandy and Andriacchi, 2010).

As mentioned in section 2.2, transfemoral amputees experience gait asymmetries and different loading between their intact and residual limb. They have shown atrophy in their residual limb hip muscles and a higher risk of hip OA in their intact limb (Jaegers et al., 1995b, Mattes et al., 2000, Segal et al., 2006, Hof et al., 2007, Goujon-Pillet et al., 2008, Highsmith et al., 2010, Pinard and Frossard, 2012, Wentink et al., 2013). However, none has reported either hip contact forces in the two limbs or the functional roles of individual muscles to hip contact forces in transfemoral amputees. Determining rehabilitation strategies to reduce hip loading asymmetry can be achieved by understanding muscle contributions to hip contact forces.

2.7 Summary of the literature review

This review summarized the biomechanical behavior of transfemoral amputees during walking. First, a definition of transfemoral amputation was presented. Then, spatiotemporal, kinematics and kinetics parameters, as well as muscle EMG during walking of transfemoral amputees, were reviewed. Much of the current literature paid particular attention to two issues: i) musculoskeletal modeling to explain the need for using simulation to understand walking mechanism in transfemoral amputees and ii) induced acceleration analysis method to investigate individual muscle contribution to forward progression, body support, and mediolateral balance during walking as well as contribution to hip contact forces. In view of all that has been mentioned so far, too little attention has been paid to using musculoskeletal modeling for analyzing compensatory mechanism in transfemoral amputees. Thus, chapter 3 will focus on developing a musculoskeletal model to represent transfemoral amputee. Chapters 4 and 5 will comprehensively elaborate the muscles behavior amongst amputees with socket (passive and active knee joint) and amputees with osseointegration prosthesis.

Chapter 3. Experimental and computational methods

The methodology used in this chapter is based on the two published and submitted papers mentioned at the beginning of chapters 4 and 5.

3.1 An overview of experimental and computational approaches in this study

Two major steps including human motion experiments and computational modeling were conducted in this study. The accurate recording of motion data is crucial for developing three-dimensional musculoskeletal modeling and computational analyses. In turn, the realistic predictions of muscle forces, as well as muscle contribution to COM acceleration and joint contact forces, depending on the quality of motion data and educated assumptions. A total of ten participants with transfemoral amputation were recruited for motion data collection at the MOVE lab of the Royal Melbourne's Hospital, Australia.

This chapter describes in detail the experimental and musculoskeletal modeling development and computational methods used to collect and analyze the walking data for investigating gait asymmetry in amputees. This includes subject recruitment, muscle contribution and loading on the lower limb joints. For clarity, the methodology explained in this chapter will also be stated briefly in the methods section of the studies of Chapters 4 and 5.

3.2 Experimental data collection

3.2.1 Subject recruitment

Six transfemoral amputee wearing a conventional socket prosthesis (herein referred to SP users), with a mean ± standard deviation (SD) age, 48.83 ± 18.71 yr.; mass, 71.33 ± 8.57 kg; height, 1.77 ± 0.15 m (Table 3.1), and four osseointegrated transfemoral amputees (herein referred to OI users) with age, 56 ± 3.46 yr.; mass: 80.38 ± 12.45 kg; height:1.80 ± 0.13 m (Table 3.2), participated in this study. The inclusion criterion for this study was a unilateral amputation of participants who were able to walk without assistive devices such as crutch. Eligible subjects had their own prosthesis during experiments. Ethical approval was obtained by the Melbourne Health Human Research Ethics Committee with the number HREC 2015.148, and each participant provided written informed consent. This study was performed at the MOVE Lab of The Royal Melbourne's Hospital, Melbourne, Australia.

Table 3.1. Subject specification of SP users. The amputation level is medium for all subjects.

Subject	Sex	Cause of amputation	Prosthetic Socket Type	Knee Joint	Foot	Residuum length
S1	Male	trauma	quadrilateral	3R92	1C30	22
S2	Male	osteosarcoma	ischial containment	GENIUM	1C60	19
S3	Male	trauma	quadrilateral	SPECTRUM	TRUESTEP	25
S4	Male	trauma	ischial containment	GENIUM	1C61	27
S5	Male	trauma	quadrilateral	3R49	MULTIFLEX	18
S6	Male	trauma	ischial containment	GENIUM	1C61	20

Table 3.2. Subject specification of OI users. The amputation level is medium for all subjects.

Subject	Gender	Cause	Knee	Knee type	Foot	Residuum length
A1	Female	trauma	C-LEG3	Mircroprocessor	1C30	27
A2	Male	osteoarcoma	GENIUM	Mircroprocessor	1C60	21
A3	Male	trauma	RHEO3	Mircroprocessor	PROFLEX	23
A4	Female	trauma	3R80	Mechanical	1C30	24

3.2.2 Body measurements

Each participant's body mass was measured using a digital standing scale. For the residual limb measurements, the subjects were asked to stand using the contralateral limb without the prosthesis. The proximal circumference, which was the largest one at the hip joint, was measured using a flexible tape measure. The circumference of the distal end, which was at the last bony prominence, was measured. Then, the residual limb's length, which was the distance from the femur head to the most distal aspect of the residual limb, was measured. Thereafter, the subject wore their prosthesis. The prostheses alignment and fitting were checked by an experienced prosthetist before data collection. Prior to the experiment, the mass and length, width and depth of prosthesis segments (knee joint, socket for SP users, pylon and foot) were obtained using a digital caliper, tape measure and digital scales to further calculation of inertia (Harandi et al., 2020).

3.2.3 Marker attachments

A total of thirty eight retro-reflective markers with 14 mm diameter were alcohol-cleaned, then mounted bilaterally on body segments of the intact and residual limb including trunk, arms, thigh and feet following a previously published marker set (Figure 3.1, Table

3.3)(Schache et al., 2011, Dorn et al., 2012b). On the prosthesis, the markers were attached over anatomical landmarks based on the intact limb (Harandi et al., 2020).

3.2.4 Walking protocol

Each subject performed several walking trials and three successful trials of over-ground walking were chosen at their self-selected speed. The speed for each trial was measured using two infrared timing gates located in a 4-meter walking way. A successful trial was defined in which the participants stepped firmly with their feet within the boundaries of the force plates, starting from heel-strike and ending at toe-off. This part of the gait cycle is defined as the stance phase.

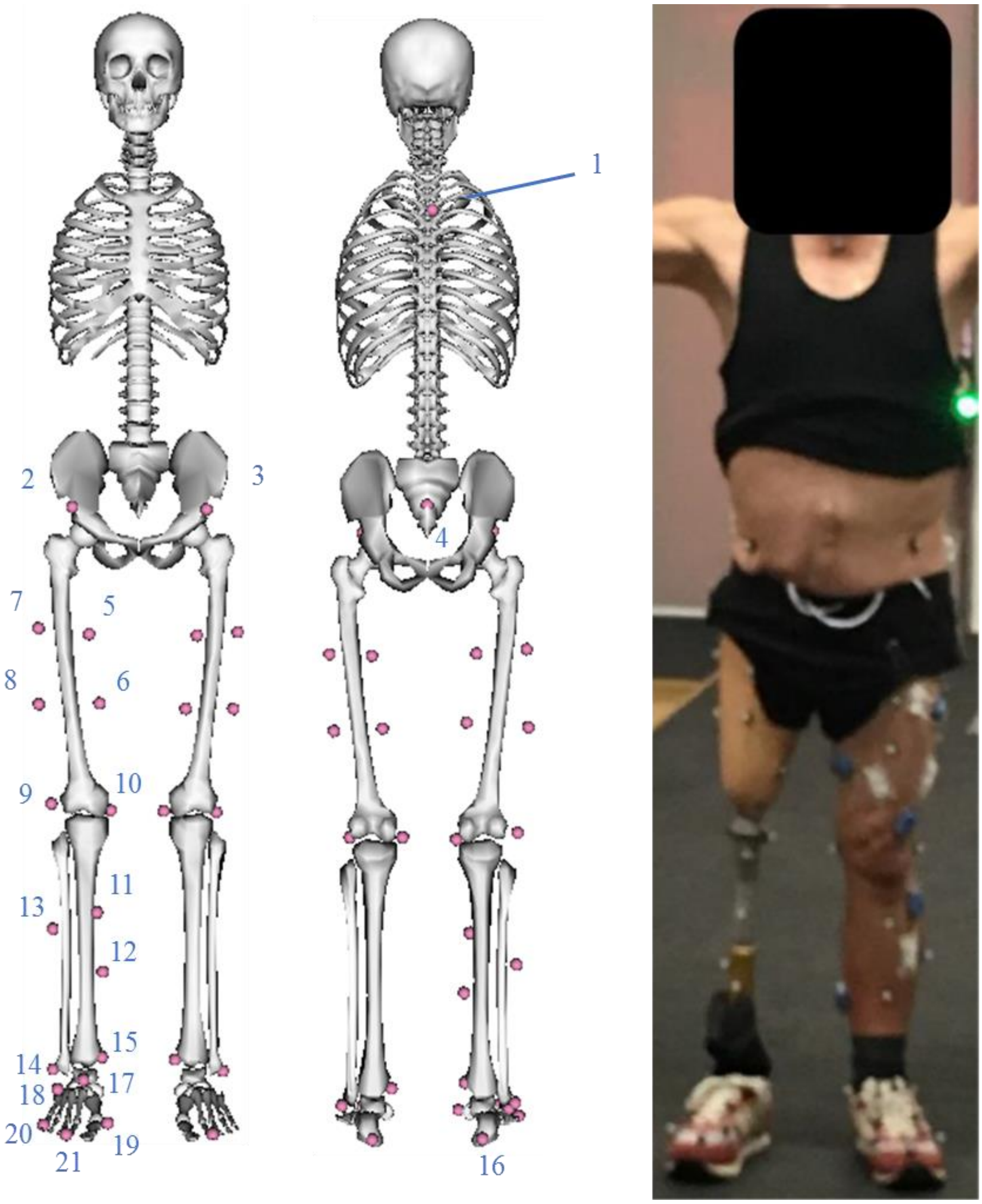

Figure 3.1- Marker set used in this study (Left). The numbers are described in Table 3.3. An illustration of an individual with markerset.

Table 3.3. Markers locations used to motion data capture. For the prosthetic leg, it follows the marker locations of the intact leg.

Marker	Trunk	
1	C7	14mm marker over spinous process of 7th cervical vertebra
	Pelvis	
2	RASI	14mm marker placed over right anterior superior iliac spine (ASIS)
3	LASI	14mm marker placed over left anterior superior iliac spine (ASIS)
4	SACR	14mm marker placed over midpoint between left and right posterior superior iliac spines
	Intact Limb Thigh	
5	RTHAP	14mm marker located at the proximal anterior aspect of the right thigh
6	RTHAD	14mm marker located at the distal anterior aspect of the right thigh
7	RTHLP	14mm marker located at the proximal lateral aspect of the right thigh
8	RTHLD	14mm marker located at the distal lateral aspect of the right thigh
9	RLEPI	14mm marker over lateral epicondyle of right femur
10	RMEPI	14mm marker over medial epicondyle of right femur
	Intact Limb Shank	
11	RTIAP	14mm marker located on the proximal 1/3 of the anterior shaft of the right tibia
12	RTIAD	14mm marker located on the distal 1/3 of the anterior shaft of the right tibia
13	RTILAT	14mm marker located on the mid lateral aspect of the right tibia
14	RLMAL	14mm marker located over the right lateral malleolus
15	RMMAL	14mm marker located over the right medial malleolus
	Intact Limb Foot	
16	RHEEL	14mm marker on distal aspect of bisection of right posterior calcaneum
17	RMFS	14mm marker on medial right midfoot
18	RMFL	14mm marker on lateral right midfoot
19	RP1MT	14mm marker on medial aspect of right 1st MTP joint
20	RP5MT	14mm marker on lateral aspect of right 5th MTP joint
21	RTOE	14mm marker on nail of 1st toe of right foot
	Residual Limb	
	On the soft tissue of the residual limb, the markers followed the intact limb marker set	
	On the prosthesis, the markers were mounted over anatomical landmarks based on the intact limb in medial and lateral knee and ankle, heel and toe	

3.2.5 Data processing

Lower limb and upper body COM kinematics were derived by tracking three-dimensional positions of the reflective markers using an eight-camera motion capture system (Vicon, Oxford Metrics) sampling at 120 Hz. Marker trajectories and GRF were low-pass filtered with a cut-off frequency of 4 and 60 Hz, respectively using a 4th order Butterworth filter (Lin et al., 2015). Surface electromyography (EMG) data were recorded at 1000 Hz using pairs of surface electrodes and Cometa system with 16 channels (Cometa, Milan, Italy). Each amputee's skin was shaved with a disposable feather razor and cleaned with alcohol before electrode placement. EMG electrode placement followed a previously described guidelines (Hermens et al., 2000), and EMG data were checked prior to testing to ensure suitable electrode placement and output (Hermens et al., 1999). Pairs of pre-gelled Ag/ AgCl bipolar electrodes were placed on the intact limb’s muscles including *gluteus maximus, gluteus medius, soleus,* medial and lateral *gastrocnemius*, and vastus medialis and lateralis and residual limb’s muscles including *gluteus maximus* and *gluteus medius* (Table 3.4). During walking trials, GRFs were simultaneously measured using three AMTI force platforms embedded in the floor (Watertown, USA) at a sample rate of 1000 Hz (Harandi et al., 2020). Vicon cameras , force plates and EMGs were automatically synced to each other.

Table 3.4. EMG electrode placements used for EMG data capture

Muscle	Location	Subject pose
Gluteus maximus	Over greatest prominence of the middle of the buttocks. Electrodes positioned 50% along a line connecting middle of sacrum and GT. Line connecting electrodes is parallel to line connecting PSIS and mid posterior thigh	Prone
Gluteus medius	Electrodes positioned 50% along a line connecting iliac crest and GT (or 3cm inferior to ASIS-PSIS, on a line with (GT). Line connecting electrodes is parallel to iliac crest-GT line	Side lying
Vastus lateralis	Over area of greatest muscle bulk. Electrodes placed approx 33%) up from patella along a line connecting ASIS to lateral margin of patella. Line connecting electrodes is parallel to muscle fibers	Supine, quads over Fulcrum
Vastus medialis	Over area of greatest muscle bulk. Electrodes placed approx 20% up from MFC along a line connecting ASIS and MFC. Line connecting electrodes is perpendicular to the ASIS-MFC line	Supine, quads over Fulcrum
Gastrocnemius		Prone, fulcrum under

medialis	Over area of greatest muscle bulk, along a line from medial tibial condyle to heel. Line connecting electrodes is parallel to line of leg	ankle, foot plantar flexed
Gastrocnemius lateralis	Over area of greatest muscle bulk. Electrodes positioned approx 33% down from head of fibula along a line from head of fibula to heel. Line connecting electrodes is parallel to line of head of fibula to heel	Prone, fulcrum under ankle, foot plantar flexed
Soleus	Electrodes positioned approx 66% down from MFC along a line connecting MFC and medial malleolus. Line connecting electrodes is parallel to line of MFC to medial malleolus	Supine with knee flexed to 90 degrees

3.3 Musculoskeletal modeling

In this section, musculoskeletal modeling development will be explained in detail. The marker trajectories, GRFs, and EMG data were extracted from C3D format and transformed into a suitable format as input to OpenSim model using a freely available Gait-Extract toolbox (https://simtk.org/home/c3dtoolbox) developed in MATLAB (The MathWorks, Inc., MA, USA).

Table 3.5. The intact and residual leg muscles included in the model. * represents EMG data collected of the intact limb muscles; ¥ represents EMG data collected of the contralateral side muscles. ϕ represent the muscles not included in the model for the residual limb.

Muscle	**Muscle group**
Gluteus medius *¥ (anterior, posterior and middle compartments) Gluteus minimus (anterior, posterior and middle compartments)	GMED
Gluteus maximus *¥ (anterior, posterior and inferior compartments)	GMAX
Hamstrings (Semimembranosus, Semitendinosus, Gracilis, Biceps femoris long head)	HAM
Biceps femoris short head ϕ	BFSH
Adductor longus, Adductor brevis, Pectineus, Quadratus femoris, Adductor magnus (superior, middle and inferior compartments)	ALAM
Iliacus, Psoas	IL
Gemellus	GEM
Piriformis	PIRI
Peroneus brevis	PERBREV
Proneus longus	PERLONG
Rectus femoris *	RF
Sartorius	SAR
Vasti *ϕ (medialis, intermedius and lateralis compartments)	VAS
Gastrocnemius *ϕ (lateral and medial compartments)	GAS
Soleus *ϕ	SOL
Tibialis posterior ϕ	TP
Tibialis anterior *ϕ	TA
Flexor digitorum longus ϕ	FDL

Extensor digitorum longus $^{\phi}$	EDL
Flexor hallucis longus $^{\phi}$	FHL
Extensor hallucis longus $^{\phi}$	EHL
Tensor fascia late $^{\phi}$	TFL
Erector spinae	ERCSPN
Internal oblique	INTOBL
External oblique	EXTOBL

3.3.1 Healthy subject model

A generic three-dimensional musculoskeletal model was developed in OpenSim 3.2 (Delp et al., 2007). Each 23-degrees-of-freedom model comprised lower limb and trunk segments actuated by 76 muscle-tendon units (Table 3.5). The Hill-type model in series with an elastic tendon of the musculotendon unit was used to reflect muscle mechanics (Thelen, 2003). Physiological musculotendon parameters including muscle architecture, muscle physiological cross-sectional area (PCSA), optimal fiber length, pennation angle, maximum isometric force, and tendon slack length were derived from previous cadaver studies (Wickiewicz et al., 1983, Delp et al., 1990, Friederich and Brand, 1990). The maximum isometric force of each muscle is defined by multiplying the muscle PCSA and muscle tension. The inertial properties (mass, center of mass and moment of inertia) of the twelve body segments (torso, pelvis, femur, tibia, calcaneus, talus and toes) were derived from (Anderson and Pandy, 2001a) study. The joints frame coordinates were defined based on Delp et al (Delp et al., 1990). A single rigid body including the combined head, arm and torso was considered to articulate with pelvis via a ball-and-socket back joint. The hip joints, the knee and metatarsal joints, and each ankle-subtalar complex joint were modeled as ball-and-socket joints, hinge joints, and a universal joint, respectively.

3.3.2 Model scaling

To accurately calculate lower limb joints moments and muscle forces, a generic musculoskeletal model must be scaled for each participant. OpenSim scaling tool adjusts mass, segment length and muscle parameters based on the individual's mass, length and diameter of segments. A static standing trial was used to calculate the scaling factors for each segment, as defined by the relative distances between pairs of markers (Delp et al., 2007). This participant-specific scaled model was then modified to develop unilateral transfemoral amputee model.

3.3.3 Amputee subject model

The residual limb of the amputated leg was modeled as a frustum of a circular cone (Mattes et al., 2000), and its measurements was described in section 3.2.1. The residual limb tissue was assumed to be homogenous with a density of 1.1 g/cm^3, in order to estimate mass, the moment of inertia and COM position (Mungiole and Martin, 1990, Smith et al., 2014). Subsequently, all musculoskeletal structures below the knee were removed from the non-amputee scaled model described above. The hip adductors and hip flexors, which were known as bi-articular muscles spanning the hip and knee joints, were re-attached in the model. These re-anchored muscles were *adductor magnus*, *semimembranosus*, *semitendinosus*, *biceps femoris long head*, *rectus femoris*, *gracilis*, *sartorius* and *tensor fascia latae*. Other uni-articular muscles crossing the knee joint and those ankle-joint spanning muscles were removed from the model (Table 3.5). The re-anchored muscles' attachment points were positioned to the distal end of the amputated femur (Harandi et al., 2020).

For the physiological properties of the re-anchored muscles, the surgical procedure of muscle stabilization must be considered. In the traditional procedure, myoplasty, both agonist and antagonist muscles are sutured over the femur. However, the muscle tension is not preserved based on this method (Gottschalk, 2004), and muscle stabilization is modeled while the tendon slack length is maintained. The matter of not keeping muscle tension has led to the use of myodesis technique specifically for the medial *hamstring* and the *adductor magnus* (Gottschalk, 2004, Tintle et al., 2010). A myodesis stabilization method has been demonstrated to preserve those muscles directly reattached to the end of femur under tension. In addition, the deep soft tissue padding is secured, and the stability of muscle is preserved (Tintle et al., 2010).

This approach tends to preserve the muscle tension of the reattached muscle relative to the corresponding muscle in the intact limb during neutral position, by modifying the muscle-tendon slack length (Ranz et al., 2017). Optimal fiber length value for each re-anchored muscle-tendon unit was then calculated in equal proportion with the sum of tendon slack length and fiber length of the intact limb's muscles in neutral position (Ranz et al., 2017). In this study, the myodesis stabilization technique was used for modeling and analyses. However, the myoplasty-based modeling result will be explained further in section 4.4. The reattached muscles in this study were the adductor magnus, semimembranosus, semitendinosus, biceps femoris long head, and gracilis, which were inserted posteriorly to the medial ridge of linea aspera; *rectus femoris* and *sartorius* were inserted anteriorly to the distal part of an intertrochanteric line and medial ridge of linea aspera; tensor fascia latae was inserted laterally to lateral ridge of the linea aspera (Harandi et al., 2020).

The prosthesis segments were reverse-engineered in SolidWorks (SolidWorks, Dassault Systems Massachusetts, USA) in accordance with the measurements described in subsection 3.2.1. The moment of inertia and COM positions of each lower-limb prosthesis were calculated from the CAD model assuming homogenous material properties and virtually placed in the individualized scaled model. The knee and ankle of the prosthetic leg were modeled as hinge joint (Harandi et al., 2020). Figure 3.2 shows a healthy model, amputee model without prosthesis and amputee model with a prosthesis attached.

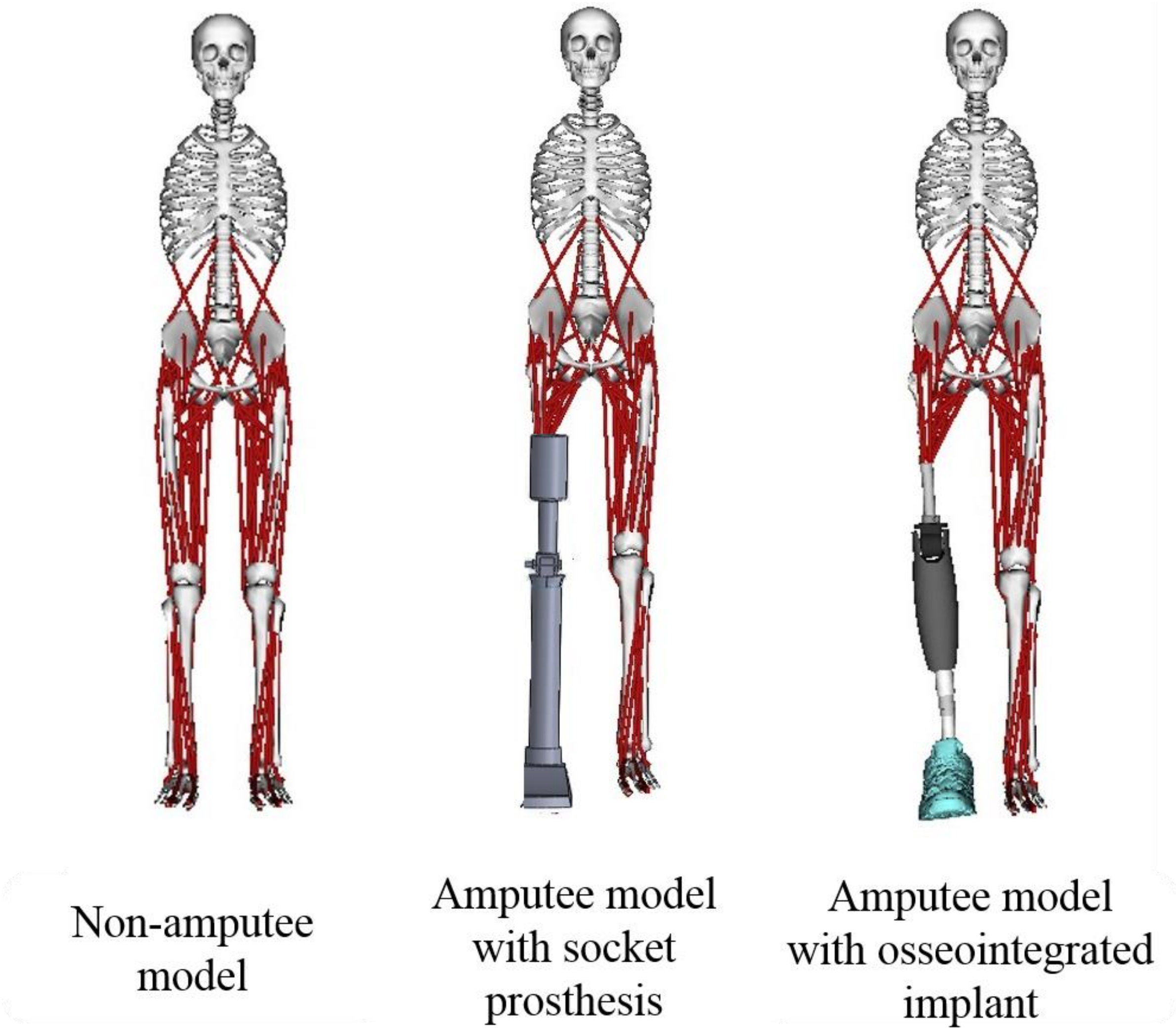

Figure 3.2. Schematics of healthy and amputee models developed in OpenSim (Harandi et al., 2020, Robinson et al., 2020).

3.3.4 Inverse kinematics

The scaled transfemoral amputee-specific model was then used to find the optimum generalized coordinates of joint motion in a multibody chain using inverse kinematics tool. This tool intends to minimize the sum of the squared differences between experimental data and virtual markers on the model (Lu and O'connor, 1999).

3.3.5 Inverse dynamics

Inverse dynamics was then used for all amputee data sets to calculate the net forces and moments of the joints of the multibody system (Remy and Thelen, 2009). This bottom-up method determined the joints moments and forces to generate the given joints movement. The GRFs applied to the distal segments of the body, the feet, were the additional information used to solve for the net moments of the ankle. This iterative upward process was used to compute all lower limb joints, from ankle to hip.

The scaled model may include kinematics and dynamics errors. Due to kinematic errors of the scaled model, large residuals are resulted between the proximal segment (pelvis) and ground to compensate for the errors. Also, incorporating GRFs in the inverse dynamics problem generates an over-determined system (Kuo, 1998). In addition, errors in inverse dynamics depend on prosthetic design (Dumas et al., 2009, Frossard et al., 2011). Therefore, the measured GRFs and kinematics may not be dynamically consistent with the skeletal model. Thus, to minimize these residual forces and moments, which will lead to experimental data and skeleton model's error, a Residual Reduction Algorithm (RRA) was used in this study. This algorithm allows the joints kinematics of the skeleton model to alter by varying the center of mass of torso with the approach of more dynamic consistency with the GRFs (Steele et al., 2012b, Dumas et al., 2016).

3.3.6 Static optimization

Since more muscles exist than joints in the lower extremity, the redundancy of the musculoskeletal system will happen. Thus, an infinite number of musculotendon force amalgamations being potentially able to generate the net joint moment is needed to reproduce the joint kinematics.

Muscle forces were computed using static optimization by decomposing the net joint moments calculated from inverse dynamics into discrete muscle actuator loads at each time instant. Static optimization used a cost function with the approach of minimizing the sum of the squared of all individual muscle activations, which is equivalent to minimizing the simultaneous mechanical stress across all muscles (Crowninshield and Brand, 1981). The predicted muscle forces by optimization were further constrained in accordance with the force-length-velocity properties of each muscle's physiological bounds.

The combination of the lower limb muscles of the musculoskeletal model, even they are fully activated, could not provide the required joint moments. For instance, when the desired knee extensor moment cannot be satisfied with the fully activated knee extensor muscles, a knee extensor strength deficiency will happen because the knee reserve actuator will generate the difference. Hence, ideal reserve torque actuators must be applied to the model. The role of these reserve actuators is to permit optimization to numerically converge; however, their contribution to the joint moments of the model during static optimization should be ideally zero. The static optimization problem is stated as follows:

calculate: $a = \begin{bmatrix} a^M \\ a^R \\ a^r \end{bmatrix}$

by minimizing: $J(a) = \overbrace{\sum_{i=1}^{nm} \omega_i (a_i{}^M)^2}^{\text{muscle}} + \overbrace{\sum_{j=1}^{6} \omega_j \left(a_j{}^R\right)^2}^{\text{residual}} + \overbrace{\sum_{k=1}^{nq} \omega_k (a_k{}^r)^2}^{\text{reserve}}$

subject to:

$$\overbrace{\sum_{i=1}^{nm}\left[a_i{}^M . f_i\left(F_0{}^M, l^M, v^M\right)\right]. s_{i,n}}^{\text{muscle}} + \overbrace{\sum_{j=1}^{6}\left[a_j{}^R . F_j{}^R\right]}^{\text{residual}} + \overbrace{\sum_{k=1}^{nq}\left[a_k{}^r . F_k{}^r\right]}^{\text{reserve}} = \tau_n \qquad 3.1$$

$$0 < \mathrm{a}^{\mathrm{M}} < 1$$

where the variables of the equation are defined as follows: muscles a^M, residuals a^R and reserve actuator activation a^r. *nm* and *nq*: the number of muscles and kinematic degree of freedom in the model; the following weights were given to muscles, residual and reserve actuators to penalize the muscles' capacity to generate force respectively, ω_i, ω_j and ω_k; the force-length-velocity surface of muscle *i* is shown by $f_i\left(F_0{}^M, l^M, v^M\right)$; the peak strength of the residual actuator *j* is $F_j{}^R$, the peak strength of the reserve actuator *j* is $F_j{}^r$; the moment arm of muscle *i* about coordinate *n* is $s_{i,n}$; the net joint moment of generalized coordinate *n*, as derived from RRA or inverse dynamics is τ_n.

Static optimization method cannot consider the time-dependent activation dynamics of muscle because this technique solves muscle forces at each time instant. The contribution of muscles is calculated in static optimization incorporating GRF and joint movements. Most of the time, the ideal reserve torques must be applied due to the lack of actuator force in the model. The reserve torques will equilibrate between actuator forces and joint moments. Static optimization problem aims to converge optimization problem by minimizing the effect of residuals and reserve torques; ideally should be zero.

3.3.7 Validation of the musculoskeletal model

Non-invasive measuring methods of muscle forces during walking maneuver are impossible. Therefore, the accurate evaluation of muscle forces prediction techniques has remained limited. One of the common methods to temporally validate muscle forces of the computer-based musculoskeletal models is to use EMG signals (Erdemir et al., 2007, Pantall and Ewins, 2013). EMG measures the electrical activity across a muscle, which leads to its activation and force generation. However, this is not very empirical method since during amputee's walking one may not be able to measure the EMG signals of the deep muscles. Although well correlated with the timing of muscle force prediction by the model and the timing of EMG signals (Anderson and Pandy, 2001b, Liu et al., 2008, Hamner et al., 2010), the validation process of the EMG magnitudes is difficult due to the non-linear relationship between the magnitudes of muscle force and EMG (Lloyd and Besier, 2003, Buchanan et al., 2004, Buchanan et al., 2005). For instance, if a muscle, which can be fully activated, does not operate inside its force-length-velocity properties, the generated force will be very minimal.

In this dissertation, EMGs of gluteal muscles in the intact and residual limb, and EMGs of *soleus*, *gastrocnemius* and *vasti* of the intact limb were recorded. The residual limb muscles have been shown to produce a non-stationary random signal, which is due to intensity and duration fluctuation of the muscle contraction (Bonato et al., 2001, Pantall and Ewins, 2013). Thus, only EMG of *gluteal* muscles was successfully employed from the residual limb. The timing of muscle force computed by the model was further evaluated using EMG signals. EMG offset signals were removed and the waveforms rectified and low-pass filtered at 10 Hz using a 2nd order Butterworth filter to create linear envelopes (Lin et al., 2015).

3.3.8 Induced acceleration analysis

The purpose of induced acceleration analyses is quantifying the constitution of each force to the total GRFs and the net joint acceleration. In this analytical technique, the superposition principles should be satisfied. This means that differences between the sum of all action forces to the GRFs or joint acceleration and the total GRFs measured experimentally must be zero (Anderson and Pandy, 2003). In this section, the term *action force* represents the forces of the musculoskeletal model and the term *actuator* represents all model actuators, which are residual loads, reserve torques, arm torques, and musculotendon forces.

To implement induced acceleration analysis, mechanical constraints are required to act between the foot and ground. The GRFs' generation in the computational musculoskeletal model will be facilitated using the mechanical constraints known as a *ground contact model,* which was adapted from Lin's study (Lin et al., 2012) and the OpenSim plug-in.

A five-point model was assumed as a contact between the foot and the ground (Anderson and Pandy, 2003, Liu et al., 2006). These five points attached to the OpenSim musculoskeletal model consisted of two heel markers (H) located on medial and lateral sides of the mid calcaneus, two metatarsal markers (M) located at the first and fifth metatarsal junctions, a toe marker (T) located at the anterior boundary of the foot, the line between the heel markers representing an approximate heel hinge axis, and the line between the metatarsal markers forming an approximate metatarsal axis (Figure 3.3).

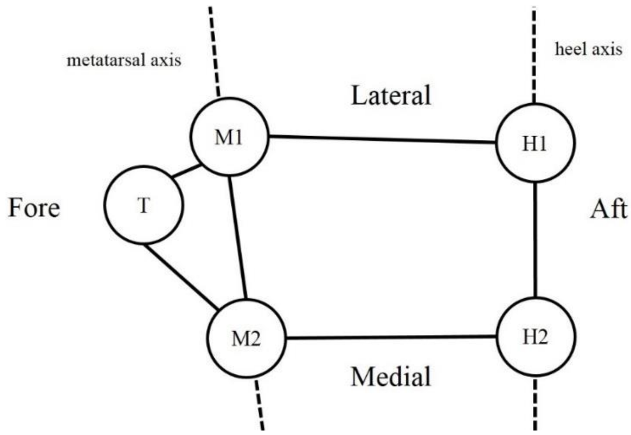

Figure 3.3. A five-point model of contact between the foot and the ground. T, M and H are representatives of toe marker, metatarsal marker and heel marker, respectively. The labels of markers are described in Table 3.6.

The location of these five points were defined by a set of five markers attached to the coordinate frame of foot (Table 3.6)

Table 3.6. The location of five foot-ground contact points over the sole of feet. The body coordinates (x, y, z) are in (anterior, vertical, lateral) directions, respectively.

Leg	Marker Name	Marker Body	Marker Location (m) in Body coordinates
Right	T	calcn_r	(0.275, 0.00, 0.02)
	M1	calcn_r	(0.135, 0.00, 0.07)
	M2	calcn_r	(0.205, 0.00, -0.05)
	H1	calcn_r	(0.00, 0.00, 0.03)
	H2	calcn_r	(0.01, 0.00, -0.05)
Left	T	calcn_l	(0.275, 0.00, -0.02)
	M1	calcn_l	(0.135, 0.00, -0.07)
	M2	calcn_l	(0.205, 0.00, 0.05)
	H1	calcn_l	(0.00, 0.00, -0.03)
	H2	calcn_l	(0.01, 0.00, 0.05)

The dynamic equation of motion for the n degree-of-freedom skeleton model with k musculotendon unit is stated as follows:

$$M(q)\ddot{q} = C(q,\dot{q}) + G(q) + \begin{bmatrix} 0_{6\times 1} \\ S(q)F^{M} \end{bmatrix} + \begin{bmatrix} R_{6\times 1} \\ r_{n\tau\times 1} \end{bmatrix} + E(q)F_{ext} \qquad 3.2$$

where q, $\dot{q}$, and $\ddot{q}$ are the $n \times 1$ generalized positions, velocities, and accelerations vectors, respectively, which include both translational (e.g. pelvis location relative to the ground) and rotational (e.g. joint angles) degrees of freedom; $\mathbf{M}(q)$ is the $n \times n$ model mass matrix or inertia matrix to describe the mass and inertial properties of the body segments; $C(q,\dot{q})$ is the $n \times 1$ vector to specify generalized force vector due to Coriolis or centripetal forces; $\mathbf{G}$(q) is an $n \times 1$ generalized gravity force vector; $\mathbf{S}(q)$ is an $n \times k$ muscular moment arms matrix; $\mathbf{F}^{M}$ is a $k \times 1$ muscle forces vector; $\mathbf{F}_{ext}$ is a $3f \times 1$ external reaction forces vector applying between the foot and ground by the f contact points; $\mathbf{E}(q)$ is an $n \times 3f$ matrix of linear generalized Jacobian which defines the relationship between the generalized velocity vector $\dot{q}$ and the linear velocity vector of the foot-ground contact points $\dot{X}$. This Jacobian matrix is defined as follows:

$$E(q) = \frac{\partial \dot{X}}{\partial \dot{q}}(q) = \frac{\partial \ddot{X}}{\partial \ddot{q}}(q)$$

$$= \left[\begin{array}{cccc|ccc} \frac{\partial \dot{x}_1 X}{\partial \dot{q}_1} & \frac{\partial \dot{x}_1 Y}{\partial \dot{q}_1} & \frac{\partial \dot{x}_1 Z}{\partial \dot{q}_1} & \cdots & \frac{\partial \dot{x}_f X}{\partial \dot{q}_1} & \frac{\partial \dot{x}_f Y}{\partial \dot{q}_1} & \frac{\partial \dot{x}_f Z}{\partial \dot{q}_1} \\ \frac{\partial \dot{x}_1 X}{\partial \dot{q}_2} & \frac{\partial \dot{x}_1 Y}{\partial \dot{q}_2} & \frac{\partial \dot{x}_1 Z}{\partial \dot{q}_2} & \cdots & \frac{\partial \dot{x}_f X}{\partial \dot{q}_2} & \frac{\partial \dot{x}_f Y}{\partial \dot{q}_2} & \frac{\partial \dot{x}_f Z}{\partial \dot{q}_2} \\ \vdots & \vdots & \vdots & \ddots & \vdots & \vdots & \vdots \\ \frac{\partial \dot{x}_1 X}{\partial \dot{q}_n} & \frac{\partial \dot{x}_1 Y}{\partial \dot{q}_n} & \frac{\partial \dot{x}_1 Z}{\partial \dot{q}_n} & \cdots & \frac{\partial \dot{x}_f X}{\partial \dot{q}_n} & \frac{\partial \dot{x}_f Y}{\partial \dot{q}_n} & \frac{\partial \dot{x}_f Z}{\partial \dot{q}_n} \end{array}\right] \qquad 3.3$$

where X, $\dot{X}$, and $\ddot{X}$ represent the linear positions, velocities, and accelerations of all f foot-ground contact points. All internal generalized force contributions such as muscle forces, reserve forces/torques, residual forces/torques, gravity forces, and Coriolis/centripetal forces are grouped as $\mathbf{F}_{int}$. So, equation 3.2 is rewritten as:

$$M.\ddot{q} = F_{int} + E.F_{ext} \qquad 3.4$$

The linear velocity of the *i*th foot point can also be calculated using a Jacobian matrix:

$$\dot{X}_i = E_i^T \dot{q} \qquad i = 1,2, \ldots, f \qquad 3.5$$

The linear acceleration of the *i*th foot point will be the time derivative of equation 3.5 as:

$$\ddot{X}_i = E_i^T \ddot{q} + \dot{E}_i^T \dot{q} \qquad i = 1,2, \ldots, f \qquad 3.6$$

When foot point *i* is in contact with the ground, the linear acceleration of point *i* is equal to zero in all directions due to the rigid contact principles assumption. Considering $K_i = \dot{E}_i^T \dot{q}$, so:

$$E_i^T \ddot{q} + K_i = 0 \qquad i = 1,2, \ldots, f \qquad 3.7$$

Prompt and quick touching on and off between each foot point and ground would result in discontinuities in the constraint set of equations and then induced acceleration results. Therefore, a diagonal weighting matrix **W** is defined to smooth transitions between constrain the contact points and contact phases to remain consistent with the actual foot motion during stance phase:

$$W_{f\times f}\{K + E^T \ddot{q}\}_{3f\times 1} = 0_{3f\times 1} \qquad 3.8$$

where **W** elements were themselves a 3×3 diagonal matrix that weighted the X, Y and Z components of the linear acceleration constraint equally:

$$W(i,i) = \begin{bmatrix} w & & \\ & w & \\ & & w \end{bmatrix} \qquad i = 1,2,\dots,f \qquad 3.9$$

where w is a weighting factor which is between zero and one. This factor indicates the magnitude of the foot point constraint. Thus, $\mathbf{W}(\mathrm{i}) = 0$ implies no contact force for the point *i* and $\mathbf{W}(\mathrm{i}) = 1$ imply when the *i*th point is fully constrained. $0 < \mathbf{W}(\mathrm{i}) < 1$ implies a partially constrained contact point i.

These weightings were determined by examining the experimental data of the trial's kinetics. The weightings estimation was based on the study done by Dorn et al. (Dorn et al., 2012a). In this regard, all foot contact points would set to zero if the Euclidean norm of the ground reaction force was below a user defined threshold. It means that the foot was accounted to be off. For other conditions, at least one point of the foot was in contact with the ground, so the weightings for the foot point constraint must be specified. As shown in Figure 3.4, four locomotion phased were defined. The experimental center of pressure (CoP) position was used to determine the foot contact point weightings.

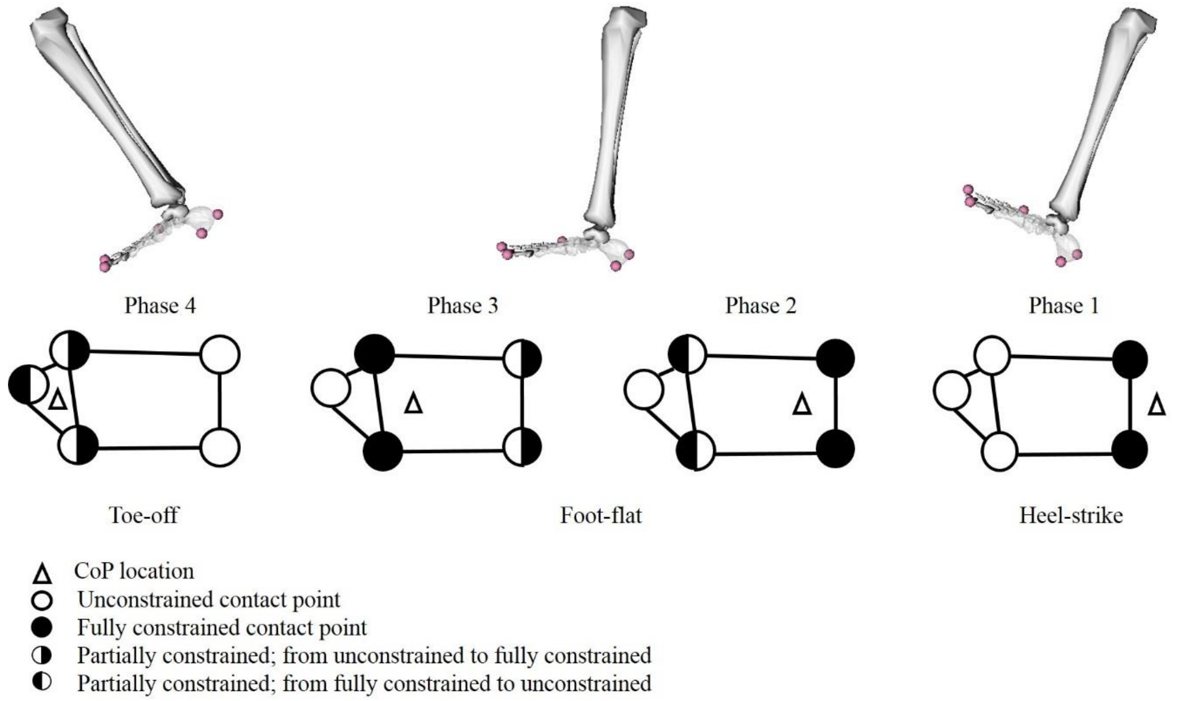

Figure 3.4. Foot-ground contact constraints during stance phase at heel-strike started from right (phase 1), foot-flat (phase 2,3) and toe-off (phase 4).

Phase 1 was defined at heel-strike when the CoP lies posteriorly relative to the heel axis, both heel markers were fully constrained while the other three were free. The foot-ground interaction at this phase was approximated as a hinge constraint in which a rotation of the foot about the heel axis can occur.

Phase 2 was defined between heel-strike and foot flat when the CoP lies posteriorly relative to half of the hind-foot boundary of the quadrilateral consisted of H and M markers. A weighting function ϕ was introduced to implement transition between phase 1 and phase 2 as:

$$\emptyset(d_h, d_m) = \frac{d_h}{d_h + d_m} \quad 3.10$$

where d_h and d_m are the shortest distance from the CoP to both heel and metatarsal axes, respectively. In this phase, the heel markers remained fully constrained, while the metatarsal points weightings were equal to 2ϕ as they remained partially constrained. Thus, as the CoP moved towards the metatarsal axis, the metatarsal points weightings increased from 0 to 1. At this stage, the interaction between the foot and ground was transformed from a hinge constraint about the heel axis to a weld constraint.

Phase 3 was defined when the CoP crosses the anterior half of the hind-foot boundary of the quadrilateral (ϕ = 0.5). At this stage, metatarsal points remained fully constrained, while the weightings of the heel markers decreased to zero according to 2(1 – ϕ). Therefore, the foot-ground constraint was transformed from a weld constraint to a hinge constraint about the metatarsal axis. At the time when the heel and metatarsal points were fully constrained, the CoP lies exactly half way between the heel and metatarsal axes. Hence, a weld constraint was considered during the foot-flat pose.

Phase 4 was defined when the CoP lies inside the boundary of the triangle consisting of the metatarsal and toe points. A weighting function γ was introduced to implement a transition from phase 3 to phase 4 as:

$$\gamma(d_m, d_t) = \frac{d_m}{d_t} \qquad 3.11$$

where d_t is the shortest distance from toe point to the metatarsal axis. When reaching this stage: heel points are free; metatarsal points weightings begin to decrease according to 1- γ; the toe point weighting begins to increase according to γ. Thus, the foot-ground interaction's constraint was transformed from a hinge constraint about the metatarsal axis to a ball constraint about toe point. Table 3.7 is the summary of the kinematic constraint weightings.

Table 3.7: Constraint weightings w for the five foot-ground interaction points. d_h and d_m are the shortest distance from the CoP to both heel and metatarsal axes, respectively. d_t is the shortest distance from toe point to the metatarsal axis.

Foot-ground interaction points	Phase 1	Phase 2	Phase 3	Phase 4
H1	1	1	$2(1-\frac{d_h}{d_h+d_m})$	0
H2	1	1	$2(1-\frac{d_h}{d_h+d_m})$	0
M1	0	$2(\frac{d_h}{d_h+d_m})$	1	$1-\frac{d_m}{d_t}$
M2	0	$2(\frac{d_h}{d_h+d_m})$	1	$1-\frac{d_m}{d_t}$
T	0	0	0	$\frac{d_m}{d_t}$

The contribution of each *action force* $\boldsymbol{\alpha}$ (e.g. individual muscles, gravity and Coriolis forces) to the net GRFs and acceleration at each joint was calculated when the *action force* is applied in isolation to the model. Regarding equations 3.4 and 3.8, the equation 3.12 was generated as follows:

$$\begin{cases} M.\ddot{q}^{\alpha} = F_{int}^{\alpha} + E.F_{ext}^{\alpha} \\ W\{K^{\alpha} + E^{T}\ddot{q}^{\alpha}\} = 0 \end{cases} \tag{3.12}$$

At a specific time, **M**, **E** and **W** are constant for all "*action forces*"; so, these values were computed outside the "*action force*" loop. The vectors of $\mathbf{F}_{int}^{\alpha}$, which is the generalized force resulting from the isolated application of the *action force,* and $\mathbf{K}^{\alpha}$, which forms part of the zero-acceleration foot point constraint, must be uniquely calculated for each "*action force*" $\boldsymbol{\alpha}$.

For the velocity related forces (Coriolis/centrifugal), equation 3.6 was rearranged to calculate $\mathbf{K}^{vel}$ since $\mathbf{K}^{\alpha}$ is zero for all *action forces* due to disability of the velocity in these terms ($\mathbf{K}^{\boldsymbol{\alpha}} = \dot{\mathbf{E}}^{\mathbf{T}}\dot{\mathbf{q}}$ and $\dot{\mathbf{q}} = \mathbf{0}$):

$$K^{vel} = \ddot{X} - E^T\ddot{q} \qquad 3.13$$

The unknown contributions of α to the GRFs at each foot-ground contact point and generalized acceleration after considering the zero-acceleration constraint related equations are represented by $\mathbf{F}^{\alpha}_{ext}$ and $\ddot{\mathbf{q}}$, respectively. To calculate these quantities from equation 3.12, an equality-constrained-least-square optimization problem is solved. In this case, an objective function, $\boldsymbol{J}$, is chosen to minimize the weighted squared sum of foot contact point forces:

$$J = \frac{1}{w}.\sum_{i=1}^{f} F^{\alpha}_{exti}F^{\alpha}_{exti} \qquad 3.14$$

A matrix form can be used to represent the equations 3.12 and 3.14 due to the being linear of the $\mathbf{F}^{\alpha}_{ext}$ and $\ddot{\mathbf{q}}$:

$$\widetilde{W}\begin{bmatrix} M & -E \\ W.E^T & 0_{3f\times 3f} \\ 0_{3f\times n} & W^{-1} \end{bmatrix}\begin{Bmatrix} \ddot{q}^{\alpha} \\ F^{\alpha}_{ext} \end{Bmatrix} = \widetilde{W}\begin{Bmatrix} F^{\alpha} \\ -W.K^{\alpha} \\ 0_{3f\times 1} \end{Bmatrix} \qquad 3.15$$

where $\widetilde{\mathbf{W}}$ is a global diagonal matrix with weights placed on the diagonal elements to emphasize the relative importance of the solution satisfying the equation of motion equality constraint (Row 1), foot point acceleration equality constraint (Row 2) and cost function (Row 3). $\widetilde{\mathbf{W}}$ is defined as:

$$\widetilde{W} = \begin{bmatrix} 10^4 I_{n\times n} & & \\ & 10^2 I_{3m\times 3m} & \\ & & I_{3m\times 3m} \end{bmatrix} \qquad 3.16$$

A more compact form of equation 3.15 can be replaced as follows:

$$A\begin{Bmatrix} \ddot{q}^{\alpha} \\ F_{ext}^{\alpha} \end{Bmatrix} = b \tag{3.17}$$

where **A** is an $(n + 6f) \times (n + 3f)$ matrix and **b** is an $(n + 6f) \times 1$ vector. The **A** matrix is constant for all *action forces* and the **b** vector is unique for each individual *action force* at a given time instant. Therefore, the superposition principles will be satisfied:

$$\begin{gathered} AX_1 = b_1 \\ \vdots \\ AX_m = b_m \\ A(X_1 + \cdots + X_m) = b_1 + \cdots + b_m \end{gathered} \tag{3.18}$$

An optimal analytical solution to the over-determined problem of equation 3.17 is provided using a least-square pseudo-inverse operator with no numerical iterations:

$$\begin{Bmatrix} \ddot{q}^{\alpha} \\ F_{ext}^{\alpha} \end{Bmatrix} = A^{+} b \tag{3.19}$$

where $\mathbf{A}^{+}$ is the Moore-Penrose pseudo-inverse of the matrix **A**. The least square error of the solution, which represents how well the solution matched the constraints, is computed as:

$$\begin{Bmatrix} err\_eom_{n\times 1} \\ err\_footconstraint_{3f\times 1} \\ err\_costfunction_{3f\times 1} \end{Bmatrix} = A^{+}\begin{Bmatrix} \ddot{q}^{\alpha} \\ F_{ext}^{\alpha} \end{Bmatrix} - b \tag{3.20}$$

Equation 3.19 was repeatedly solved for each *action force* $\boldsymbol{\alpha}$ at each time instant. Finally, the individual contributions of $\boldsymbol{\alpha}$ on each foot point, each foot and each direction were summed to determine the contribution of $\boldsymbol{\alpha}$ to the net GRFs. The sum of all *action forces* contributions may not be equal to the experimental GRFs, which leads to lack of satisfaction of the superposition principle. Anderson and Pandy mentioned that such superposition errors appear due to the rigid foot-ground contact assumption which is not quite accurate (Anderson and Pandy, 2003). Hence, to consider these inaccuracies, an inertial force (i.e. a fictitious force) was defined. This inertia force is required to satisfy the superposition principle by equating the model results and experimental data. To compute the inertial force's contribution to the joint acceleration and GRFs, equation 3.15 was modified as stated:

$$\begin{bmatrix} M & -E \\ I_{n\times n} & 0_{3f\times 3f} \end{bmatrix} \begin{Bmatrix} \ddot{q}^{I} \\ F^{I}_{ext} \end{Bmatrix} = \begin{Bmatrix} 0_{n\times 1} \\ (\ddot{q}^{Exp} - \ddot{q}^{Model}) \end{Bmatrix} \qquad 3.21$$

where $\ddot{\mathbf{q}}^{Exp}$ is the experimental generalized joint acceleration vector and $\ddot{\mathbf{q}}^{Model}$ is the sum of all induced accelerations of all *action forces*:

$$\ddot{q}^{Model} = \sum_{\alpha=1}^{numActionForces} \ddot{q}^{\alpha} \qquad 3.22$$

Regarding equation 3.21, the cost function related row (the third row in equation 3.15) does not exist. Therefore, it reduces to a discriminative problem and $\ddot{\mathbf{q}}^{\mathbf{I}}$ and $\mathbf{F}^{\mathbf{I}}_{\mathrm{ext}}$ were uniquely solved:

$$\ddot{q}^{I} = \ddot{q}^{Exp} - \ddot{q}^{Model} \qquad 3.23$$

$$F^{I}_{ext} = E^{+}(M.\ddot{q}^{I}) \qquad 3.24$$

3.3.8 Joint reaction loads and muscle contribution

Resultant forces and moments at joints were calculated in OpenSim based on the predicted muscle forces. Joint reaction analysis aims to calculate all loads acting on the model between consecutive bodies. Joint structure carries the internal loads, which are representative of the un-modeled joint structure generating the desired joint movement. The resultant loads at the joint are applied at the mobilizer frame/joint center of the two successive bodies.

To calculate joint reaction forces, a recursive bottom-up procedure beginning from distal bodies and progressing to the proximal bodies was used at each time instant during walking (Steele et al., 2012a). The recursive algorithm was based on resolving the applied point at the joint to stabilize the forces and motions using a free body diagram principle for every single rigid body. The desired joint resultant forces were calculated using the known generalized coordinates, GRFs and muscle forces as stated below:

$$\vec{R}_o = \begin{bmatrix} \vec{\tau}_o \\ \vec{F}_o \end{bmatrix} = M_i(\vec{q})\vec{a}_i + \vec{F}_{constraint} - \left(\sum \vec{F}_{external} + \sum \vec{F}_{muscles} + \vec{R}_{i+1}\right) \quad 3.25$$

where $\vec{\mathbf{R}}_0$ represents the joint forces and moments at the origin of body; $\mathbf{M}_i(\vec{q})$ represents the six-by-six mass matrix for body segment *i*; $\vec{\mathbf{a}}_i$ is the six-dimensional vector of known linear and angular acceleration of the body distal to joint *i*. $\vec{\mathbf{F}}_{constraint}$ expresses constraint forces applied to the body; $\vec{\mathbf{F}}_{external}$ and $\vec{\mathbf{F}}_{muscles}$ are the previously calculated forces and moments applied by external loads and musculotendon actuators, respectively; $\vec{\mathbf{R}}_{i+1}$ is the joint reaction force applied at the distal joint; $\vec{\boldsymbol{\tau}}_o$ and $\vec{\mathbf{F}}_o$ are the moment and force to balance the equation. Finally, the joint reaction forces and moments at the joint center were calculated by a shifting vector from body origin to center joint:

$$\vec{R}_i = \begin{bmatrix} \vec{\tau}_i \\ \vec{F}_i \end{bmatrix} := \begin{bmatrix} \vec{\tau}_o \\ \vec{F}_o \end{bmatrix} - \begin{bmatrix} \vec{r} \times \vec{F}_o \\ \vec{o} \end{bmatrix} \quad 3.26$$

where $\vec{\mathbf{r}}$ represents the vector from the body origin to the joint center.

The induced acceleration analysis approaches described in section 3.3.8 can also provide the calculation of the individual muscle contributions to joint contact forces. At each time step, muscle contributions to joint contact forces were obtained by i) using the results of muscle contribution to GRFs or acceleration; ii) remaining only the muscle interest and the corresponding muscle force and ground reaction forces in the model; and iii) solving joint contact force calculation described above. This procedure was repeated for each muscle throughout gait cycle (Sasaki and Neptune, 2010).

Chapter 4. Gait biomechanics in transfemoral amputees during: individual muscle contribution to COM acceleration

This chapter is based on the following published work:

- **Vahidreza Jafari Harandi,** David Charles Ackland, Raneem Haddara, L. Eduardo Cofré Lizama, Mark Graf, Mary Pauline Galea, Peter Vee Sin Lee – Gait compensatory mechanism in unilateral transfemoral amputees. *Medical Engineering and Physics*, Published.

4.1 Introduction

Transfemoral amputees have been shown to walk with 30% reduced speed and between 30 and 60% higher energy consumption than those of able-bodied individuals (Vaughan et al., 1992, Jaegers et al., 1995b, Boonstra et al., 1996, Genin et al., 2008). Increased hip joint range of motion and larger ground reaction forces (GRFs) during single-leg stance of the intact limb during walking have been observed relative to those of the residual limb (Sjödahl et al., 2002, Sjödahl et al., 2003, Goujon-Pillet et al., 2008, Schaarschmidt et al., 2012, de Cerqueira et al., 2013). The intact limb has also been shown to exhibit larger hip, knee and ankle joint moments and powers compared to those in the residual limb (Seroussi et al., 1996, Segal et al., 2006, Prinsen et al., 2011, Okita et al., 2018, Harandi et al., 2020, Robinson et al., 2020). These asymmetric gait patterns in transfemoral amputees have the potential to lead to an increased risk of lower back pain and hip osteoarthritis of the intact limb (Morgenroth et al., 2010, MPhty, 2012, Devan et al., 2014, Matsumoto et al., 2018).

In addition, about 30% of transfemoral amputees fitted with socket prosthesis experience severe socket related problems such as chronic skin pain (Rommers et al., 1996, Hagberg and Brånemark, 2001a, Meulenbelt et al., 2009, Butler et al., 2014), which leads to problems with mobility and a low quality of life (Pezzin et al., 2000, Demet et al., 2003, Pezzin et al., 2004b). Although new socket designs have improved walking, skin problems are still a major concern (Van de Meent et al., 2013). As a result, osseointegrated prosthesis have been sought as a way to combat these problems and have been recognized as the better alternative in some cases (Haggstrom et al., 2013, Pantall and Ewins, 2013, Van de Meent et al., 2013, Brånemark et al., 2014, Al Muderis et al., 2018, Frossard, 2019, Robinson et al., 2020). In contrast to SP users, there have only been a few studies that have investigated gait biomechanics in bone-anchored prostheses. Osseointegrated transfemoral amputees have shown greater hip range of motion, better walking ability, quicker cadence, shorter gait duration and increase in walking speed than SP users as well as slower cadence and larger gait period compared to non-amputees (Hagberg et al., 2005, Frossard et al., 2010, Tranberg et al., 2011, Van de Meent et al., 2013, Leijendekkers et al., 2017, Robinson et al., 2020). In addition, one study found that the function of the hip residual limb muscles was similar to those in non-disabled individuals (Pantall and Ewins, 2013).

Lower extremity muscles generate propulsion, support, and balance of the body during walking. Several studies investigating individual muscle contribution to the anterior-posterior, vertical and mediolateral acceleration of the body center of mass (COM) in able-bodied individuals (Neptune et al., 2001, Neptune et al., 2004, Liu et al., 2006, Pandy et al., 2010). In transfemoral amputees, a number of lower limb muscles required during ambulation may be missing in the residual limb, affecting the overall motor control strategy. Most notably, *vasti* (VAS), *soleus* (SOL) and *gastrocnemius* (GAS) are typically absent. In healthy individuals, VAS contributes to braking, while GAS and SOL generate forward propulsion (Lim et al., 2013, Lin et al., 2015). SOL and GAS contribute substantially to the vertical COM acceleration in the second half of stance, while VAS and the gluteus muscles generate body support in the first half of stance (Lim et al., 2013, Lin et al., 2015). Other muscles such as *hamstrings* (HAM) and the inferior compartment of adductor magnus may be re-anchored to the end of the residual limb, affecting their force-length properties. At present, the way in which muscles in the intact and residual limbs, and the transfemoral prosthesis, generate forward propulsion, vertical support, and mediolateral balance is not well understood.

The present study aimed to use three-dimensional personalized musculoskeletal modeling to quantify lower limb joint kinematics and kinetics as well as muscle and prosthesis contributions to body COM acceleration in the socket and osseointegrated fitted transfemoral amputees during walking. Previous studies have shown significant differences in spatiotemporal parameters, joint kinematics, and kinetics between the intact limb relative to that of the residual limb (Dumas et al., 2016, Ranz et al., 2017, Okita et al., 2018, Frossard, 2019). We, therefore, hypothesized that the contributions of the hip muscles in the intact limb to the fore-aft, vertical and mediolateral COM acceleration would be significantly different from that of the residual limb. The results of this study will provide new information about the gait compensatory mechanisms adopted by transfemoral amputees, which may assist in prescribing rehabilitation post-amputation.

4.2 Materials and Methods

The detail of materials and methods used in this study has been comprehensively discussed in Chapter 3. In this section, a brief explanation of the methods is presented. However, the relevant section in the methods chapter is mentioned to avoid repetition.

4.2.1 Participants

Gait experiments were performed on six individuals with unilateral transfemoral amputation wearing socket and four osseointegrated unilateral transfemoral amputees. All subjects wore their own prosthesis and were able to walk without assistive devices (Table 3.1, Table 3.2). The prostheses alignment and fitting were checked by an experienced prosthetist prior to data collection. Ethical approval was obtained by the Melbourne Health Human Research Ethics Committee with the number HREC 2015.148, and each participant provided written informed consent.

4.2.2 Testing protocol

Each subject performed three successful trials of over-ground walking at their preferred speed (1.16m/s±0.23 for SP users and 1.29m/s±0.10 for OI users). Lower limb and body COM kinematics were derived by tracking three-dimensional positions of reflective markers using an eight-camera motion capture system (Vicon, Oxford Metrics) sampling at 120 Hz. Retro-reflective markers were mounted bilaterally on body segments of the intact and residual limb following a previously published marker set (Dorn, 2011). On the prosthesis, the markers were mounted over anatomical landmarks based on the intact limb in the medial and lateral knee and ankle, heel, and toe. During walking trials, GRFs were measured using three AMTI force platforms embedded in the floor (Watertown, USA) at a sample rate of 1000 Hz. EMG data were simultaneously recorded at 1000 Hz using pairs of surface electrodes placed on the intact muscles including GMAX, GMED, SOL, GAS and VAS and residual limb muscles including GMAX and GMED (Cometa, Milan, Italy) (Table 3.5). EMG electrode placement followed a previously described procedure (Hermens et al., 2000), and EMG data were checked prior to testing to ensure suitable electrode placement and output (Hermens et al., 1999).

4.2.3 Data processing

Marker trajectories and GRF were low-pass filtered with a cut-off frequency of 4 and 60 Hz, respectively using a 4^{th} order Butterworth filter (Lin et al., 2015). EMG offset signals were removed and the waveforms rectified and low-pass filtered at 10 Hz using a 2^{nd} order Butterworth filter to create linear envelopes (Lin et al., 2015). Three successful gait cycles of each subject were selected and averaged for analyses.

4.2.4 Musculoskeletal modelling

Subject-specific three-dimensional musculoskeletal models of each subject were developed in OpenSim 3.2 (Delp et al., 2007). Each model comprised 10 lower limb and trunk segments actuated by 76 Hill-type muscle-tendon units. The head, arm, and torso were combined as a single rigid body that articulated with the pelvis via a ball-and-socket back joint. The hip joints were modeled as ball-and-socket joints, the knee and metatarsal joints as hinge joints, and each ankle-subtalar complex as a universal joint. All segment lengths and muscle-tendon parameters were scaled from a generic musculoskeletal model to the subject's mass and anthropometry. A static standing trial was used to calculate the scaling factors for each segment, as defined by the relative distances between pairs of markers (Delp et al., 2007).

For the prosthetic leg, all musculoskeletal structures below the knee were removed from the scaled model. A myodesis stabilization technique was employed in modeling muscle architecture, including re-anchoring of the amputated muscles in the residual limb (Ranz et al., 2017). The myodesis stabilization technique re-attaches muscles that were detached in the amputation process directly to the distal end of the residual femur (Ranz et al., 2017). Specifically, the adductor magnus, semimembranosus, semitendinosus, biceps femoris long head, and gracilis were inserted posteriorly to the medial ridge of linea aspera; *rectus femoris* and *sartorius* were inserted anteriorly to the distal part of an intertrochanteric line and medial ridge of linea aspera; *tensor fascia latae* was inserted laterally to lateral ridge of the linea aspera. In the model of the amputee, the tendon slack length of each reattached muscle in the residual limb was modified to ensure that the muscle-tendon unit tension in the neutral position was equivalent to that of the same muscle in the intact limb (Ranz et al., 2017, Harandi et al., 2020). Optimal fiber length value for each re-anchored muscle-tendon unit was varied in equal proportion to match the pre-operative muscle-tendon length of the intact in the neutral position

(Ranz et al., 2017, Harandi et al., 2020). The mass and dimensions (length, width, height) of the prosthesis knee joint, socket, pylon and foot segments were measured using digital calipers, tape measure and digital scales, and the prosthesis reverse-engineered in SolidWorks (SolidWorks, Dassault Systems Massachusetts, USA). Homogenous, isotropic material properties were assumed, and a residual limb density of 1.1 g/cm^3 was assumed (Mungiole and Martin, 1990, Ferris et al., 2017). The moment of inertia and COM positions of each lower-limb prosthesis were calculated from the CAD model and integrated into the musculoskeletal model (Harandi et al., 2020).

Joint angles were calculated using inverse kinematics, and joint moments computed from inverse dynamics using the joint kinematics and measured GRFs (Lu and O'connor, 1999). Residual Reduction Analysis was performed to vary the model's torso COM position and minimize dynamic inconsistency between the collected GRFs and the measured kinematics (Thelen and Anderson, 2006, Delp et al., 2007). Muscle forces were computed using static optimization by decomposing the net joint moments calculated from inverse dynamics into discrete muscle actuator loads (Anderson and Pandy, 2001b). The optimization problem minimized the sum of squares of all muscle activations and was constrained by each muscle's force-length and force-velocity relations. Contributions of muscle forces, gravity, inertia, and other external forces to the fore-aft, vertical and mediolateral COM acceleration represent the contribution to body propulsion, support and balance, respectively. Pseudo-inverse GRF decomposition method employing a five foot-ground contact point model for the stance limb was used to quantify the contributions to walking (Dorn et al., 2012a). The foot-ground contact model of the residual limb was assumed the same as that of the intact limb. In this thesis, N/BW and Nm/kg stand for "Newton per Body Weight" and "Newton-meter per kilogram", respectively.

4.2.5 Data analysis

Spatiotemporal parameters, kinematics, kinetics, muscle forces and muscle contributions to whole-body COM acceleration were evaluated during the stance phase of walking at four gait events which included ipsilateral heel-strike (IHS), contralateral toe-off (CTO), contralateral heel-strike (CHS) and ipsilateral toe-off (ITO). A non-parametric Wilcoxon signed-rank test was used to analyze non-normally distributed data. Comparisons of each dependent variable (i.e. joint angles and moments, muscle forces and muscle contribution) between the intact and residual limbs, were analyzed at each gait event and also during the whole stance phase. The results of the Wilcoxon were quantified by h-values, in which h=1 rejects the null hypothesis of no difference between the two legs, while h=0 accepts the null hypothesis. Significance level was set at $p<0.05$. All statistical analyses were performed using IBM-SPSS 24 (IBM Corp., USA).

4.3 Results

In this section, the results of both SP and OI users are separately presented. Then, a sensitivity analysis on alterations in inertial properties of prosthesis for one amputee is presented.

4.3.1 SP users

Significantly different spatiotemporal parameters were observed between the intact leg and the residual leg ($p<0.05$) (Table 4.1). Step length was significantly smaller in the intact limb compared to that of the residual limb (mean difference: 0.08±0.02 m, $p=0.03$). The step time for the residual limb was significantly greater than the intact limb (mean difference: 0.08±0.03 sec, *p*=0.03). The cadence of the intact limb was significantly larger than that of the residual limb (mean difference: 2.00±1.01 step/sec, *p*=0.04).

Table 4.1. Mean and standard deviation (SD) of spatiotemporal parameters in SP users (n=6) between the intact and residual limb.

	Limb	Mean	SD	*p* -value
Step Length (m)	Intact	0.68	0.15	0.03
	Residual	0.76	0.13	
Step Time (sec)	Intact	0.55	0.05	0.03
	Residual	0.63	0.08	
Cadence (step/sec)	Intact	100.33	9.45	0.04
	Residual	98.33	10.46	

Hip flexion was significantly greater in the intact leg compared to that in the residual limb at IHS (mean difference:10.51˚±5.29°, p = 0.03) and CTO (mean difference:17.11˚±7.10˚, p = 0.03). The hip of the intact limb also showed significantly greater ex- tension than that in the residual limb at CHS (mean differ- ence:10.10˚±2.01˚, p=0.03). Knee flexion of the intact leg was significantly greater than that in the residual limb at CTO (mean difference:21.51˚±4.60˚, p = 0.003). The intact limb also demonstrated significantly larger hip abduction than that in the residual limb at IHS (mean difference:5.13˚±0.2˚, p = 0.03), CTO (mean difference:8.64˚±0.39˚, p = 0.03), CHS (mean difference:4.05˚±0.5°, p = 0.03) and ITO (mean difference:13.80˚±0.37°, p = 0.03). There was a significant increase in anterior pelvic tilt towards the residual limb relative the intact limb at CTO (mean differ- ence:0.41˚±0.09°, p=0.03) and CHS (mean difference:6.1˚±2.1°, p = 0.03) (Table 4.2, Figure 4.1).

Table 4.2. The mean, standard deviation (SD), 95% confidence interval and p-value of the joint angles of the intact and residual legs during stance phase of SP users (n=6). Hip flexion and adduction, pelvis tilt and knee extension angles and ankle dorsiflexion are positive. IHS: ipsilateral heel strike; CTO: contralateral toe-off; CHS: contralateral heel strike; ITO: ipsilateral toe-off.

Joint angles (°)	Gait event	Limb	Mean	SD	95% Confidence Interval	*p-Value*
Hip flexion/ extension	IHS	Intact	29.41	8.06	17.74 to 36.46	0.03 *
		Residual	18.9	10.08	4.36 to 27.67	
	CTO	Intact	30.86	12.55	14.58 to 42.86	0.03 *
		Residual	13.73	12.08	-0.87 to 30.47	
	CHS	Intact	-20.38	3.82	-24.24 to -16.83	0.03 *
		Residual	-10.26	3.18	-13.90 to -5.86	
	ITO	Intact	-5.78	8.82	-14.74 to 8.25	0.06
		Residual	-10.31	6.24	-16.27 to 0.68	
Hip abduction/ adduction	IHS	Intact	-8.2	0.45	-8.67 to -7.74	0.03 *
		Residual	-3.07	0.1	-3.18 to -2.97	
	CTO	Intact	-7.3	0.72	-8.06 to -6.54	0.03 *
		Residual	1.34	0.63	0.67 to 2.01	
	CHS	Intact	3.74	0.87	2.82 to 4.66	0.03 *
		Residual	-0.31	0.84	-1.19 to 0.57	
	ITO	Intact	-11.04	0.9	-11.98 to -10.09	0.03 *
		Residual	-2.75	0.06	-2.81 to -2.68	
Knee flexion/ extension	IHS	Intact	-7.28	3.89	-10.27 to -0.90	0.31
		Residual	-4.5	4.52	-9.10 to 3.11	
	CTO	Intact	-28.26	10.01	-39.67 to -12.97	0.03 *
		Residual	-6.71	5.31	-11.96 to 2.23	
	CHS	Intact	-15.39	4.39	-22.90 to -11.05	0.06
		Residual	-8.14	3.4	-11.70 to -2.55	
	ITO	Intact	-44.16	5.86	-53.97 to -35.89	0.09
		Residual	-34.4	4.5	-41.36 to -27.86	
Pelvis tilt	IHS	Intact	-1.47	3.15	-5.84 to 2.90	0.65
		Residual	-0.044	2.17	-3.21 to 2.26	
	CTO	Intact	0.29	2.8	-3.67 to 4.24	0.03 *
		Residual	0.71	1.72	-1.20 to 3.60	
	CHS	Intact	-1.57	2.71	-5.43 to 2.29	0.03 *
		Residual	4.54	3.01	-0.87 to 7.87	
	ITO	Intact	-0.94	3.21	-5.37 to 3.50	0.12
		Residual	1.42	5.57	-6.18 to 7.81	
Ankle dorsiflexion	IHS	Intact	-2.7	12.16	-21.39 to 12.76	0.09
		Residual	-6.1	8.51	-18.40 to 5.65	
	CTO	Intact	-10.93	13.9	-32.83 to 5.95	0.81
		Residual	-11.93	8	-24.50 to -2.18	
	CHS	Intact	-1.96	16.13	-22.21 to 23.03	0.31
		Residual	4.3	6.2	-3.56 to 13.83	
	ITO	Intact	-29.44	15.5	-51.01 to -7.15	0.03 *
		Residual	-6.95	7.73	-18.65 to 3.13	

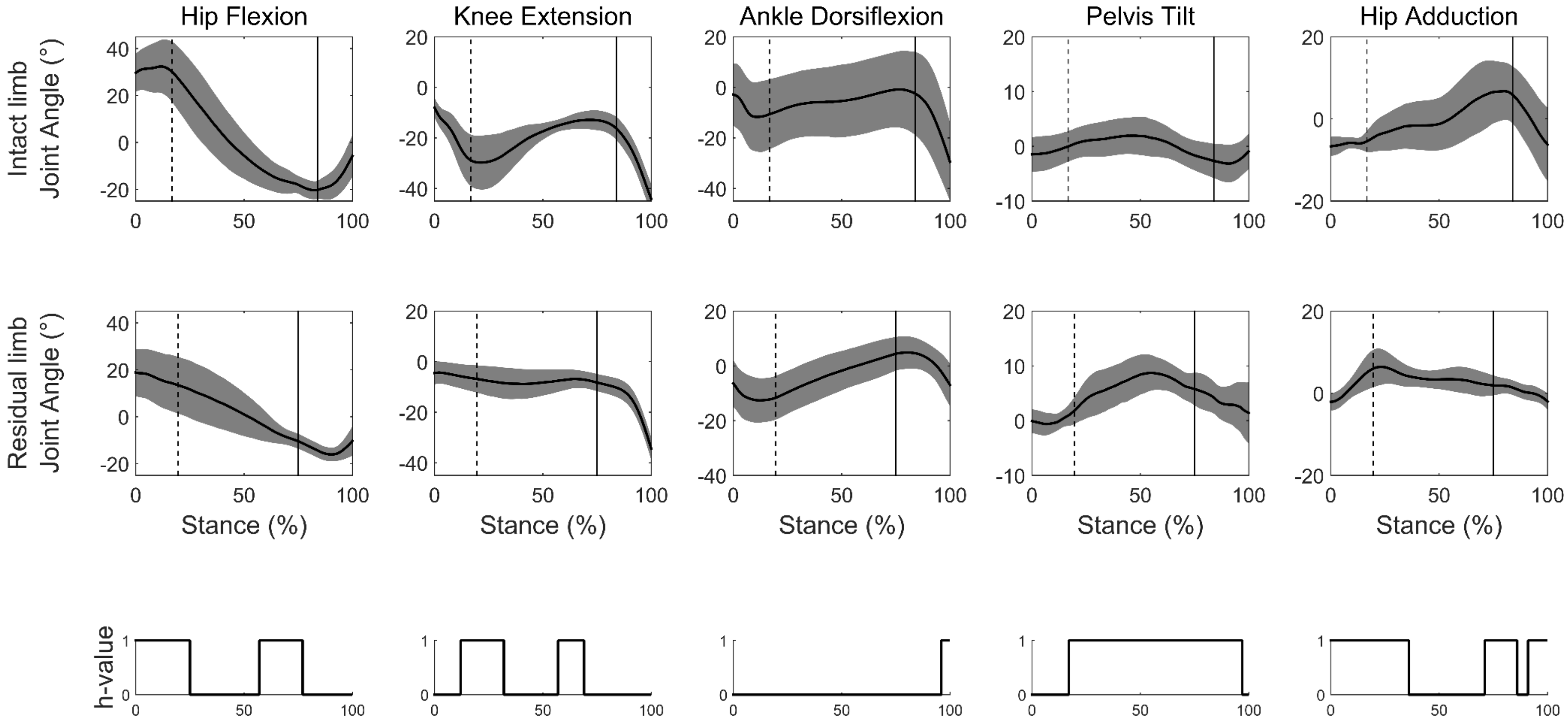

Figure 4.1. Joint angles in the intact and residual limb of transfemoral amputees (n=6). The gray shaded areas represent ±1 standard deviation from the mean. The vertical dashed line represents contralateral toe-off (CTO); the vertical solid line represents contralateral heel strike (CHS). Statistical analyses obtained between the two legs are demonstrated by h = 1 in the h-value plots.

There were significant differences in the joint moments at hip, knee, and ankle joints between the residual and intact limbs (Table 4.3, Figure 4.2) (p<0.05). The hip flexion moment of the residual limb was significantly smaller compared to that in the intact leg at IHS (mean difference:0.41 ±0.05Nm/kg, p = 0.03) and CHS (mean difference:0.39 ±0.09Nm/kg, p = 0.03). Further- more, significantly different hip muscle forces were found be- tween the two legs (Table 4.4, Figure 4.3). For instance, GMED in the intact limb exhibited larger force than GMED in the residual limb at IHS (mean difference:1.14 ±0.72 N/kg, p = 0.03), CTO (mean difference:18.45 ±2.58 N/kg, p = 0.03) and CHS (mean difference:13.83 ±1.16 N/kg, p = 0.03).

Table 4.3. The mean, standard deviation (SD), 95% confidence interval and p-value of the joint moments of the intact and residual legs during stance phase for SP users (n=6). Hip flexion, knee extension and ankle dorsiflexion moments are positive. IHS: ipsilateral heel strike; CTO: contralateral toe-off; CHS: contralateral heel strike; ITO: ipsilateral toe-off.

Joint moments (Nm/kg)	Gait event	Limb	Mean	SD	95% Confidence Intacterval	*p-Value*
Hip flexion/ extension	IHS	Intact	0.43	0.09	0.33 to 0.53	0.03 *
		Residual	-0.02	0.07	-0.10 to 0.06	
	CTO	Intact	-0.89	0.34	-1.25 to -0.53	0.16
		Residual	-0.69	0.38	-1.10 to -0.28	
	CHS	Intact	0.58	0.09	0.49 to 0.68	0.03 *
		Residual	0.19	0.19	-0.01 to 0.39	
	ITO	Intact	0.23	0.26	-0.03 to 0.51	0.84
		Residual	0.13	0.14	-0.01 to 0.27	
Knee flexion/ extension	IHS	Intact	-0.005	0.18	-0.20 to 0.19	0.69
		Residual	-0.02	0.13	-0.15 to 0.11	
	CTO	Intact	0.81	0.43	0.36 to 1.27	0.03 *
		Residual	-0.04	0.13	-0.18 to 0.09	
	CHS	Intact	-0.06	0.16	-0.24 to 0.10	0.31
		Residual	-0.19	0.13	-0.33 to -0.05	
	ITO	Intact	-0.02	0.03	-0.06 to 0.01	0.43
		Residual	0.03	0.12	-0.10 to 0.16	
Ankle dorsiflexion	IHS	Intact	0.01	0.007	0.004 to 0.02	0.16
		Residual	0.05	0.04	0.01 to 0.09	
	CTO	Intact	0.28	0.1	0.17 to 0.38	0.84
		Residual	0.28	0.1	0.17 to 0.38	
	CHS	Intact	-1.46	0.08	-1.54 to -1.37	0.03 *
		Residual	-1.09	0.23	-1.34 to -0.85	
	ITO	Intact	0.03	0.002	0.03 to 0.03	0.16
		Residual	0.002	0.03	-0.04 to 0.04	

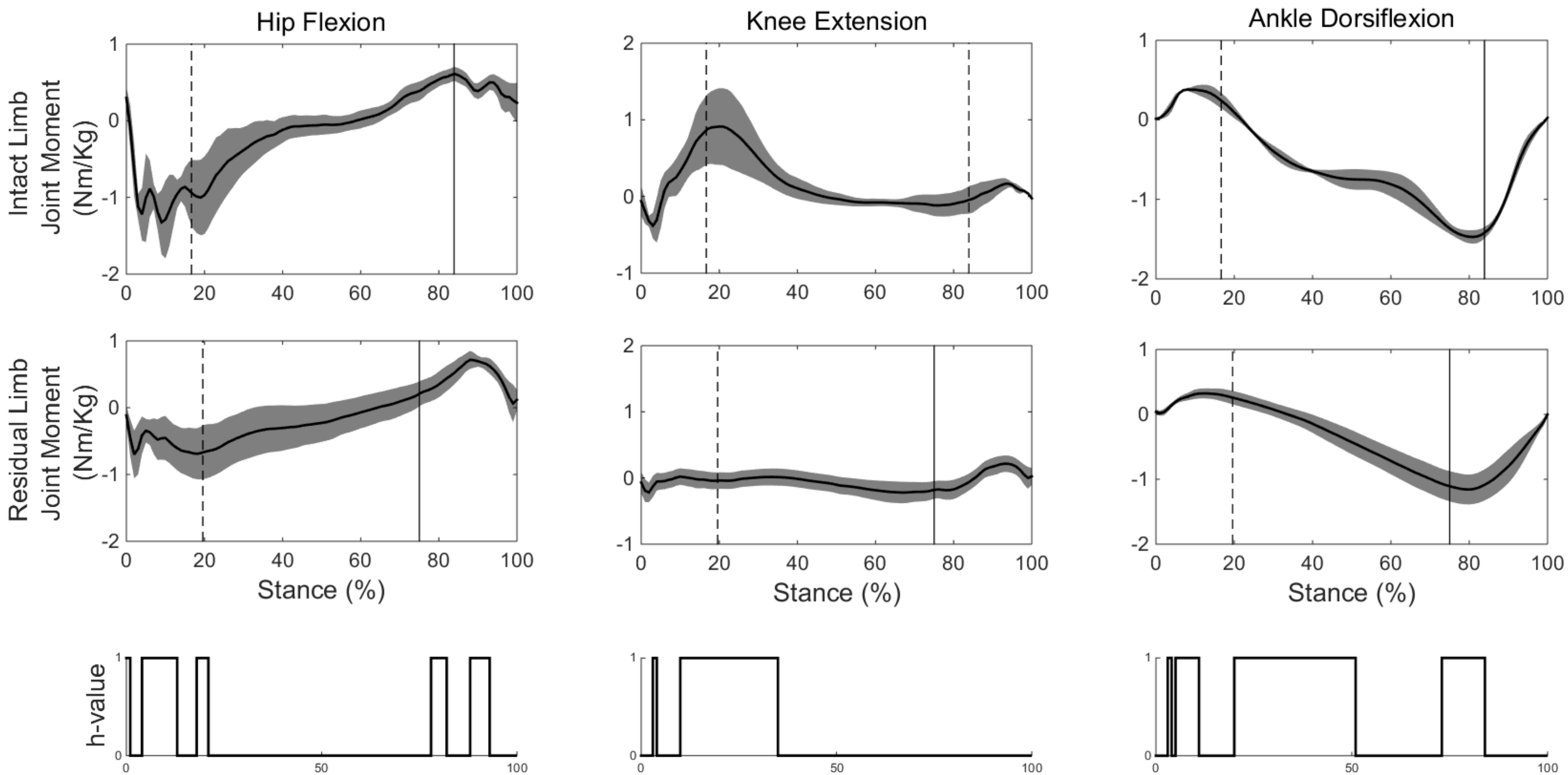

Figure 4.2. Joint moments in the intact and residual limb of transfemoral amputees (n=6). The gray shaded areas represent ±1 standard deviation from the mean. The vertical dashed line represents contralateral toe-off (CTO); the vertical solid line represents contralateral heel strike (CHS). Statistical analyses obtained between the two legs are demonstrated by h = 1 in the h-value plots.

As described in section 3.3.7, we used EMG signals to evaluate the onset and offset of the subject-specific model-predicted muscle forces. The timing of muscle contractions predicted by the model was correlated well with the EMG signals (Figure 4.3, Figure 4.4).

The results showed that in general, the intact limb hip muscles generated more forces during the whole stance than the residual limb (Table 4.4, Figure 4.3). GMAX force was significantly greater in the intact limb than the residual limb at CTO (mean difference: 1.74 N/kg, p=0.03). GMED of the intact limb was significantly greater at IHS, CTO and CHS than the residual limb (mean difference: 0.14, 18.45 and 13.83 N/kg, respectively, p=0.03). The intact limb IL had also significantly greater forces in the intact limb than the residual limb at IHS and CHS (mean difference: 2.83 and 9.33 N/kg, respectively, p=0.03). HAM demonstrated greater forces at ITO of the intact limb than the residual limb (mean difference: 2.83 N/kg, p=0.03) (Table 4.4, Figure 4.3). Figure 4.4 shows muscle forces of the intact limb for SOL, GAS, and VAS with the period of EMG activity recorded for the specific muscles.

Table 4.4. Mean, standard deviation (SD), 95% confidence interval and p-value of the muscle forces of the intact and residual legs during stance phase for SP users (n=6). IHS: ipsilateral heel strike; CTO: contralateral toe-off; CHS: contralateral heel strike; ITO: ipsilateral toe-off.

Muscle forces (N/kg)	Gait event	Limb	Mean	SD	95% Confidence Intacterval	*p-Value*
GMAX	IHS	Intact	0.52	0.36	0.14 to 0.90	0.03 *
		Residual	1.2	0.61	0.56 to 1.84	
	CTO	Intact	6.91	1.83	5.00 to 8.83	0.03 *
		Residual	4.17	1.33	2.77 to 5.57	
	CHS	Intact	0.04	0.04	0.01 to 0.08	0.03 *
		Residual	0.41	0.13	0.27 to 0.55	
	ITO	Intact	0.17	0.22	0.07 to 0.41	0.87
		Residual	0.2	0.12	0.07 to 0.32	
GMED	IHS	Intact	2.81	1.75	0.97 to 4.65	0.03 *
		Residual	1.67	0.30	1.36 to 1.98	
	CTO	Intact	22.72	6.07	16.34 to 29.09	0.03 *
		Residual	4.27	1.79	2.39 to 6.16	
	CHS	Intact	17.22	2.83	14.25 to 20.19	0.03 *
		Residual	3.39	0.25	3.13 to 3.65	
	ITO	Intact	0.71	0.65	0.03 to 1.39	0.17
		Residual	0.44	0.38	0.03 to 0.84	
IL	IHS	Intact	2.89	0.77	2.07 to 3.69	0.03 *
		Residual	0.06	0.068	0.00 to 0.13	
	CTO	Intact	0.001	0.001	0.00 to 0.002	0.03 *
		Residual	0.19	0.22	0.00 to 0.42	
	CHS	Intact	14.61	1.30	13.24 to 15.97	0.03 *
		Residual	5.28	3.66	1.44 to 9.11	
	ITO	Intact	3.14	1.46	1.60 to 4.68	0.09
		Residual	1.67	1.91	0.00 to 3.84	
RF	IHS	Intact	0.69	0.85	0.00 to 2.09	0.31
		Residual	0.08	0.12	0.00 to 0.27	
	CTO	Intact	0.001	0.05	0.00 to 0.01	0.06
		Residual	0.53	0.37	0.14 to 0.91	
	CHS	Intact	6.96	2.61	4.22 to 9.71	0.06
		Residual	4.14	1.50	2.56 to 5.70	
	ITO	Intact	1.83	1.30	0.47 to 3.19	0.09
		Residual	0.61	0.29	0.31 to 0.91	
HAM	IHS	Intact	0.02	0.01	0.00 to 0.06	0.03 *
		Residual	2.01	0.28	1.28 to 2.72	
	CTO	Intact	3.21	0.23	2.61 to 3.82	0.6
		Residual	2.65	0.74	0.76 to 4.54	
	CHS	Intact	0.02	0.01	0.00 to 0.06	0.9
		Residual	0.004	0.001	0.001 to 0.006	
	ITO	Intact	0.52	0.04	0.40 to 0.63	0.03 *
		Residual	0.01	0.001	0.005 to 0.01	

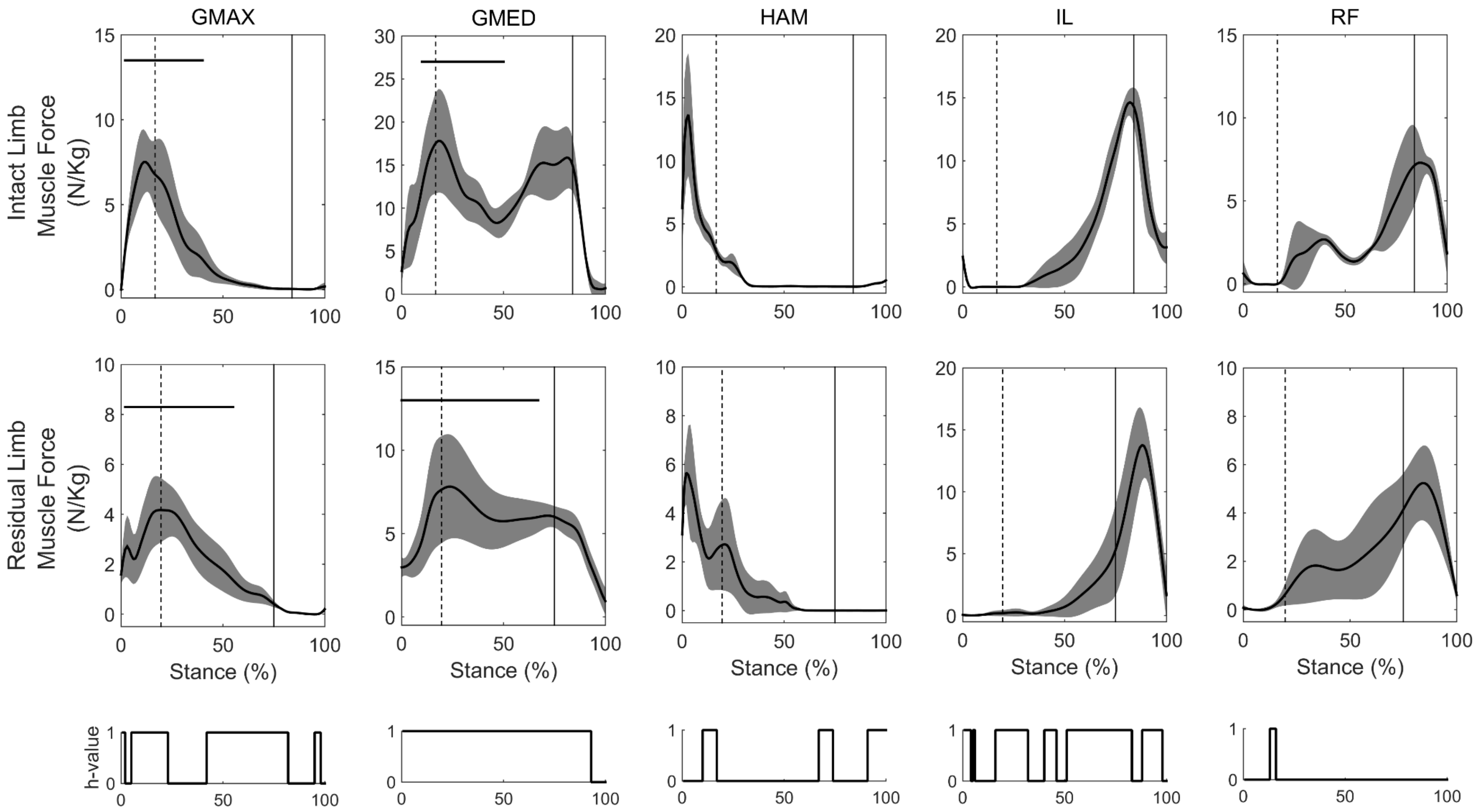

Figure 4.3. Forces of muscles in the intact and residual limb of transfemoral amputees (n=6). The gray shaded areas represent ±1 standard deviation from the mean. The vertical dashed line represents contralateral toe-off (CTO); the vertical solid line represents contralateral heel strike (CHS). The horizontal solid line indicates the period of EMG activity recorded for muscles. Statistical analyses obtained between the two legs are demonstrated by h = 1 in the h-value plots.

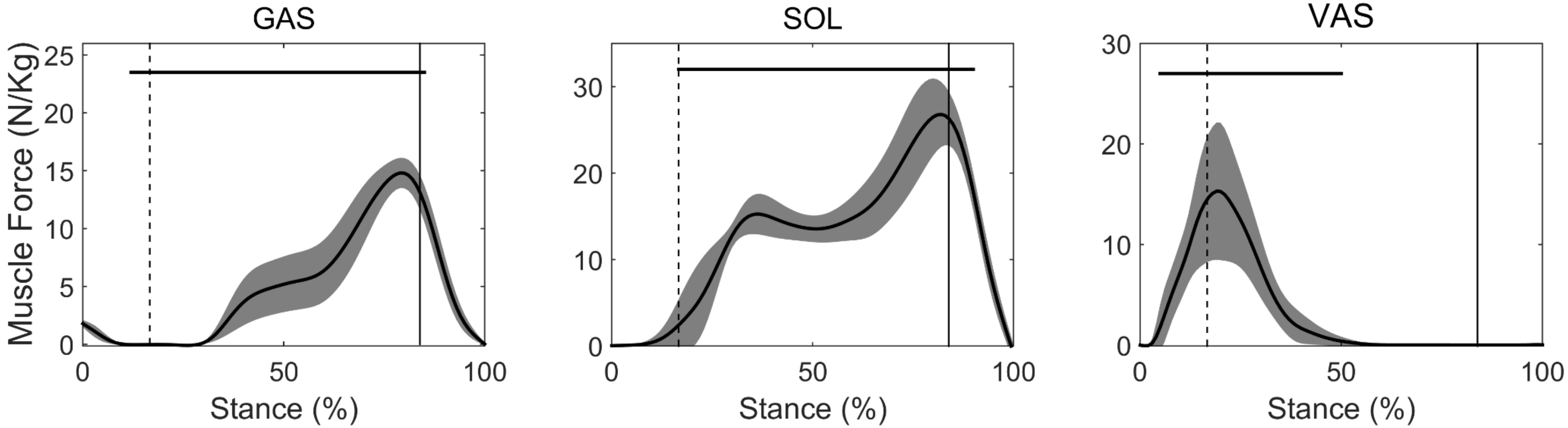

Figure 4.4. Forces of muscles in the below-knee of the intact of SP users (n=6). The gray shaded areas represent ±1 standard deviation from the mean. The horizontal black line indicates the activity time of the muscles. The vertical dashed line represents contralateral toe-off (CTO); The vertical solid line represents contralateral heel strike (CHS). The horizontal solid line indicates the period of EMG activity recorded for muscles.

RF showed larger contribution to the fore-aft body COM acceleration in the intact limb than that in the residual limb at CTO (mean difference: -0.02 m/s^2, p=0.04) and CHS (mean difference: -0.38 m/s^2, p=0.03), while the contribution of the intact limb GMAX was larger at IHS (mean difference: -0.07 m/s^2, p=0.03) and during mid-stance when compared to the residual limb. In addition, HAM generated higher contribution at IHS (mean difference: 0.07 m/s^2, p=0.04), CHS (mean difference: 0.16 m/s^2, p=0.04) and ITO (mean difference: 0.15 m/s^2, p=0.03) in the intact leg than the residual limb (Table 4.5, Figure 4.5). In early to mid-stance, VAS in the intact limb contributed substantially to breaking, while SOL and GAS contributed to both breaking and propulsion during the second half of stance. In the residual limb, the prosthesis contributed primarily to braking and propulsion in the first and second half of stance, respectively (Figure 4.5).

The prosthesis generated the greatest amount of support throughout stance compared to any residual limb muscle, while the intact leg's SOL, GAS and VAS provided most of the contribution to support than other intact limb’s muscles (Figure 4.5). In early to mid-stance and pre-swing, GMED produced a greater contribution to the vertical COM acceleration in the intact leg than the residual leg at CTO (mean difference: 0.70 m/s^2, p=0.02) and ITO (mean difference: 0.05 m/s^2, p=0.02). GMAX showed higher contribution to the vertical acceleration of the COM than that of the residual limb at IHS (mean difference: 0.25 m/s^2, p=0.02) and CTO (mean difference: 0.64 m/s^2, p=0.04) (Table 4.5, Figure 4.5).

GMED was the largest contributor to mediolateral COM acceleration and it also contributed to medial COM acceleration during the whole of stance. The peak contribution of GMED to mediolateral COM acceleration was significantly higher in the intact leg than the residual leg at IHS (mean difference: 0.10 m/s^2, p=0.04), CTO (mean difference: 1.00 m/s^2, p=0.02), CHS (mean difference: 0.30 m/s^2, p=0.02) and ITO (mean difference: 0.02 m/s^2, p=0.04). GMAX in the residual leg contributed to medial COM acceleration, whereas GMAX in the intact limb generated lateral COM acceleration, with significant differences at IHS (mean difference: 0.01 m/s^2, p=0.03), CTO (mean difference: 0.15 m/s^2, p=0.03), CHS (mean difference: 0.02 m/s^2, p=0.03) and ITO (mean difference: 0.02 m/s^2, p=0.03). VAS, SOL and GAS of the intact limb contributed to medial acceleration of the COM. Conversely, the prosthesis contributed to lateral body COM acceleration during stance (Table 4.5, Figure 4.6).

Table 4.5. The *p*-value of the muscle contribution to the COM acceleration during stance phase of SP users (n=6) between the intact and the residual limb at four gait events including IHS: ipsilateral heel strike; CTO: contralateral toe-off; CHS: contralateral heel strike; ITO: ipsilateral toe-off.

	Muscle	IHS	CTO	CHS	ITO
Muscle contribution to fore-aft COM acceleration	ALAM	0.69	0.03 *	0.03 *	0.09
	GMAX	0.03 *	0.09	0.31	0.84
	GMED	0.09	0.69	0.84	0.69
	HAM	0.22	0.92	0.03 *	0.06
	IL	0.03 *	0.09	0.03 *	0.09
	RF	0.22	0.06	0.03 *	0.31
Muscle contribution to vertical COM acceleration	ALAM	0.91	0.03 *	0.03 *	0.84
	GMAX	0.03 *	0.06	0.06	0.09
	GMED	0.69	0.03 *	0.69	0.03 *
	HAM	0.31	0.84	0.09	0.03 *
	IL	0.03 *	0.92	0.03 *	0.09
	RF	0.31	0.09	0.03 *	0.06
Muscle contribution to mediolateral COM acceleration	ALAM	0.06	0.03 *	0.03 *	0.03 *
	GMAX	0.06	0.03 *	0.03 *	0.03 *
	GMED	0.06	0.03 *	0.03 *	0.06
	HAM	0.06	0.22	0.06	0.93
	IL	0.03 *	0.03 *	0.03 *	0.03 *
	RF	0.03 *	0.43	0.31	0.84

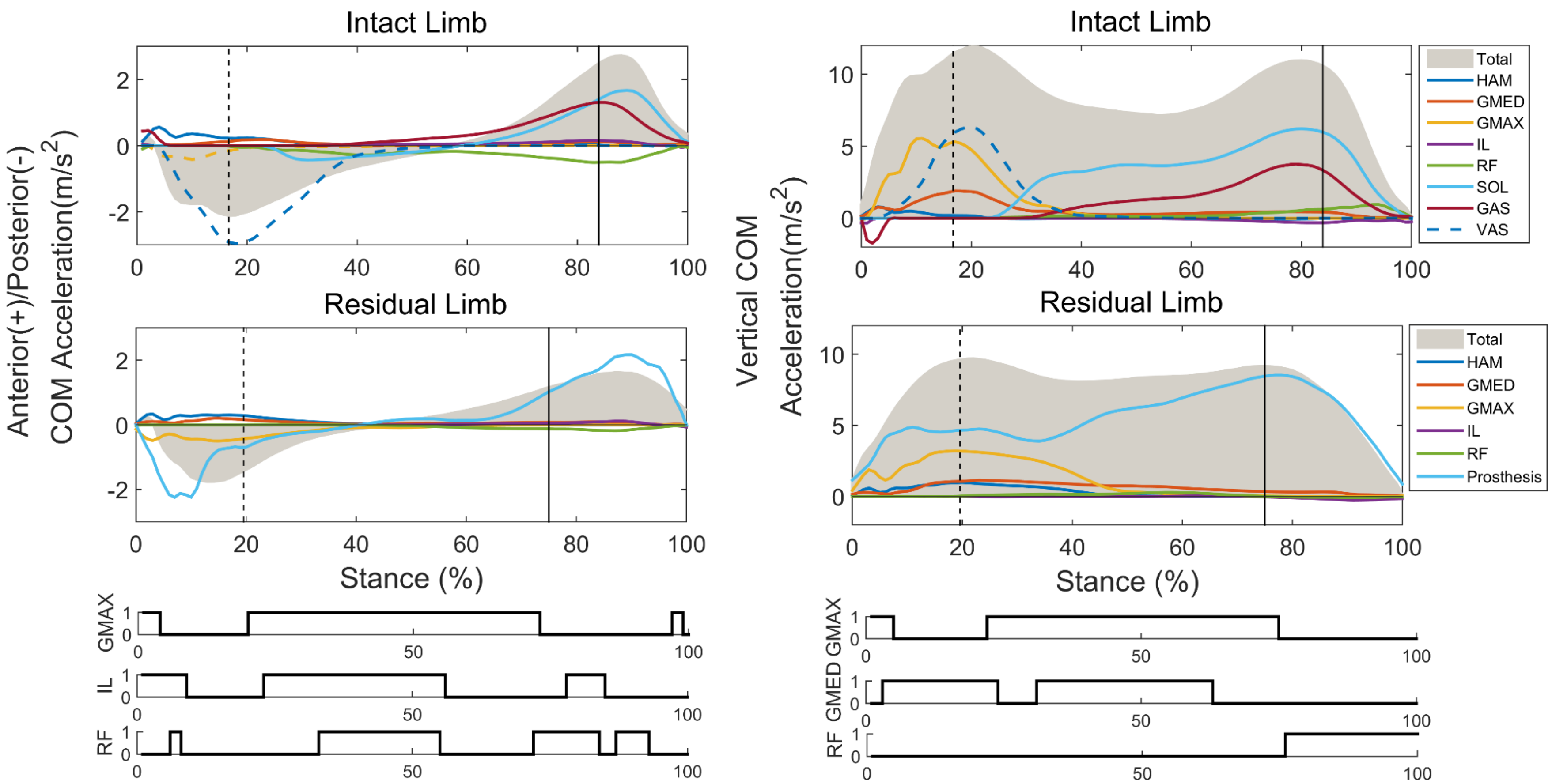

Figure 4.5. Individual muscle and prosthesis contribution to anterior-posterior and vertical COM acceleration in transfemoral amputees (n=6). The shaded area represents the summed contribution from all actuators. The vertical dashed line represents contralateral toe-off (CTO); the vertical solid line represents contralateral heel strike (CHS). Statistical analyses obtained between the two legs are demonstrated by h = 1 in the h-value plots.

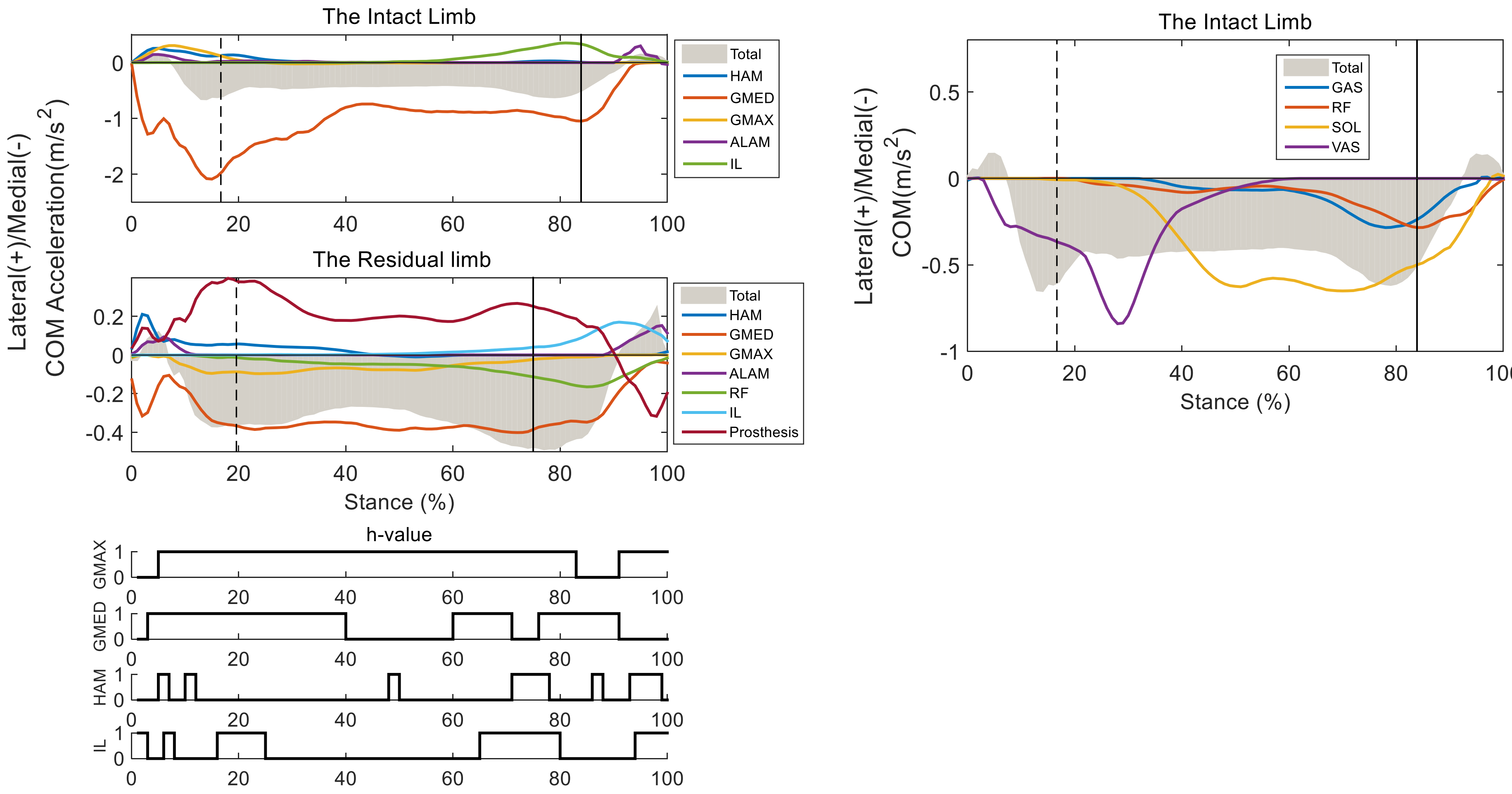

Figure 4.6. Individual muscle and prosthesis contribution to mediolateral COM acceleration in transfemoral amputees (n=6). The shaded area represents the summed contribution from all actuators. The vertical dashed line represents contralateral toe-off (CTO); the vertical solid line represents contralateral heel strike (CHS). Statistical analyses obtained between the two legs are demonstrated by h = 1 in the h-value plots.

4.3.2 OI users

The step time of the intact limb was lower than the residual limb (mean difference: 0.01sec, respectively). The cadence and stride length of the intact limb was slightly greater than the residual limb (mean difference: 0.05 steps/sec and 0.01 m) (Table 4.6).

Table 4.6. Mean and standard deviation (SD) of spatiotemporal parameters in OI users between the intact and residual limb of OI users (n=4).

	Limb	Mean	SD
Step Length (m)	Intact	0.80	0.02
	Residual	0.79	0.02
Step Time (sec)	Intact	0.52	0.02
	Residual	0.53	0.01
Cadence (step/sec)	Intact	110.67	3.05
	Residual	110.00	2.46

The intact limb flexed hip less compared to the residual limb at CTO (mean difference: 5.27˚). The intact limb knee flexion was greater than the residual limb at CTO (mean difference: 3.20˚) and CHS (mean difference: 7.90˚) (Table 4.7, Figure 4.7).

The hip moment depicted greater flexion at IHS (mean difference: 0.20 Nm/kg) and ITO (mean difference: 0.36 Nm/kg) than the residual limb, whereas the hip extension moment of the residual limb was larger than the intact limb at CTO (mean difference: 0.15 Nm/kg) and CHS (mean difference: 0.05 Nm/kg). The intact knee also generated larger peak moment at CTO (mean difference: 0.40 Nm/kg) than that in the residual limb (Table 4.8, Figure 4.7).

Table 4.7. The mean, standard deviation (SD) and 95% confidence interval of the joint angles of the intact and residual legs during stance phase of OI users (n=4). Hip flexion and adduction, and knee extension angles and ankle dorsiflexion are positive. IHS: ipsilateral heel strike; CTO: contralateral toe-off; CHS: contralateral heel strike; ITO: ipsilateral toe-off.

Joint angles (°)	Gait event	Limb	Mean	SD	95% Confidence Interval
Hip flexion/ extension	IHS	Intact	25.11	2.65	23.13 to 27.08
		Residual	29.37	3.85	26.48 to 32.26
	CTO	Intact	22.22	2.73	19.89 to 24.52
		Residual	27.49	4.69	22.90 to 30.07
	CHS	Intact	-19.51	3.43	-21.33 to -16.22
		Residual	-16.79	3.65	-21.10 to -14.30
	ITO	Intact	-1.89	2.01	-4.23 to 1.65
		Residual	-1.83	3.62	-1.97 to 2.20
Hip abduction/ adduction	IHS	Intact	3.25	0.11	3.01 to 3.65
		Residual	2.63	0.15	2.18 to 3.08
	CTO	Intact	10.06	1.23	9.21 to 11.14
		Residual	7.26	1.27	6.39 to 8.14
	CHS	Intact	9.42	1.11	8.02 to 10.82
		Residual	6.96	0.46	6.11 to 7.42
	ITO	Intact	1.97	0.65	1.22 to 2.45
		Residual	1.65	0.23	1.51 to 1.83
Knee flexion/ extension	IHS	Intact	-9.81	2.65	-11.79 to -7.85
		Residual	-8.89	2.47	-9.97 to -6.78
	CTO	Intact	-20.24	4.25	-23.43 to -18.72
		Residual	-17.04	3.45	-21.22 to -15.25
	CHS	Intact	-11.03	2.66	-13.19 to -9.29
		Residual	-4.18	0.85	-4.64 to -3.23
	ITO	Intact	-41.67	4.45	-45.27 to -38.05
		Residual	-39.89	1.03	-40.44 to -38.09
Ankle dorsiflexion	IHS	Intact	8.39	1.67	6.28 to 10.49
		Residual	-1.27	0.12	-1.78 to -1.02
	CTO	Intact	-1.57	2.66	-3.87 to 0.07
		Residual	-0.25	2.03	-2.10 to 1.43
	CHS	Intact	8.79	1.45	7.34 to 10.23
		Residual	9.11	1.14	7.53 to 9.98
	ITO	Intact	-21.05	3.59	-25.12 to -18.97
		Residual	-0.51	0.91	-1.62 to 0.36

Table 4.8. The mean, standard deviation (SD) and 95% confidence interval of the joint moments of the intact and residual legs during stance phase of OI users (n=4). Hip flexion, knee extension and ankle dorsiflexion moments are positive. IHS: ipsilateral heel strike; CTO: contralateral toe-off; CHS: contralateral heel strike; ITO: ipsilateral toe-off.

Joint moment (Nm/kg)	Gait event	Limb	Mean	SD	95% Confidence Interval
Hip flexion/ extension	IHS	Intact	0.22	0.19	-0.41 to 0.83
		Residual	0.02	0.09	-0.27 to 0.27
	CTO	Intact	-1.01	0.08	-1.27 to -0.75
		Residual	-1.16	0.07	-1.37 to -0.96
	CHS	Intact	0.46	0.08	0.18 to 0.69
		Residual	0.51	0.04	0.37 to 0.65
	ITO	Intact	0.39	0.08	0.14 to 0.65
		Residual	0.03	0.06	-0.17 to 0.23
Knee flexion/ extension	IHS	Intact	0.01	0.05	-0.15 to 0.16
		Residual	-0.05	0.03	-0.15 to 0.04
	CTO	Intact	0.44	0.03	0.33 to 0.55
		Residual	0.01	0.03	-0.10 to 0.09
	CHS	Intact	-0.24	0.04	-0.36 to -0.12
		Residual	-0.25	0.03	-0.35 to -0.15
	ITO	Intact	0.17	0.02	0.01 to 0.08
		Residual	0.05	0.03	0.01 to 0.07
Ankle dorsiflexion	IHS	Intact	0.04	0.01	0.02 to 0.06
		Residual	0.01	0.01	-0.01 to 0.02
	CTO	Intact	0.14	0.05	-0.03 to 0.31
		Residual	-0.13	0.02	-0.21 to -0.06
	CHS	Intact	-1.34	0.02	-1.40 to -1.27
		Residual	-1.39	0.02	-1.45 to -1.30
	ITO	Intact	0.04	0.01	0.02 to 0.05
		Residual	-0.06	0.04	-0.18 to 0.05

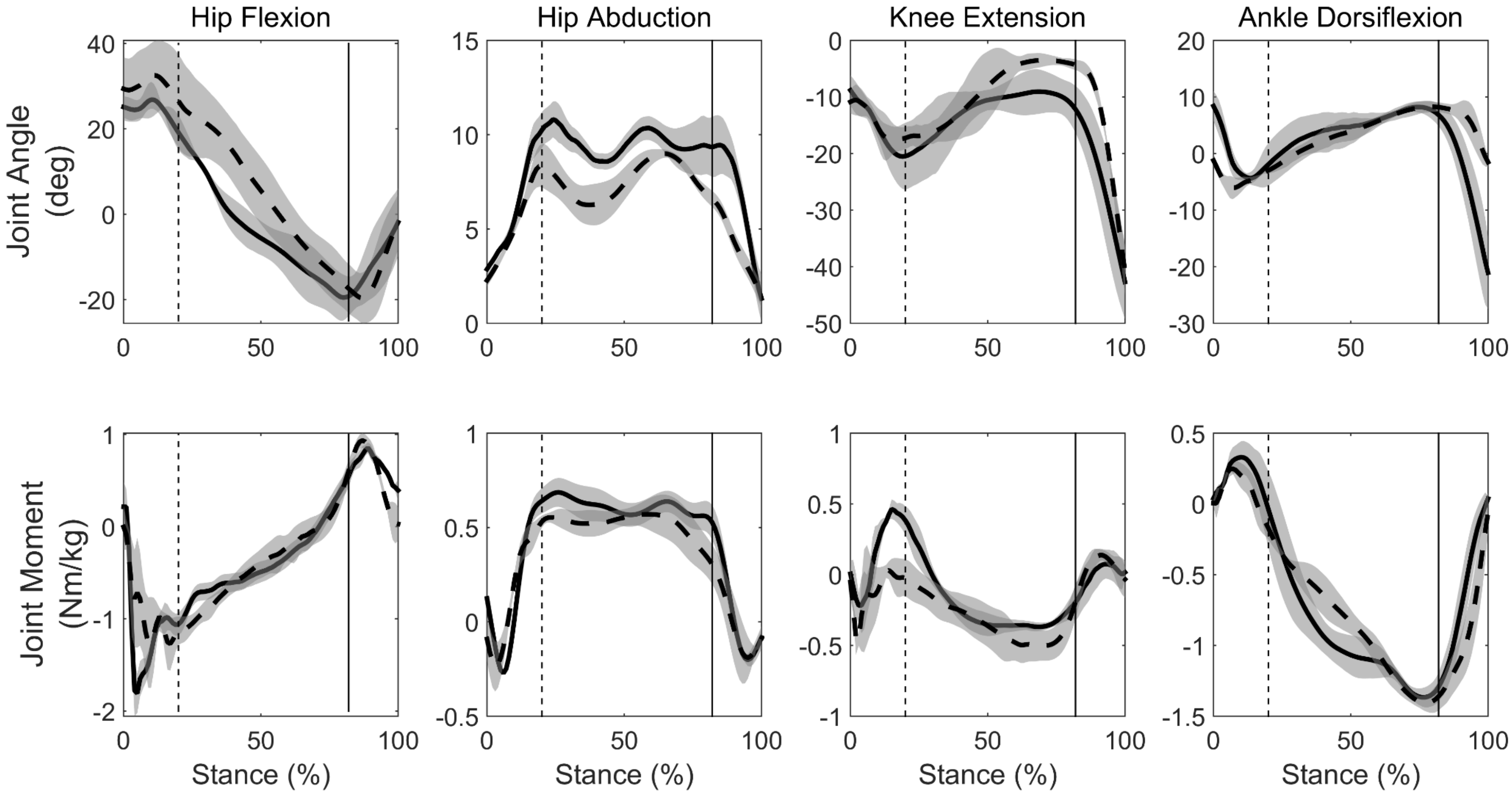

Figure 4.7. Joint angles and moments of the intact (solid line) and residual (dashed line) limbs of OI users (n=4). The gray shaded areas represent ±1 standard deviation from the mean. The vertical dashed line represents contralateral toe-off (CTO); the vertical solid line represents contralateral heel strike (CHS).

Similar to SP users model validation, the timing of muscle contractions predicted by the model for OI users was similar to those exhibited by EMG signals (Figure 4.8, Figure 4.9).

Peak muscle forces of the intact limb were greater than those in the residual limb for GMED (mean difference: 5.53 N/kg), IL (mean difference: 1.0 N/kg) and HAM (mean difference: 2.09 N/kg). The intact limb's peak force of GMAX (mean difference: 0.30 N/kg) was smaller than the residual limb, while the peak of RF forces of the intact limb was greater compared to the residual limb during the first and the second half of stance (mean difference: 9.52 and 0.37 N/kg, respectively) (Table 4.9, Figure 4.8).

Table 4.9. The mean, standard deviation (SD) and 95% confidence interval of the muscle forces of the intact and residual legs during stance phase of OI users (n=4). IHS: ipsilateral heel strike; CTO: contralateral toe-off; CHS: contralateral heel strike; ITO: ipsilateral toe-off.

Muscle forces (N/kg)	Gait event	Limb	Mean	SD	95% Confidence Interval
GMAX	IHS	Intact	0.29	0.12	0.09 to 0.67
		Residual	1.11	0.33	0.07 to 2.15
	CTO	Intact	8.53	0.46	7.05 to 10.02
		Residual	8.59	0.13	8.19 to 9.01
	CHS	Intact	0.02	0.15	0.00 to 0.07
		Residual	0.07	0.03	0.00 to 0.16
	ITO	Intact	0.01	0.01	0.00 to 0.01
		Residual	0.73	0.29	0.00 to 1.67
GMED	IHS	Intact	3.46	0.54	1.74 to 5.20
		Residual	3.11	0.51	1.51 to 4.69
	CTO	Intact	20.67	2.44	17.10 to 25.25
		Residual	17.89	0.33	16.85 to 18.92
	CHS	Intact	8.89	2.77	0.08 to 17.69
		Residual	5.52	0.09	5.22 to 5.82
	ITO	Intact	1.01	0.45	0.09 to 1.90
		Residual	0.27	0.15	0.11 to 0.44
IL	IHS	Intact	2.19	0.91	0.00 to 5.05
		Residual	0.17	0.12	0.00 to 0.55
	CTO	Intact	<0.01	<0.01	<0.01
		Residual	<0.01	<0.01	<0.01
	CHS	Intact	14.51	1.86	8.59 to 20.41
		Residual	10.66	0.43	9.38 to 11.95
	ITO	Intact	1.95	0.71	0.00 to 3.21
		Residual	0.62	0.51	0.00 to 1.25
RF	IHS	Intact	<0.01	<0.01	<0.01
		Residual	0.04	0.02	0.00 to 0.06
	CTO	Intact	2.86	0.12	2.48 to 3.23
		Residual	<0.01	<0.01	<0.01
	CHS	Intact	9.17	0.41	7.87 to 10.47
		Residual	8.84	0.21	8.19 to 9.51
	ITO	Intact	4.01	0.23	3.28 to 4.71
		Residual	1.05	0.14	1.25 to 0.89
HAM	IHS	Intact	0.44	0.27	0.00 to 1.31
		Residual	1.28	0.25	0.97 to 1.49
	CTO	Intact	1.11	0.36	0.00 to 1.45
		Residual	7.63	1.24	6.23 to 8.89
	CHS	Intact	0.03	0.02	0.00 to 0.10
		Residual	<0.01	<0.01	<0.01
	ITO	Intact	0.16	0.01	0.00 to 0.03
		Residual	0.73	0.03	0.62 to 0.83

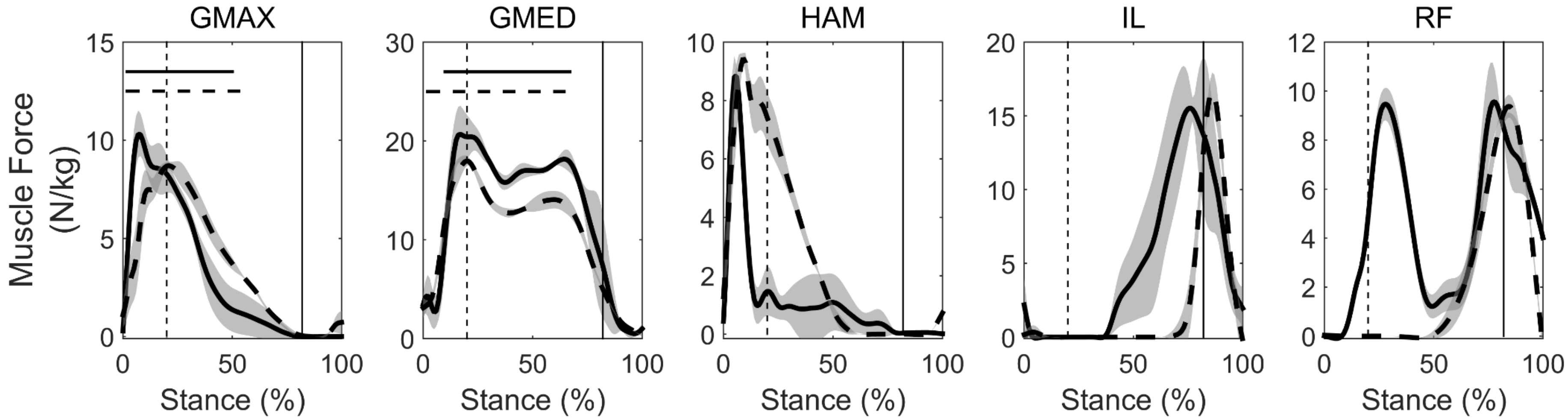

Figure 4.8. Hip muscle forces of the intact (solid line) and residual (dashed line) limbs during stance of OI users (n=4). The gray shaded areas represent ±1 standard deviation from the mean. The horizontal line for GMAX and GMED indicates the EMG activity period. The vertical dashed line represents contralateral toe-off (CTO); the vertical solid line represents contralateral heel strike (CHS).

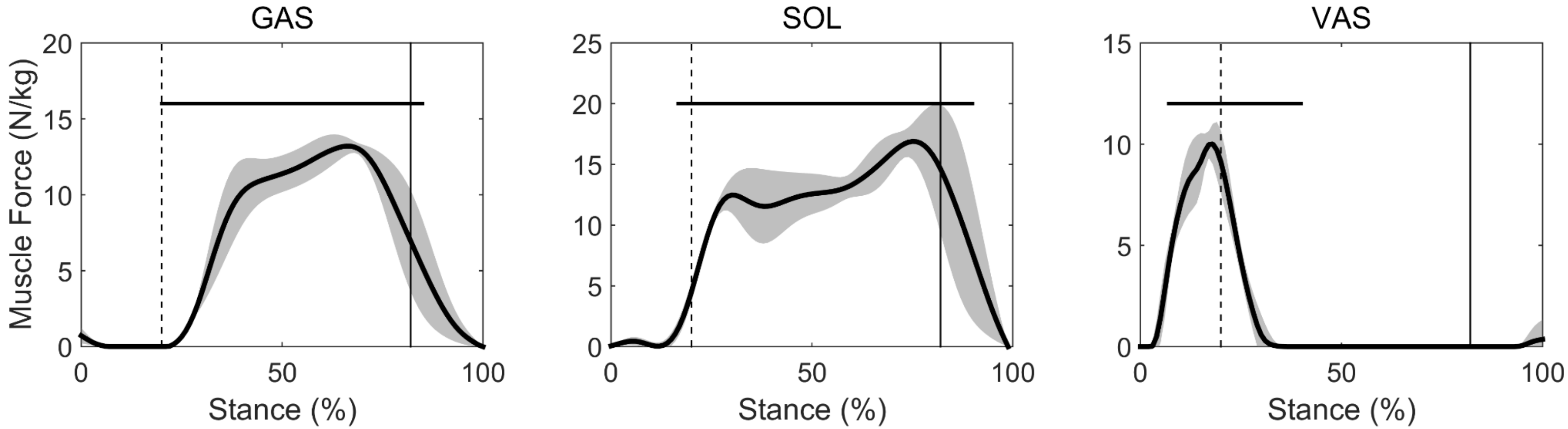

Figure 4.9. Muscle forces of the intact limb's VAS, GAS and SOL during stance of OI users (n=4). The gray shaded areas represent ±1 standard deviation from the mean. The horizontal lines indicate the EMG activity period. The vertical dashed line represents contralateral toe-off (CTO); the vertical solid line represents contralateral heel strike (CHS).

The results also showed that VAS contributed mostly to braking in the first half of stance, whereas SOL and GAS were prominent contributors to propulsion in the second half of stance. RF's peak contribution to braking was higher in the intact limb than the residual limb (mean difference: 0.20 m/s^2). The prosthesis generated most of the anterior-posterior COM acceleration in the whole stance in the residual limb. Body support was primarily provided by VAS in early to mid-stance and SOL and GAS in the second half of stance of the intact limb. GMAX contributed more to vertical COM acceleration in the intact limb compared to that in the residual limb (mean difference: 0.75 m/s^2).

The largest contribution to mediolateral COM acceleration was generated by GMED, which contributed medially throughout the whole stance. The peak GMED contribution to medial acceleration was greater in the intact limb than the residual limb (mean difference: 0.34 m/s^2). The intact limb GMAX contributed laterally to COM acceleration, which contrasts with the medial contribution of GMAX in the residual limb. The peak IL contribution to lateral COM acceleration was higher in the intact limb than that in the residual limb (mean difference: 0.09 m/s^2). The peak amount of HAM contribution to balance was smaller in the intact limb compared to the residual limb (mean difference: 0.25 m/s^2). The prosthesis generated lateral contribution to COM acceleration in the residual limb, while VAS contributed medially, and SOL and GAS contributed laterally during stance of the intact limb (Figure 4.10).

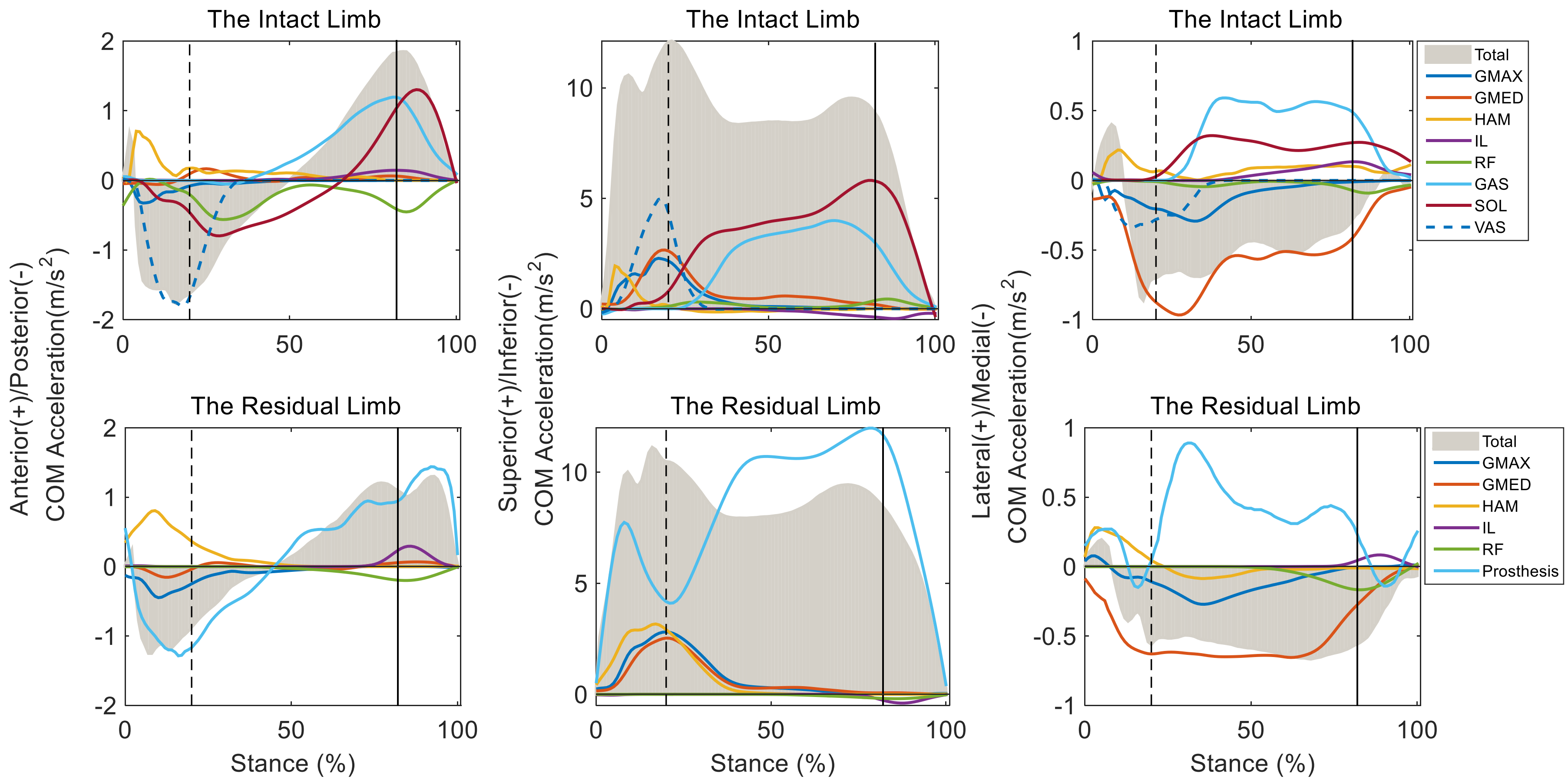

Figure 4.10. Individual muscle and prosthesis contribution to anterior-posterior, vertical and mediolateral COM acceleration of OI users (n=4). The shaded area represents the summed contribution from all actuators. The vertical dashed line represents contralateral toe-off (CTO); the vertical solid line represents contralateral heel strike (CHS).

4.3.3 Sensitivity analysis

Sensitivity analyses were performed to determine the effects of independently changing moment of inertia and center of mass of the prosthetic leg on knee moment of the intact and residual limb for one SP amputee. The following alterations were applied to the prosthetic inertial properties:

i) Increasing the moment of inertia (MOI) of all prosthetic segments by 25% and 50%, keeping the center of mass (COM) constant.

ii) Moving distally the center of mass of all prosthetic segments by 25% and 50%, keeping the moment of inertia constant.

iii) Decreasing the moment of inertia of all prosthetic segments by 25% and 50%, keeping the center of mass constant.

iv) Decreasing the center of mass of all prosthetic segments by 25% and 50%, keeping the moment of inertia constant.

No significant differences were found in the knee moment of the intact and the residual limb (Figure 4.11), which is in agreement with previous modeling prosthetic study (Smith et al., 2014, Narang et al., 2015).

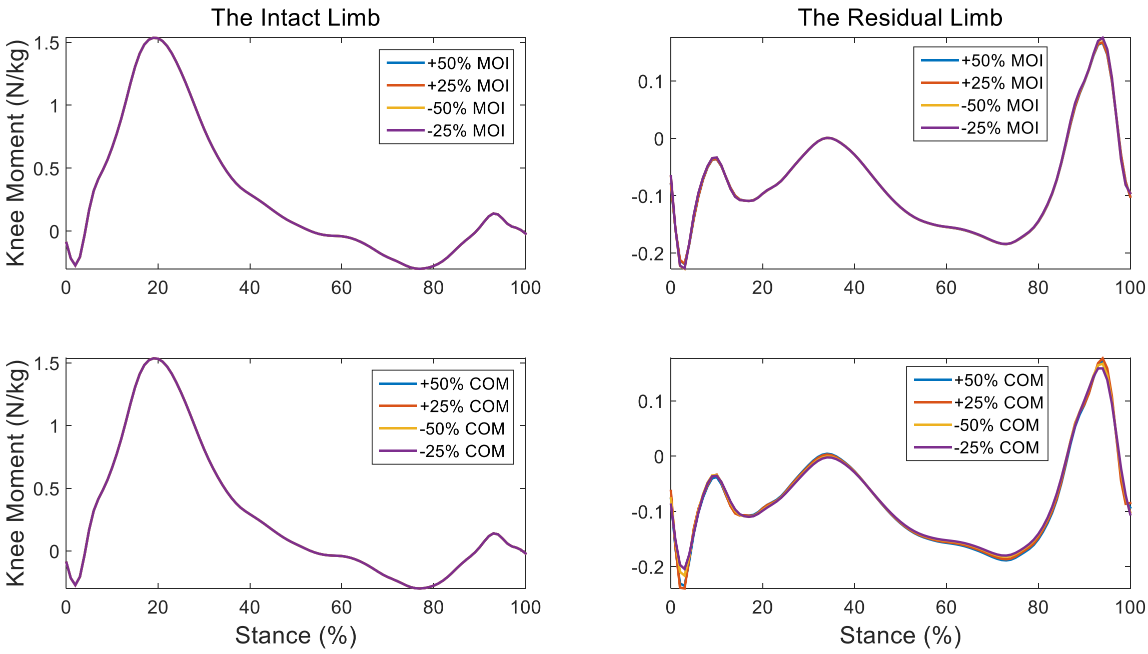

Figure 4.11. Knee moment of intact limb and residual limb for one amputee. ±50 (25) % MOI represents when MOI increased or decreased by 50(25) %; ±50(25) % COM represents when COM increased (decreased) by 50(25) %.

4.4 Discussion

The objective of this study was to employ 3D musculoskeletal modeling to investigate gait asymmetry in unilateral transfemoral amputees during gait. This was achieved by determining how the lower limb muscles and prosthesis of unilateral transfemoral amputees generate forward progression, vertical support, and mediolateral acceleration of the body COM. Consistent with our hypothesis, hip muscle contributions to propulsion, support and balance in the intact limb were significantly greater than those in the residual limb for both socket and osseointegrated groups. The prosthesis was found to function as the major contributor to support, progression and mediolateral balance in the residual limb. The knee and ankle extensors of the SP users contributed to the medial acceleration of the COM, while it is known that these muscles contribute to lateral acceleration of the COM in healthy non-amputees (Pandy et al., 2010, Silverman and Neptune, 2012). However, the ankle extensors (SOL and GAS) of the OI users contributed to lateral COM acceleration, which was similar to non-amputee's muscle behavior according to literature.

In agreement with previous studies (Nolan et al., 2003, Gard, 2006, Hof et al., 2007), a significantly longer stance phase was shown in the intact limb of the SP users compared to that in the residual limb. This may be due to the greater dependence of the amputee's intact limb on generation of support and propulsion of the body COM, which was evidenced from greater vertical and anterior-posterior components of the GRFs compared to those in the residual limb (Nolan et al., 2003, de Cerqueira et al., 2013, Harandi et al., 2020). For example, the amputees' inability to flex their prosthetic knee during weight transfer to the intact limb may necessitate greater compensatory hip motion from the intact limb during the swing phase of the residual limb, thus prolonging the stance in the intact limb (Gard, 2006). The shorter residual limb stance phase may also be exacerbated by contrasting mass and inertial properties between the two legs (Mattes et al., 2000, Harandi et al., 2020). Regarding the OI users, the spatiotemporal parameters of the intact limb were greater than those of the residual limb. However, the differences in each parameter between the intact and residual limb were smaller in the OI users than those of the SP users. This may be due to the greater self-selected walking speed of the OI users than the SP users, which might be affected by the direct anchorage of the femur to the residual limb (Frossard et al., 2010).

The present study showed that hip flexion and extension in the residual limb were significantly reduced at IHS, CTO and CHS compared to that in the intact limb in SP users. This reduced femoral motion may be affected by socket-pelvis interference. The femoral rotation relative to the pelvis is restricted in the acetabulum of the hip due to the anatomical constraints imposed by the skeletal anatomy (Jaegers et al., 1995b, Rabuffetti et al., 2005). The amputees also tilted their pelvis more in the stance phase of the residual limb than the that of the intact limb, which was mostly observed during hip extension. This may be associated with an increase in hip abduction and extension of the intact limb as a compensatory mechanism for the reduced hip function in the residual limb (Cappozzo et al., 1982, Sjödahl et al., 2003, Goujon-Pillet et al., 2008). For the OI users, the hip extension and adduction of the intact limb were greater than those in the residual limb. The OI users extended their residual limb's hip more to reach their intact limb's hip extension when compared with SP users (Rabuffetti et al., 2005, Tranberg et al., 2011). It may be correlated with differences in step length values between the intact and residual limb. The step length of the residual limb in the SP users was significantly smaller than that of the intact limb, which is in contrast to OI users. This may lead to a reduced hip extension during stance (Kerrigan et al., 1998, Sawicki and Ferris, 2009). The difference in step length of the SP and OI users between their intact and residual limb may also be due to the influence of direct attachment of the femur to the implant, which allows the hip joint moves in a larger range than socket type (Tranberg et al., 2011). On the other hand, the

SP users tilted their pelvis more anteriorly, when the residual limb was in stance phase, to compensate the reduced residual limb's hip extension due to restrictions caused by the socket (Kerrigan et al., 1998).

The present study about both SP and OI users showed that VAS and GMAX in the intact limb were the major contributors to the fore-aft and vertical body COM acceleration in early to mid-stance, which has already been shown in studies of healthy adults (Lim et al., 2013, Lin et al., 2015). Also, RF in the intact limb contributed more to posterior COM acceleration than that in the residual limb, while the intact limb's IL contributed more to anterior COM acceleration compared to those contributions in the residual limb. Furthermore, VAS and GMAX contributed significantly more to support, and VAS also contributed more considerably to breaking. The greater contribution to COM acceleration of the hip muscles in the intact limb compared to those in the residual limb may be due to the lower hip joint motions and smaller hip joint moments in the residual limb, which led to an increase in hip motion, greater hip moments and higher hip muscles forces of the intact limb (Lim et al., 2013, Lin et al., 2015). Regarding the OI users, the peak of hip muscles forces and contributions to COM acceleration in the intact limb were greater than those in the residual limb; however, the difference between the two limbs was smaller than that of the SP users.

While this study did not quantify muscle and joint function in healthy controls, forces generated by VAS, SOL and GAS in the intact limb of the transfemoral amputees were greater than those previously measured in non-amputees (Lim et al., 2013, Harandi et al., 2020). In addition, previous studies on healthy individuals have shown that VAS, SOL, and GAS contribute to lateral body COM acceleration, whereas our study on SP users showed that these muscles contributed to medial body COM acceleration (Silverman and Neptune, 2012). This difference may be associated with the greater step width and hip abduction in the intact limb compared to the residual limb (Silverman and Neptune, 2012). For example, the maximum and average values of the intact limb hip abduction angle were 11.04˚ and 4.64˚, respectively, which were higher than those in non-amputees reported previously (4.3˚ and 1.0˚, respectively) (Silverman and Neptune, 2012, Harandi et al., 2020). For the OI users, VAS generated medial contribution, but SOL and GAS contributed to lateral body COM acceleration, which was in contrast with the medial contribution of the two latter muscles in SP users. OI users showed 6.76˚ and 3.82˚ as the maximum and average values of the intact limb hip abduction, respectively. These values were smaller and greater than those in SP users described above. This intact foot's inclination to the lateral body COM may also be associated with the increase in stability due to loss of ankle plantarflexors of the residual limb (Kerrigan et al., 1998). The contribution of SP users' VAS, SOL and GAS to the medial acceleration of the body COM in transfemoral amputees may be caused by the placement of the intact limb's foot relative to the body COM more laterally than that in the residual limb to control mediolateral balance. This difference in foot placement may be a result of the loss of ankle plantarflexors to increase the stability of the body during walking (Kerrigan et al., 1998). However, the OI users showed similarity in the contribution of SOL and GAS to lateral COM acceleration with non-amputees in the literature.

The prosthesis of the SP and OI users provided the major contribution to body support during stance in the residual limb, but it also contributed to braking and progression in the first and second half of stance, respectively. The function of the prosthesis to braking, propulsion, and support was similar to the overall role of VAS, SOL, and GAS in the intact limb during walking. While the prosthesis contributed to lateral COM acceleration, GMED in the residual limb contributed substantially to medial COM acceleration. However, contributions from GMED and GMAX of the residual limb were smaller relative to those in the intact leg. This may be related to smaller hip moments and hip muscle forces accompanying smaller hip range of motion in the residual limb, as demonstrated in previous lower limb amputee studies (Renström et al., 1983, Moirenfeld et al., 2000).

One may raise question about the SP users in this dissertation is that they are divided into two groups (three with the passive knee joint and three with active knee joint). The type of knee joint has been demonstrated to affect knee flexion angle and moment of the intact limb (Kaufman et al., 2007, Frossard et al., 2010, Kaufman et al., 2012, Frossard et al., 2019), which has also been confirmed by our result (Figure 4.12-Figure 4.13). Furthermore, all the musculoskeletal modeling and computational procedures were separately performed for the SP users with passive and active knee joint. The results of induced acceleration analysis showed consistency in the overall pattern of muscle recruitment during walking between the passive and active knee prosthesis (Figure 4.14-Figure 4.15). However, the magnitudes of individual muscle contribution to COM acceleration were different between the two groups fitted with passive and active knee prosthesis (Harandi et al., 2020). The aim of this study was to investigate the dynamic~~s~~ role of muscles when generating walking movement in transfemoral amputees with socket and osseointegration prosthesis. So, one view might be doing average amongst all the SP users ignoring their type of knee joint and considering only the effect of socket on their walking.

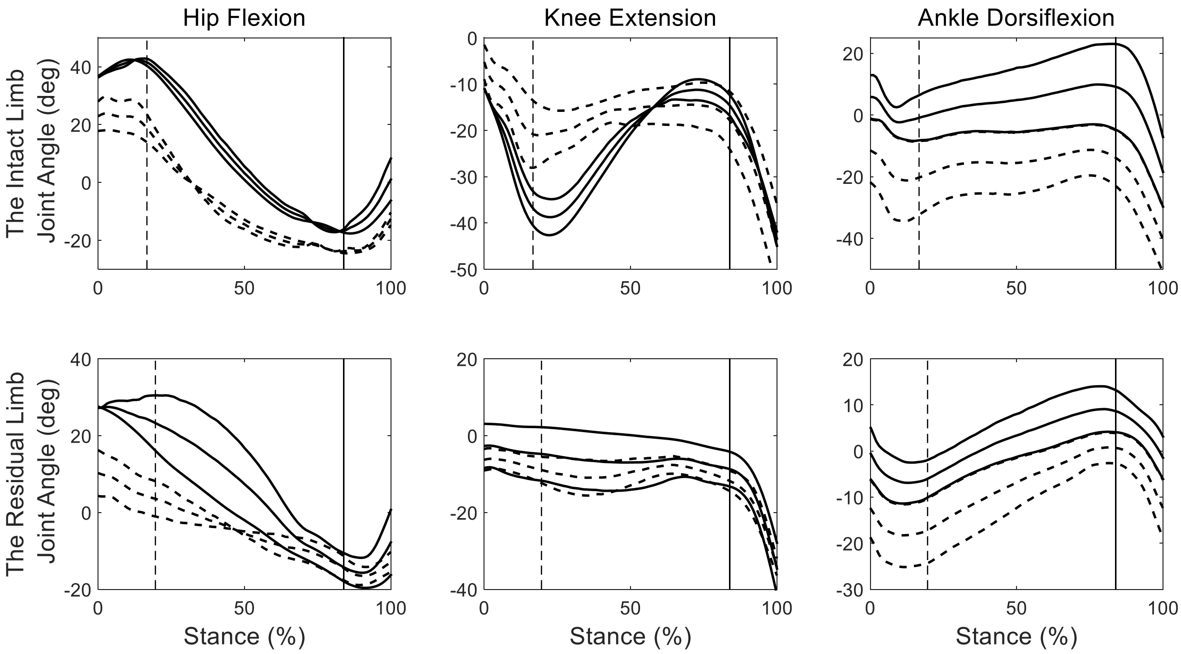

Figure 4.12. The intact and residual limb's joints angles of the amputees with passive (solid line, n=3) and active (dashed line, n=3) prosthesis. The vertical dashed line represents contralateral toe-off (CTO); the vertical solid line represents contralateral heel strike (CHS).

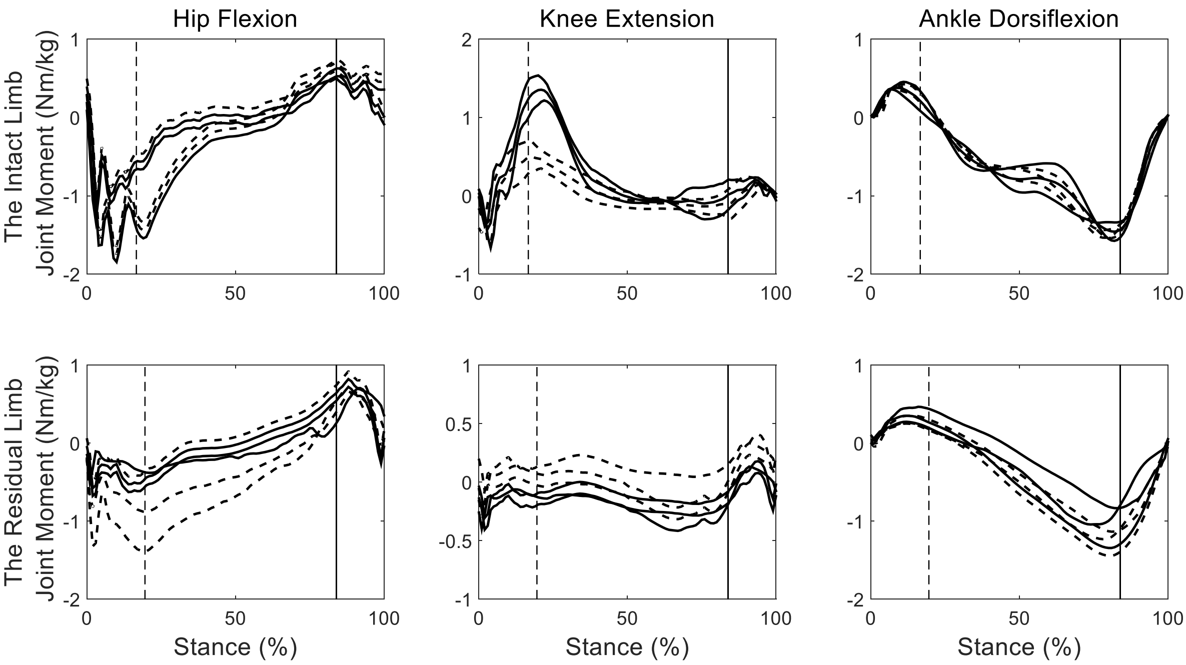

Figure 4.13. The intact and residual limb's joints moments of the amputees with passive (solid line, n=3) and active (dashed line, n=3) knee prosthesis. The vertical dashed line represents contralateral toe-off (CTO); the vertical solid line represents contralateral heel strike (CHS).

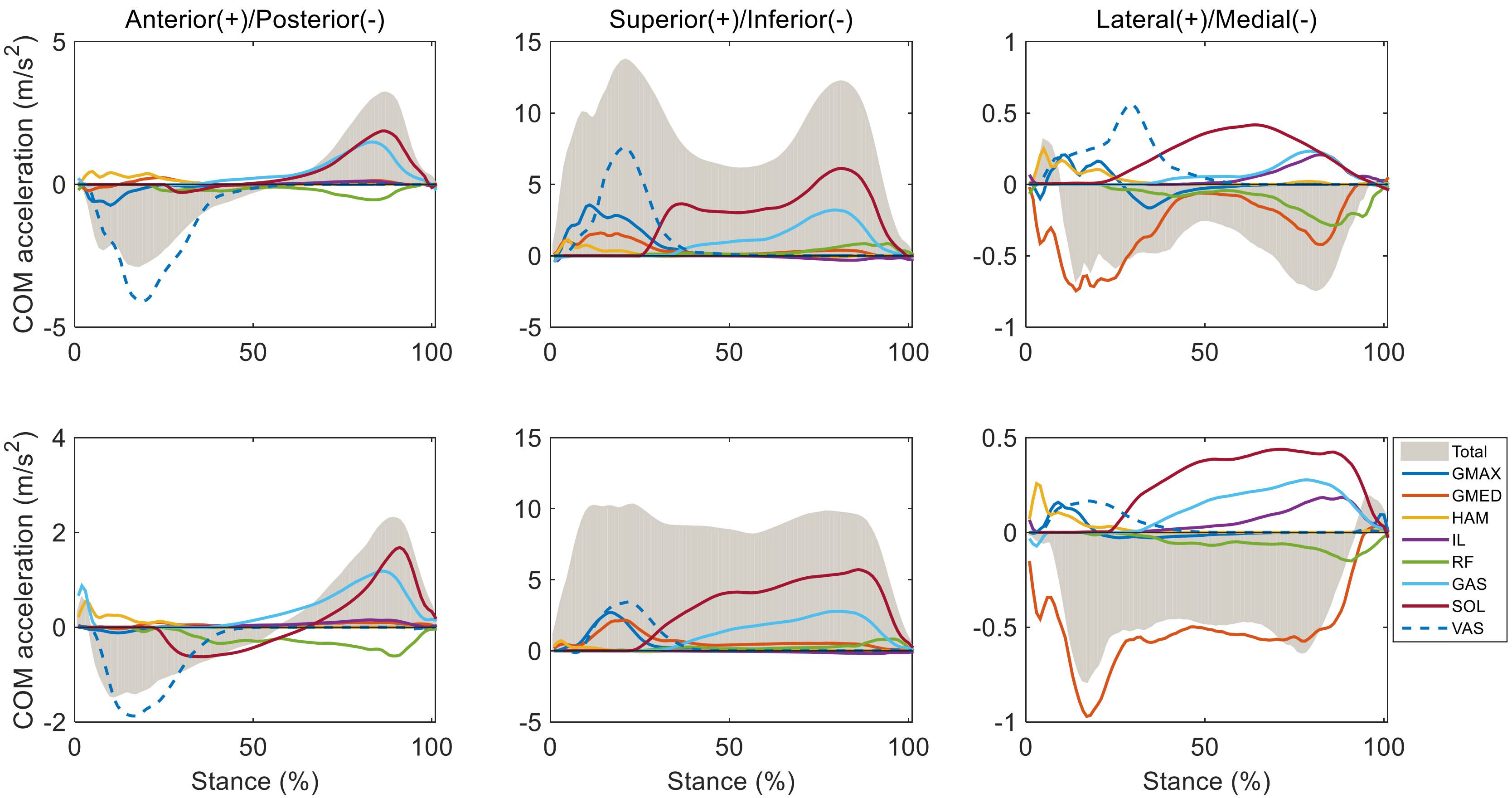

Figure 4.14. The intact limb muscle contribution to COM acceleration for amputees with passive (mechanical) knee joint (top, n=3) and active (microprocessor) knee joint (bottom, n=3). The shaded area represents the summed contribution from all actuators.

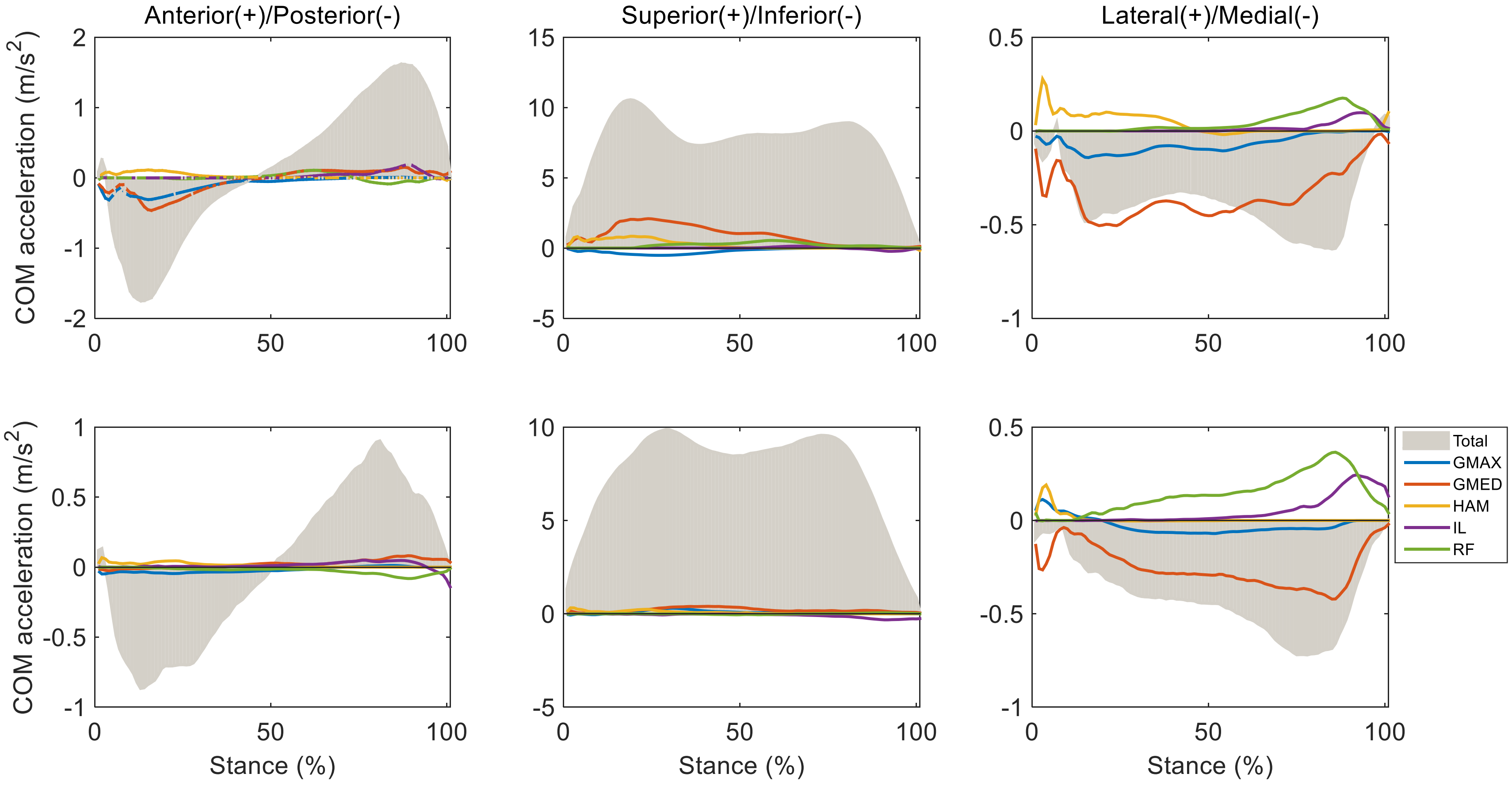

Figure 4.15. The residual limb muscle contribution to COM acceleration for amputees with passive (mechanical) knee joint (top, n=3) and active (microprocessor) knee joint (bottom, n=3). The shaded area represents the summed contribution from all actuators.

Another questionable issue might present the stabilization method for modeling the physiological properties of the re-attached muscles. As previously mentioned, the results of this study were based on myodesis stabilization technique. However, the re-attached muscles for one amputee were also modeled based on myoplasty method. As shown in Figure 4.16, in myoplasty, the re-attached muscles generated no forces, and moments generated by the hip joint were consequently distributed to other residual limb muscles. As a result, the residual limb muscles produced greater forces in myoplasty than myodesis, although the ratio of the hip muscles was preserved in both methods. For example, GMED of the residual limb generated higher forces than GMAX in myodesis and this trend was repeated in myoplasty modeling, however, the magnitudes were different. It indicates that myodesis-based surgical technique may involve more residual limb muscles in force generation than myoplasty. It may suggest surgeons to use myodesis, which distributes hip moments to more muscles to prevent muscle atrophy (Harandi et al., 2020).

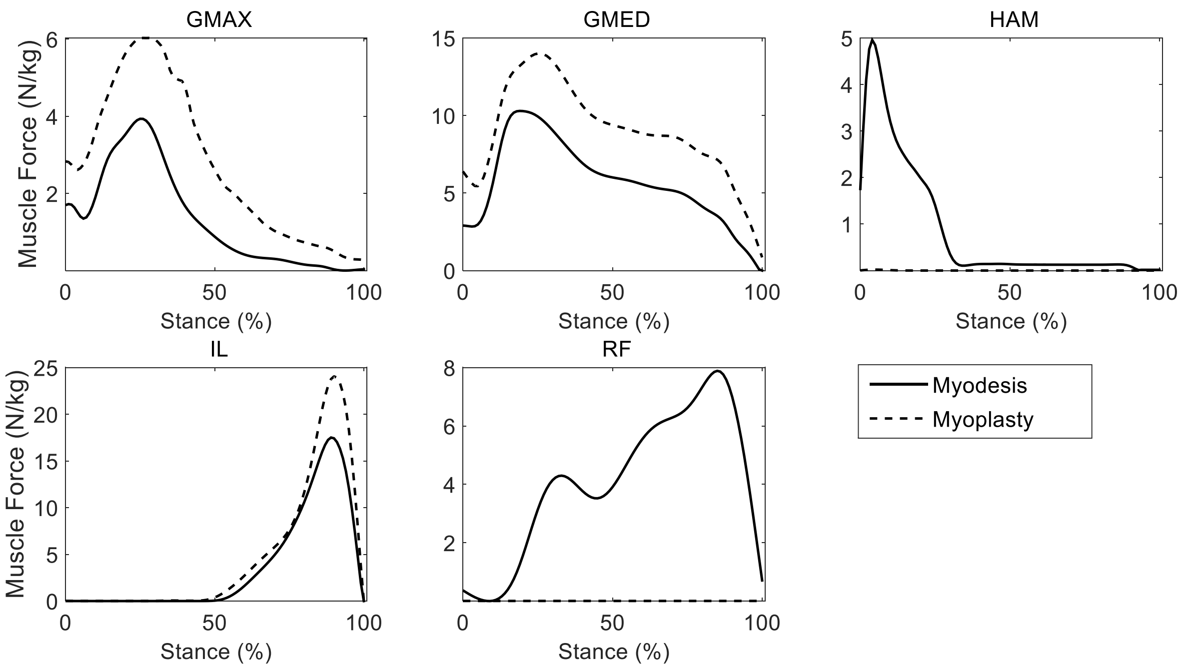

Figure 4.16. Residual limb muscle forces calculated based on myodesis and myoplasty techniques.

Moreover, the inertial properties (center of mass and moment of inertia) of prosthetic segments were estimated by the prosthetics' reverse-engineering design in SolidWorks. The results demonstrated that differences in joint moments between the initial properties estimated by SolidWorks and the alterations described in 4.3.3 were small during stance phase, which was in accordance with previous studies (Smith et al., 2014, Narang et al., 2015) (Figure 4.11). Narang et al. investigated the effects of different mass and moment of inertia on knee moment and found there would be no notable difference in the knee moment of the prosthetic leg if the inertial parameters of the prosthetic changed to 25% and 50% of the corresponding segments in the intact limb during stance. In general, it seems that the type of prosthesis and knee joint both influence the joints angles and moments (Huch et al., 1997, Bae et al., 2007, Steele et al., 2012b).

There are several limitations to the present study. Firstly, the cost function used in the static optimization minimized the sum of squares of muscle activations. Activation criterion does not consider musculoskeletal conditions for amputees. For example, muscle fatigue frequently occurs in atrophied muscles of lower limb amputees, which may influence gait compensation strategies (Ackermann and Van den Bogert, 2010). Secondly, the low number of subjects recruited may not be representative of the average data for a broad population of amputees and may affect statistically the results. However, the sample size was sufficient to detect significant differences in spatiotemporal parameters, joint angles and joint moments between limbs for the SP users. The small number size of the OI users did not permit to perform any statistical analysis.

This chapter demonstrated gait asymmetries in transfemoral amputees (SP and OI users), including increased anterior pelvis tilt during the residual limb's stance and increased hip extension in the intact limb compared to that in the residual limb. Reduced hip extension in the residual limb and a shorter residual limb stance phase was associated with increased anterior pelvis tilt. Increases in the intact limb's hip joint range of motion and hip muscle function appeared to be a compensatory mechanism associated with decreases in the residual limb's hip muscle forces and contributions to COM acceleration. For the OI users, spatiotemporal parameters, joint kinematics and kinetics, muscle forces and muscle contribution to COM acceleration in the intact limb were greater than those of the residual limb. However, the results depicted that differences in these parameters between the two limbs were smaller than those of the SP users since there was no significant difference between the two limbs. This may prove that the OI users walked more symmetrically than the SP users. However, we believe that the small sample size (four OI users) may not be representative of the transfemoral osseointegrated community and larger sample size is needed to reach a solid statement. The outcomes of this study may help with prescribing targeted rehabilitation and help with improving the design and function of prostheses.

Chapter 5. Muscle contribution to hip contact forces

This chapter is based on the following submitted paper:

- **Vahidreza Jafari Harandi,** David Charles Ackland, Raneem Haddara, L. Eduardo Cofré Lizama, Mark Graf, Mary Pauline Galea, Peter Vee Sin Lee – Muscle contribution to hip contact forces in osseointegrated transfemoral amputees during walking. *Computer Methods in Biomechanics and Biomedical Engineering*, Under Review (Submitted December 2019).

5.1 Introduction

The number of individuals with lower extremity amputation is estimated to increase by 2050 in the US (Ziegler-Graham et al., 2008). Approximately one-third of socket-worn transfemoral amputees has been reported to complaint chronic skin pain due to the interaction with socket (Rommers et al., 1996, Hagberg and Brånemark, 2001b, Meulenbelt et al., 2009, Butler et al., 2014). This tissue problem has affected their mobility and quality of life (Pezzin et al., 2000, Demet et al., 2003, Pezzin et al., 2004a), which has led to design new sockets for better walking; however, skin problems still exist (Van de Meent et al., 2013). Thus, an alternative technique, osseointegration, has been used to decrease these problems (Branemark et al., 2001, Al Muderis et al., 2018). On the other hand, the prevalence rate of pain and osteoarthritis (OA) in the hip of the intact limb has been shown in lower extremity amputees to be higher with 14% more than able-bodied individuals (Struyf et al., 2009, Welke et al., 2019).

Osseointegrated transfemoral amputees have improved gait parameters compared to those fitted with socket prosthesis. For example, they have shown greater hip range of motion, quicker cadence and increase in walking speed than conventional socket patients; however, slower cadence and larger gait duration have been recognized in osseointegrated transfemoral amputees compared to non-amputees (Hagberg et al., 2005, Frossard et al., 2010, Tranberg et al., 2011, Pinard and Frossard, 2012, Leijendekkers et al., 2017, Robinson et al., 2020). Lower cadence and stride length have been associated with lower hip contact forces (Stansfield and Nicol, 2002). One study has found improvement in hip extension of the residual limb after osseointegration surgery relative to when wearing socket prosthesis (Tranberg et al., 2011). Lewis et al. reported that increase in hip extension resulted in increase in anterior hip contact forces (Lewis et al., 2007, Lewis et al., 2010, Wesseling et al., 2015). A decreased hip extension at terminal stance has been linked to a reduction in hip contact forces (Bennett et al., 2008, Beaulieu et al., 2010, Wesseling et al., 2015). Also, increased hip contact force has been indicated to relate to increase in hip extension and adduction angles and moments in patients with total hip replacement (Foucher et al., 2009, Wesseling et al., 2015). Increasing hip loading has been illuminated as a sign for hip OA development (Felson, 2004). Transfemoral amputees also showed greater intact limb ground reaction forces (GRFs) than the residual limb (Schaarschmidt et al., 2012, Okita et al., 2018), which may result greater joint loading in the intact limb. As a result, joint loading variations between the intact and residual limb should be identified to assimilating how walking mechanisms contribute to the prevalence of hip OA.

Several instrumented implants-based studies have measured hip contact forces in daily activities (Rydell, 1966, Crowninshield et al., 1978, Bergmann et al., 1993, Bergmann et al., 2001). The in vivo approach in these studies is limited to those with total hip replacement surgery, which does not apply to amputees and healthy subjects. Therefore, musculoskeletal modeling techniques have been utilized to noninvasively calculate hip contact forces (Heller et al., 2001, Stansfield et al., 2003, Correa et al., 2010, Schache et al., 2018). The resultant hip contact forces have mostly been investigated in non-amputees during walking and running (Crowinshield et al., 1978, Röhrle et al., 1984, Read and Nigg, 1999, Giarmatzis et al., 2015). However, three studies provided a more complete understanding of muscle function to hip contact forces in healthy individuals (Correa et al., 2010, Pandy and Andriacchi, 2010, Schache et al., 2018). Despite muscles have been shown as major contributors to mechanical joint loading (Herzog et al., 2003), further study is required to analyze individual muscle role to joint contact force in amputees due to differences in walking mechanism than non-amputees.

Previous studies have investigated individual muscle contribution to the anterior-posterior, superior-inferior and medial-lateral components of the hip joint contact forces in non-amputees (Correa et al., 2010, Schache et al., 2018). The crossing hip joint muscles, *gluteus maximus* (GMAX) and *gluteus medius* (GMED), contributed more to posterior and anterior hip contact forces, respectively. In addition, the axial and mediolateral components of hip contact forces were provided by GMAX and GMED. Of those non-crossing the hip joint muscles, *vasti* (VAS) contributed more to the anterior and superior of hip contact forces during the first half of stance, while *soleus* (SOL) and *gastrocnemius* (GAS) generated greater contribution to the superior of hip contact forces during the second half of stance (Correa et al., 2010, Schache et al., 2018). Differences in spatiotemporal parameters and joint angles and moments in the intact limb than the residual limb as well as the loss of functional behavior of a number of below-knee muscles and knee extensors may be affecting walking mechanisms in unilateral transfemoral amputees. As a result, the way in which individual muscles contribute to hip contact forces in transfemoral amputees is ambiguous.

The purpose of this study was to use three-dimensional musculoskeletal modelling to investigate individual muscle contribution to hip contact forces through analysis of joint kinematics and moments, then muscle forces and muscle contribution to GRFs in SP and OI users. Our hypothesis was the hip muscles contribution to hip contact forces would be different to that of the residual limb. The outcome of this study may be important to prevent or postpone the increase rate of hip OA in amputees.

5.2 Materials and Methods

The detail of materials and methods used in this study has been comprehensively discussed in chapter Chapter 3. In this section, a brief explanation of the methods is presented. However, the relevant section in the methods chapter is mentioned to avoid repetition.

5.2.1 Subject recruitment

Gait experiments were performed on six individuals with unilateral transfemoral amputation wearing socket and four osseointegrated unilateral transfemoral amputees. All subjects wore their own prosthesis and were able to walk without assistive devices. The prostheses alignment and fitting were checked by an experienced prosthetist prior to data collection. Ethical approval was obtained by the Melbourne Health Human Research Ethics Committee with the number HREC 2015.148, and each participant provided written informed consent.

5.2.2 Testing protocol

Experimental data were collected over three trials of over-ground walking at each subject's preferred speed. The three-dimensional positions of reflective markers were recorded using an eight-camera motion capture system (Vicon, Oxford Metrics) sampling at 200 Hz. The markers were placed on body segments on the intact and residual limb, followed by the marker set protocol developed by Dorn (Dorn, 2011). On the prosthesis, the markers were mounted in medial and lateral knee and ankle, heel and toe. Three force platforms (Watertown MA, USA), embedded in the ground, were used to measure GRF, sampling at 1000 Hz. EMG was simultaneously recorded on the intact limb muscles (GMAX, GMED, SOL, GAS and VAS (supplementary material)) and residual leg muscles (GMAX and GMED) based on the previously described procedure to collect electromyography (EMG) data (Hermens et al., 2000), sampling at 1000 Hz. Muscle contraction was performed to check EMG signals prior to experiment to obtain the accuracy of electrodes (Hermens et al., 1999, Wentink et al., 2013).

5.2.3 Data processing

Marker trajectories were then low-pass filtered with a cut-off frequency of 4 Hz using a 4^{th} order Butterworth filter. A 4^{th} order Butterworth filter was used to low-pass filter GRFs data with a cut-off frequency of 60 Hz. EMG offset signals were removed and then rectified and low-pass filtered at 10 Hz using a 2^{nd} order Butterworth filter to create linear envelopes. Joint trajectories were calculated using inverse-kinematics and averaged across three successive gait cycles (Harandi et al., 2020).

5.2.4 Musculoskeletal modeling

A 10-segment, 23 degree-of-freedom generic skeletal model of the body was scaled in OpenSim 3.2 for each subject (Delp et al., 2007). The head, arm, and torso were lumped together as a single rigid body, which articulated with the pelvis via a ball-and-socket back joint. The hip was modelled as a ball-and-socket joint, both anatomical knee and metatarsal joints of the intact limb as hinge joints, and each ankle-subtalar complex of the intact limb as a universal joint. The lower limbs and trunk were actuated by 76 Hill-type muscle-tendon units (Zajac, 1989) (supplementary material). Scaled-personalized models were then developed by scaling segment length and muscle tendon parameters of the generic musculoskeletal model. A scaling factor was calculated using the relative distance between each segment’s pair of markers measured in a static standing calibration trial and the corresponding virtual markers mounted in the model (Delp et al., 2007, Schache et al., 2018).

For each subject, the dimensions of the lower-limb prosthesis’ segments including knee joint, pylon and foot were measured using digital caliper and tape measure, and the weight of the prosthesis’ segments was measured using digital scale (AND brand, model SJ-5001HS 5000g x 1g). The prosthesis was then reverse-engineered in SolidWorks (Massachusetts, USA), assuming homogeneous material, to calculate moment of inertia and center of mass position, and virtually placed in the individualized scaled model. The knee and ankle of the prosthetic leg were modeled as hinge joint. The residual limb was modeled as a frustum of a right circular cone to obtain mass, center of mass and moment of inertia (Ferris et al., 2017, Harandi et al., 2020).

The below-knee segments including tibia, talus, and foot (in concomitant with that portion of femur replaced with implant) were removed from the scaled model. Uniarticular muscles spanning the knee joint were also excluded from model. Two different surgical techniques, myodesis and myoplasty, are the most common stabilization strategies for the re-attached muscles. However, myodesis has been shown to improve the re-anchored muscle's capacity such as *hamstrings* and hip adductors to generate hip forces and moments (Gottschalk, 2004, Tintle et al., 2010, Ranz et al., 2017). Thus, the current study followed the myodesis stabilization technique for alteration, re-anchored muscle properties. This technique directly re-attaches the detached muscles to the distal end of the residual femur (Ranz et al., 2017). In this case, muscle parameters were changed to preserve the muscle tension in the neutral position based on data from the same muscle in the opposite limb (Ranz et al., 2017). Tendon slack length was changed to maintain muscle tension; optimal fibre length was then calculated in equal proportion to the sum of muscle tendon slack length and fibre length of the intact limb's muscles in neutral position (Ranz et al., 2017, Harandi et al., 2020).

Hip, knee ankle joint trajectories were calculated using inverse kinematics (IK) (Lu and O'connor, 1999). Net joint moments were obtained using inverse dynamics. Residual Reduction Analysis (RRA) was then performed to vary the model's torso center of mass to diminish the dynamic inconsistency between the collected GRFs and the measured kinematics of the model (Thelen and Anderson, 2006, Delp et al., 2007). Muscle forces were calculated using static optimization by decomposing the net joint moments into discrete muscle actuator loads (Anderson and Pandy, 2001b). The optimization problem aimed to minimize the sum of squared muscle activation constrained by each muscle's force-length-velocity property. Contribution of muscle forces, gravity, inertia and other external forces to the GRFs were subsequently quantified using a pseudo-inverse GRF decomposition method and induced acceleration analysis, considering five-point foot-ground contact model for both the intact and residual limb (Dorn et al., 2012a). The foot-ground model is required as mechanical constraint to implement induced acceleration analysis. The hip contact forces were calculated using a recursive bottom-up operation which starts from the most distal segments and ends at the most proximal body (Steele et al., 2012a). At each time step, muscle contributions to hip contact forces were computed by remaining only the muscle interest and the corresponding muscle force and muscle contribution to GRF, and then solving hip contact forces described above (Sasaki and Neptune, 2010). Hip contact forces and muscle contributions to hip contact force were calculated at four major gait events including ipsilateral heel-strike (IHS), contralateral toe-off (CTO), contralateral heel-strike (CHS) and ipsilateral toe-off (ITO) during stance phase.

5.3 Results

In this section, the results for both SP and OI users are presented. However, the reader is referred to relevant sections in some cases to avoid repetition. Overall, the SP and OI users showed differences in walking parameters including spatiotemporal, joint angles, joint moments and muscle forces between the intact and residual limb.

5.3.1 SP users

The results of spatiotemporal parameters, joint kinematics and kinetics, and muscle forces have been explained in section 4.3.1. In this section, the results of hip contact forces are shown for SP users with passive and active knee joint prosthesis.

5.3.1.1 Passive knee prosthesis SP users

The overall hip contact force was higher in the intact limb than the residual limb at CTO and CHS (mean difference: 1.07±0.5 and 2.57±0.67 N/BW, respectively) (Figure 5.1). The peak hip contact forces were greater in the intact limb than those in the residual limb at CTO (mean difference: 0.75±0.20, 0.66±0.11 and 0.38±0.09 N/BW for the anterior-posterior, superior-posterior and medial-lateral directions, respectively) (Table 5.1, Figure 5.2) and CHS (mean difference: 0.88±0.18, 2.21±0.85 and 0.98±0.24 N/BW for the anterior-posterior, superior-posterior and medial-lateral directions, respectively) (Table 5.2, Figure 5.2). The peak GMAX and GMED contribution to the anterior-posterior hip contact forces was higher in the intact limb than the residual limb at CTO (mean difference: 0.93±0.19 and 0.50±0.10 N/BW, respectively) and CHS (mean difference: 0.68±0.12 and 0.21±0.08 N/BW). GMED generated most contribution to the axial hip contact forces with the higher peak at CTO in the intact limb than the residual limb (mean difference: 0.23±0.10 N/BW) (Table 5.1, Figure 5.2). GMED also provided the most contribution to mediolateral hip contact forces, which the peak was greater in the intact than the residual limb at CTO (mean difference: 1.08±0.60 N/BW) (Table 5.1, Figure 5.2). the peak GMAX to medial hip contact forces was greater in the intact limb compared to that of the residual limb at CTO (mean difference: 0.37±0.10 N/BW) (Table 5.1, Figure 5.2).

GAS, SOL and VAS generated the most contribution to the three components of the intact limb's hip contact forces. GAS provided higher contribution to the superior hip contact forces at CTO (0.44±0.09 N/BW), followed by and VAS (0.28±0.05 N/BW) (Table 5.1, Figure 5.3). The peak VAS contribution to axial hip contact forces was greater at CHS (0.56±0.11 N/BW) than GAS (0.34±0.08 N/BW) (Table 5.2, Figure 5.3).

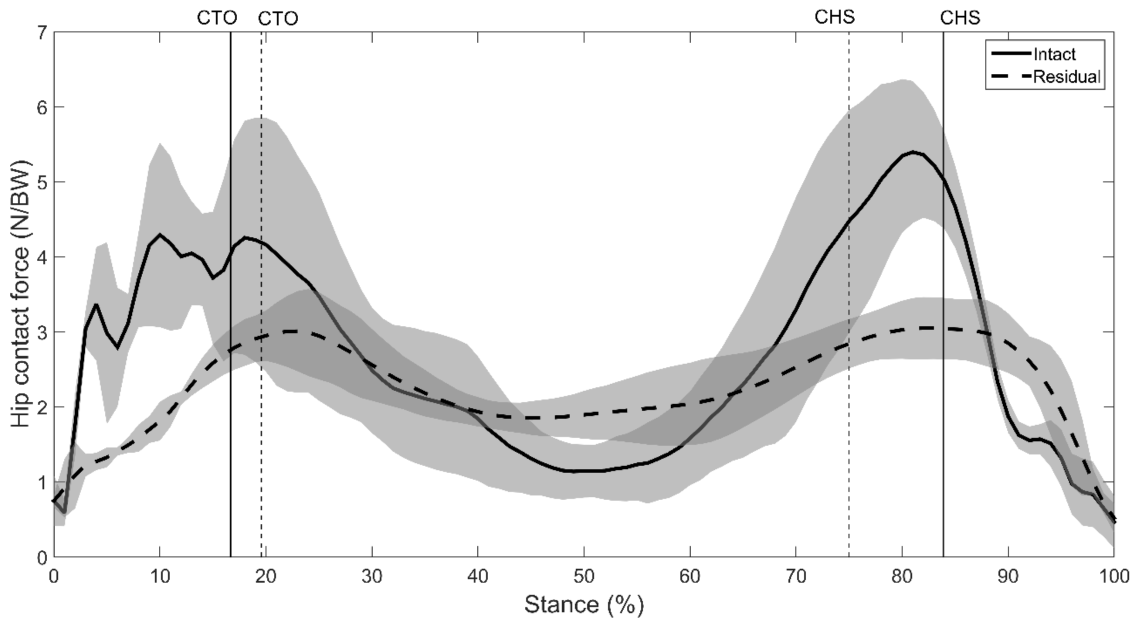

Figure 5.1. Total hip contact forces for the intact and residual limb of the SP users with only ***passive*** knee prosthesis (n=3). The vertical solid lines indicate the intact limb and the vertical dashed lines indicate the residual limb.

Table 5.1. Individual muscle contribution to the peak hip contact forces during CTO for the SP users with only ***passive*** knee prosthesis (n=3).

	Anterior(+)/ Posterior(-)		Superior(+)/ Inferior(-)		Medial(+)/ Lateral(-)	
	Intact	Residual	Intact	Residual	Intact	Residual
Hip-spanning muscles						
ALAM	0.14	0.03	0.47	0.16	0.12	0.05
GMAX	-0.94	<0.01	1.55	1.14	0.49	0.12
GMED	0.83	0.33	2.35	2.12	1.27	0.19
IL	0.20	0.12	0.75	0.05	0.16	0.04
RF	0.03	-0.01	-0.36	<0.01	<0.01	0.02
HAM	0.07	0.01	0.47	0.21	0.04	0.04
Subtotal	**0.33**	**0.48**	**5.23**	**3.68**	**2.08**	**0.46**
Non-hip-spanning muscles						
GAS	0.05	---	0.44	---	<0.01	---
SOL	0.03	---	-0.28	---	<0.01	---
VAS	0.07	---	0.28	---	0.02	---
Subtotal	**0.15**	---	**0.44**	---	**0.02**	---
Others	**0.76**	**0.01**	**-2.25**	**-0.92**	**-0.91**	**0.35**
Total	**1.24**	**0.49**	**3.42**	**2.76**	**1.19**	**0.81**

Table 5.2. Individual muscle contribution to the peak hip contact forces during CHS for the SP users with only ***passive*** knee prosthesis (n=3).

	Anterior(+)/ Posterior(-)		Superior(+)/ Inferior(-)		Medial(+)/ Lateral(-)	
	Intact	Residual	Intact	Residual	Intact	Residual
Hip-spanning muscles						
ALAM	0.15	0.02	0.66	0.15	0.06	0.03
GMAX	-0.71	-0.03	0.75	0.56	0.06	0.19
GMED	0.44	0.23	1.52	2.02	0.65	0.59
IL	0.83	0.01	2.07	0.12	0.51	0.01
RF	0.17	-0.02	0.32	-0.08	-0.02	<0.01
HAM	0.14	0.04	0.63	0.07	0.02	0.03
Subtotal	**1.02**	**0.25**	**5.95**	**2.84**	**1.28**	**0.85**
Non-hip-spanning muscles						
GAS	0.09	---	0.34	---	0.04	---
SOL	0.13	---	-0.11	---	-0.04	---
VAS	0.12	---	0.56	---	0.02	---
Subtotal	**0.34**	**---**	**0.79**	**---**	**0.02**	**---**
Others	**-0.20**	**0.03**	**-1.93**	**-0.15**	**0.39**	**-0.14**
Total	**1.16**	**0.28**	**4.81**	**2.69**	**1.69**	**0.71**

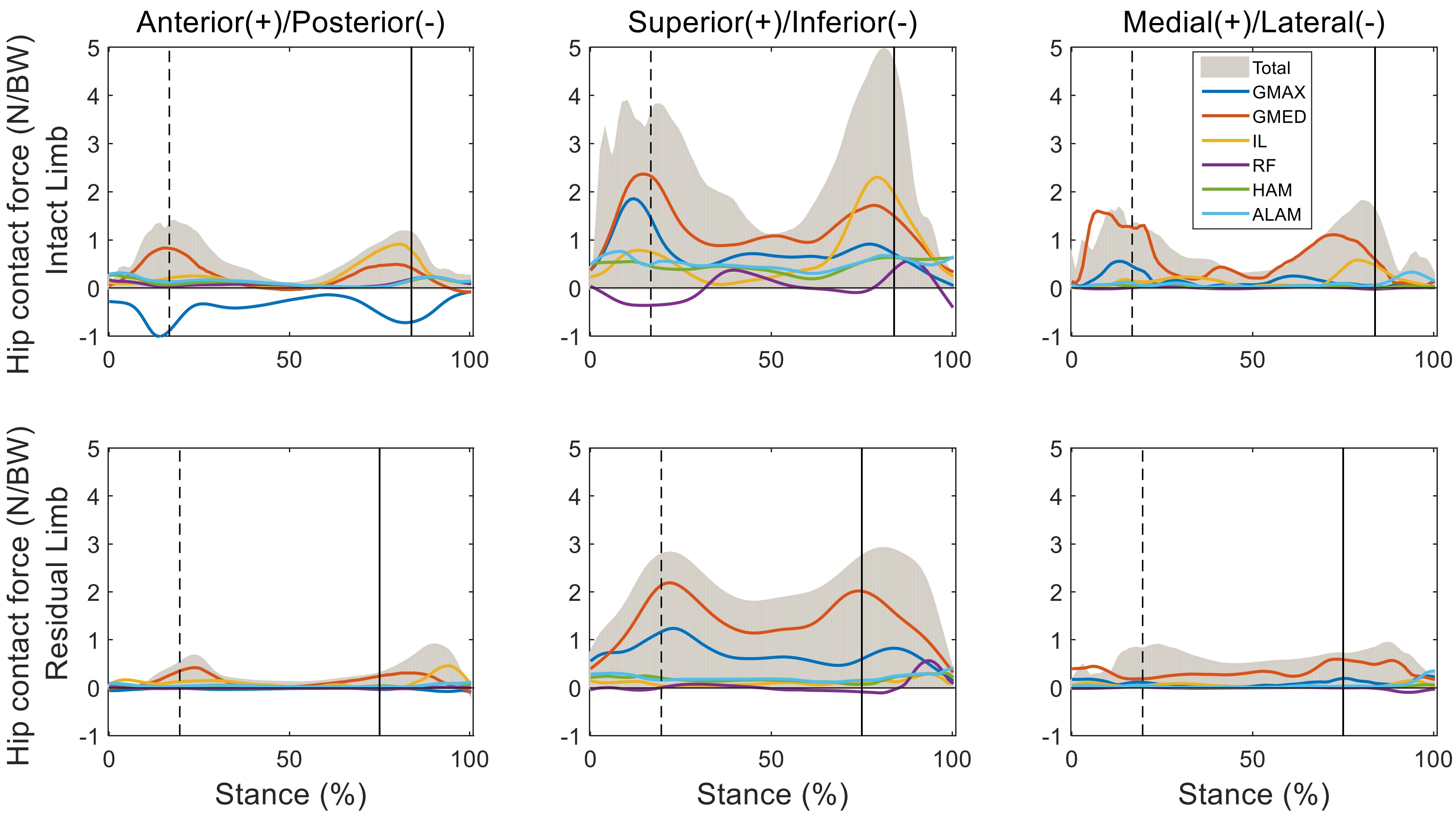

Figure 5.2. Individual hip-spanning muscles to the three components of the hip contact forces for the SP users with only ***passive*** knee prosthesis (n=3). The vertical dashed and solid lines indicate contralateral toe-off and contralateral heel-strike, respectively. The shaded area represents the total hip contact forces acting along the three coordinate directions.

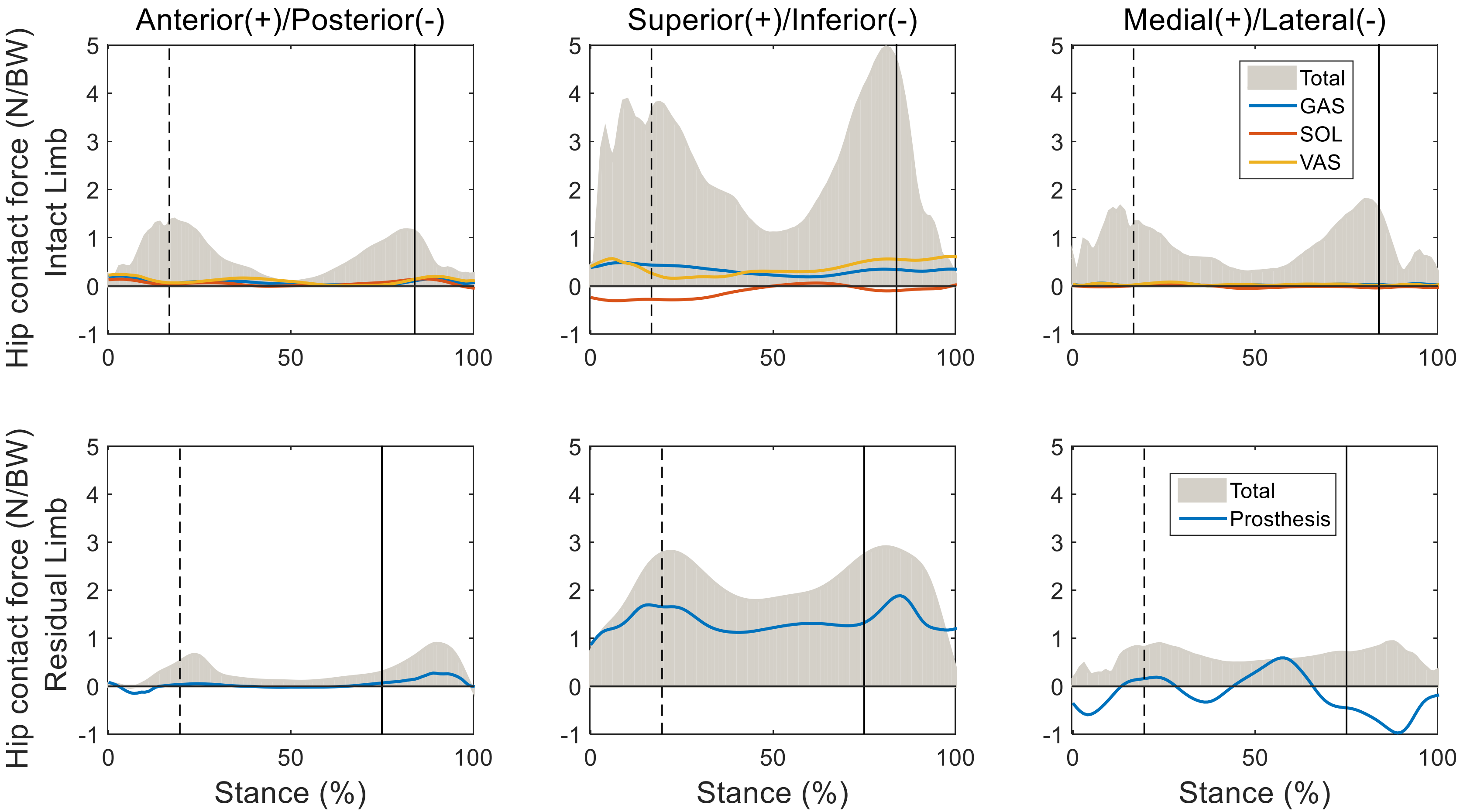

Figure 5.3. Individual non-hip-spanning muscles to the three components of the hip contact forces for the SP users with only ***passive*** knee prosthesis (n=3). The vertical dashed and solid lines indicate contralateral toe-off and contralateral heel-strike, respectively. The shaded area represents the total hip contact forces acting along the three coordinate directions.

5.3.1.2 Active knee prosthesis SP users

The hip contact forces were greater in the intact limb relative to the residual limb at CTO and CHS (mean difference: 0.04±0.01 and 0.18±0.08 N/BW, respectively) (Figure 5.4). Specifically, the anterior-posterior, superior-inferior and medial-lateral hip contact forces of the intact limb were higher than those of the residual limb at CTO (mean difference: 0.10±0.05, 0.45±0.15 and 0.44±0.20 N/BW, respectively) (Table 5.3). The peak hip contact force of the intact limb was greater than the residual limb at CHS for the superior-inferior direction (mean difference: 0.44±0.12 N/BW) (Table 5.4). GMED contributed to the anterior hip contact force, which the peak was higher in the intact limb than the residual limb at CTO (mean difference: 0.30±0.10 N/BW). The axial hip contact force was basically provided by GMED and GMAX, which the peak at CTO was greater in the intact limb than the residual limb (mean difference: 0.32±0.12 and 0.36±0.16 N/BW, respectively) (Table 5.3). The peak contribution to medial-lateral hip contact force of GMED was greater in the intact limb than the residual limb at CTO (mean difference: 0.65±0.35 N/BW) (Table 5.3) (Figure 5.5).

VAS generated most contribution to the superior hip contact forces at CTO and CHS with the peak of 0.47±0.20 and 0.41±0.25 N/BW, respectively, followed by GAS with the peak of 0.29±0.09 N/BW, respectively) (Table 5.3, Figure 5.6). While SOL contributed to the lateral hip contact force with the peak of 0.16±0.05 N/BW (Table 5.4, Figure 5.6).

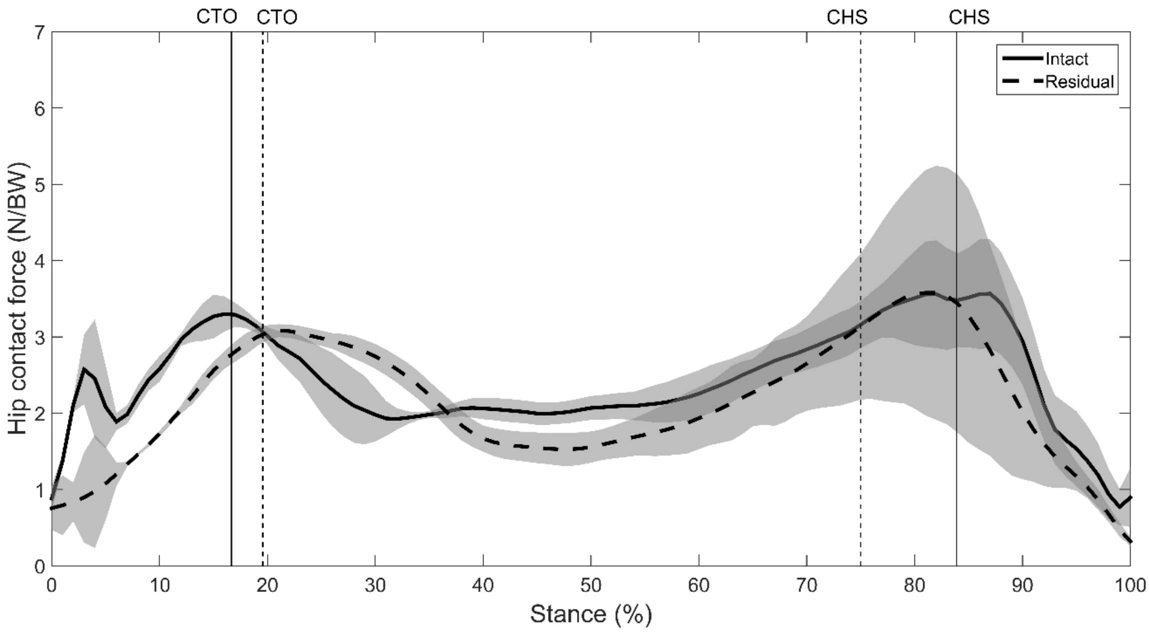

Figure 5.4. Total hip contact forces for the intact and residual limb of the SP users with only ***active*** knee prosthesis (n=3). The vertical solid lines indicate the intact limb and the vertical dashed lines indicate the residual limb.

Table 5.3. Individual muscle contribution to the peak hip contact forces during CTO for the SP users with only ***active*** knee prosthesis (n=3).

	Anterior(+)/ Posterior(-)		Superior(+)/ Inferior(-)		Medial(+)/ Lateral(-)	
	Intact	Residual	Intact	Residual	Intact	Residual
Hip-spanning muscles						
ALAM	0.05	0.02	0.52	0.43	0.03	<0.01
GMAX	-0.27	-0.25	0.92	0.58	0.32	0.05
GMED	0.81	0.51	1.82	1.50	0.97	0.32
IL	0.05	0.07	0.46	0.07	<0.01	0.04
RF	-0.01	-0.02	-0.12	0.05	<0.01	-0.02
HAM	0.04	0.02	0.34	0.34	0.02	0.02
Subtotal	**0.67**	**0.35**	**3.94**	**2.97**	**1.34**	**0.41**
Non-hip-spanning muscles						
GAS	0.03	---	0.33	---	0.01	---
SOL	-0.02	---	0.16	---	<0.01	---
VAS	0.02	---	0.47	---	<0.01	---
Subtotal	**0.03**	---	**0.96**	---	**0.01**	---
Others	**0.19**	**0.44**	**-1.87**	**-0.39**	**-0.39**	**0.11**
Total	**0.89**	**0.79**	**3.03**	**2.58**	**0.96**	**0.52**

Table 5.4. Individual muscle contribution to the peak hip contact forces during CHS for the SP users with only ***active*** knee prosthesis (n=3).

	Anterior(+)/ Posterior(-)		Superior(+)/ Inferior(-)		Medial(+)/ Lateral(-)	
	Intact	Residual	Intact	Residual	Intact	Residual
Hip-spanning muscles						
ALAM	0.16	0.04	0.55	0.41	0.05	0.02
GMAX	-0.39	-0.34	0.79	0.75	0.13	0.06
GMED	0.22	0.23	1.51	1.43	0.39	0.33
IL	0.55	0.38	1.81	0.08	0.12	0.18
RF	0.11	0.02	0.73	0.15	0.02	0.01
HAM	0.15	0.05	0.51	0.31	0.05	0.02
Subtotal	**0.80**	**0.38**	**5.90**	**3.13**	**0.76**	**0.62**
Non-hip-spanning muscles						
GAS	0.06	---	0.29	---	0.03	---
SOL	0.06	---	-0.19	---	0.01	---
VAS	0.11	---	0.41	---	0.04	---
Subtotal	**0.23**	---	**0.51**	---	**0.08**	---
Others	**-0.16**	**0.47**	**-2.99**	**-0.15**	**0.02**	**0.29**
Total	**0.87**	**0.85**	**3.42**	**2.98**	**0.86**	**0.91**

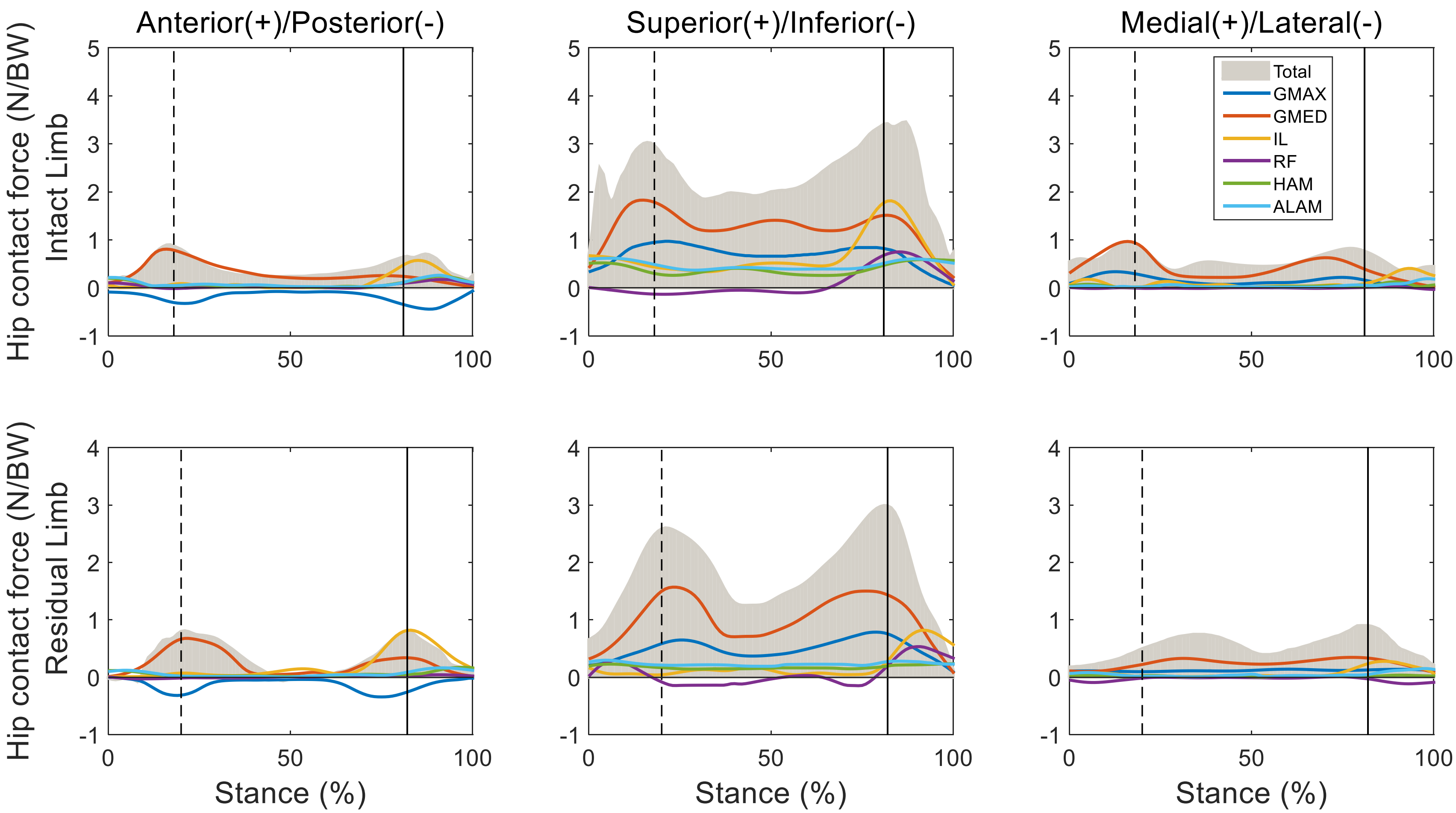

Figure 5.5. Individual hip-spanning muscles to the three components of the hip contact forces for the SP users with only ***active*** knee prosthesis (n=3). The vertical dashed and solid lines indicate contralateral toe-off and contralateral heel-strike, respectively. The shaded area represents the total hip contact forces acting along the three coordinate directions.

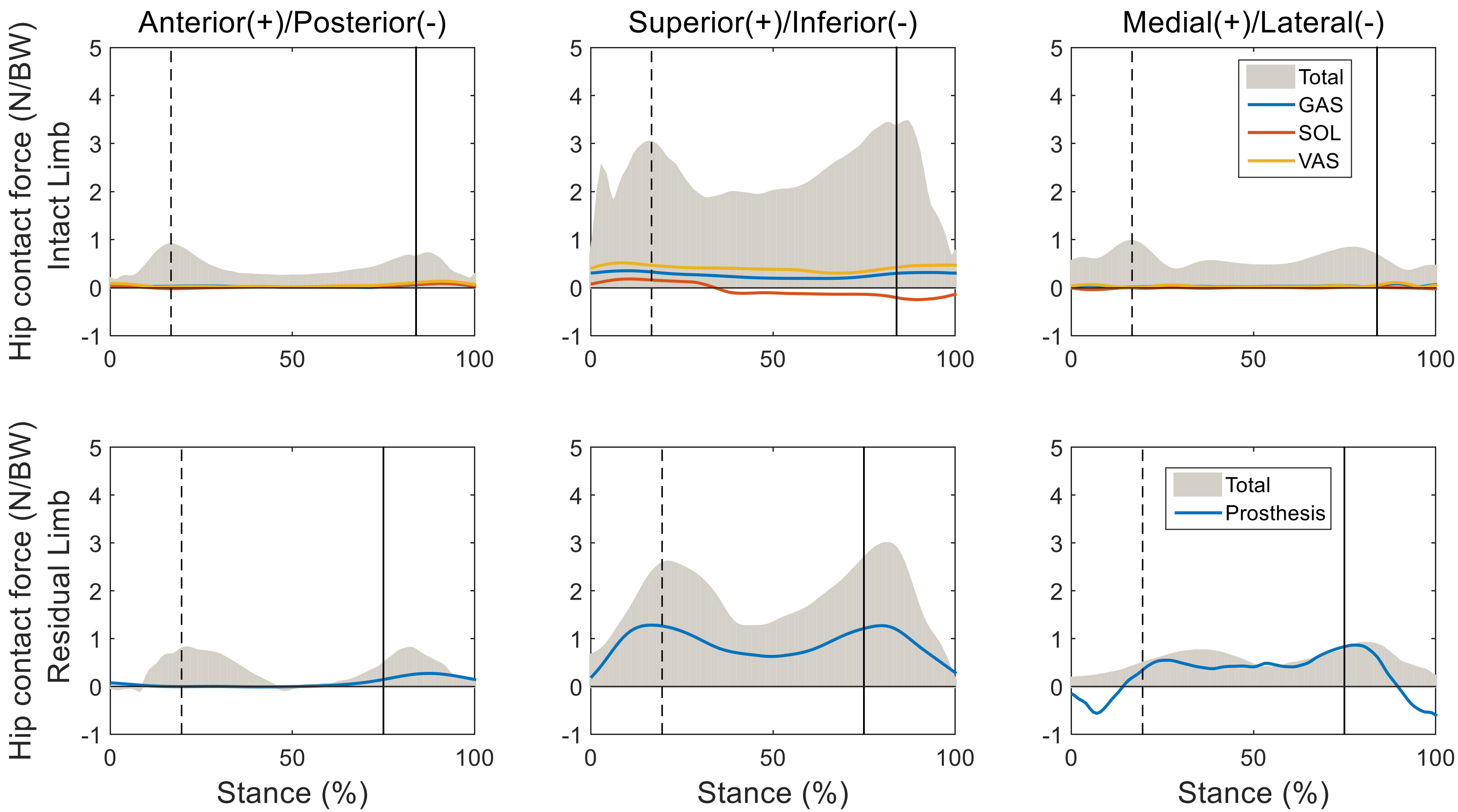

Figure 5.6. Individual non-hip-spanning muscles to the three components of the hip contact forces for the SP users with only ***active*** knee prosthesis (n=3). The vertical dashed and solid lines indicate contralateral toe-off and contralateral heel-strike, respectively. The shaded area represents the total hip contact forces acting along the three coordinate directions.

5.3.2 OI users

The hip contact forces were greater in the intact limb than the residual limb at CTO and CHS with the mean difference 0.43±0.21 and 1.50±0.90 N/BW, respectively (Figure 5.7). The peak hip contact forces were greater in the intact limb than those in the residual limb at CTO (mean difference: 0.17±0.10, 0.26±0.12 and 0.73±0.43 N/BW for the anterior-posterior, superior-posterior and medial-lateral directions, respectively) (Table 5.5, Figure 5.8). The peak anterior-posterior, superior-inferior and medial-lateral hip contact force was greater in the intact relative to the residual limb at CHS (mean difference: 0.30±0.10, 1.02±0.65 and 1.45±0.95 N/BW, respectively) (Table 5.6, Figure 5.8). The peak GMED contribution to the anterior-posterior hip contact forces was greater in the intact limb compared to the residual limb at CTO (mean difference: 0.34±0.11 N/BW). The peak GMAX in the intact limb to the posterior hip contact force was higher than that in the residual limb (mean difference: 0.05±0.01 and 0.73±0.23 N/BW at CTO and CHS, respectively) (Table 5.5, Figure 5.8). The vertical hip contact forces were mostly generated by GMED, which had a greater peak in the intact limb than the residual limb (mean difference: 0.75±0.22 and 0.20±0.11 N/BW at CTO and CHS, respectively) (Table 5.5-Table 5.6, Figure 5.8). The muscle contribution to mediolateral hip contact forces was significantly provided by GMED, which the peak was greater in the intact limb than that of the residual limb (mean difference: 1.21±0.43 and 0.82±0.26 N/BW at CTO and CHS, respectively). The contribution of GMAX to the medial hip contact force was greater in the intact limb than that in the residual limb at CTO (mean difference: 0.23±0.08 N/BW) and CHS (mean difference: 0.19±0.10 N/BW) (Table 5.5-Table 5.6, Figure 5.8).

Of those non-hip-spanning muscles, VAS generated more contribution to the anterior, superior and medial hip contact forces at CTO (0.08±0.02, 0.70±0.10 and 0.11±0.04 N/BW, respectively), followed by the posterior, superior and medial contribution of GAS (0.03±0.01, 0.50±0.10 and 0.07±0.02 N/BW, respectively). VAS also contributed more to the anterior, superior and lateral hip contact forces at CHS (0.14±0.07, 0.43±0.10 and 0.04±0.01 N/BW, respectively) (Table 5.5-Table 5.6, Figure 5.9).

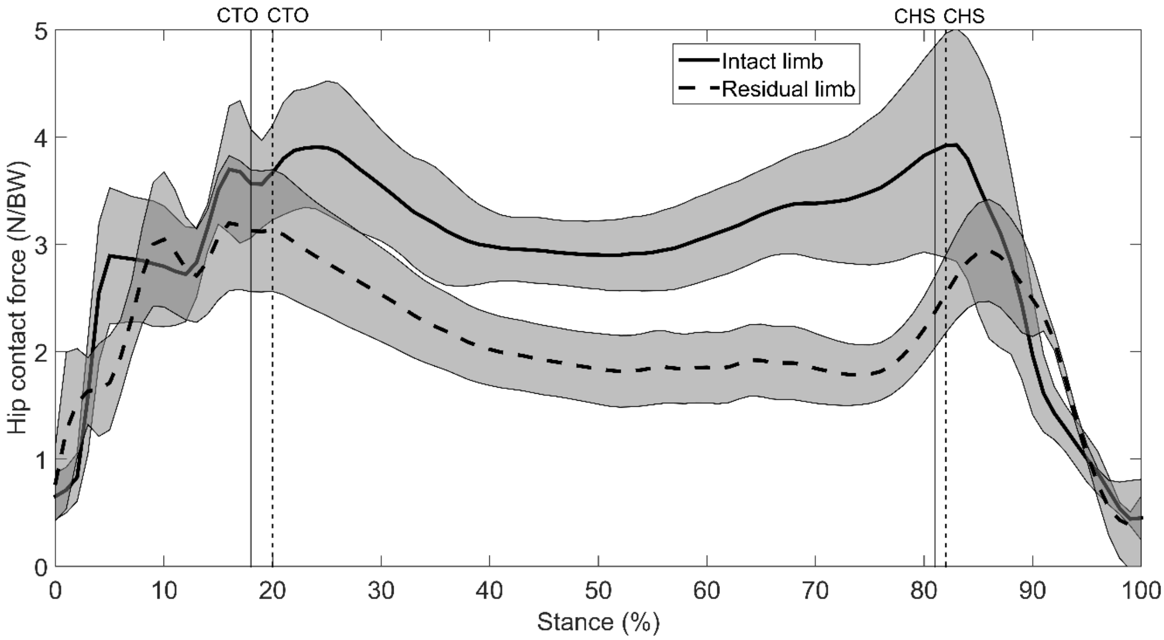

Figure 5.7. Total hip contact forces for the intact and residual limb of the OI users (n=4). The vertical solid lines indicate the intact limb and the vertical dashed lines indicate the residual limb.

Table 5.5. Individual muscle contribution to the peak hip contact forces during CTO for the OI users (n=4).

	Anterior(+)/ Posterior(-)		Superior (+)/ Inferior(-)		Medial(+)/ Lateral(-)	
	Intact	Residual	Intact	Residual	Intact	Residual
Hip-spanning muscles						
ALAM	-0.08	-0.01	0.13	0.39	0.16	0.04
GMAX	-0.23	-0.16	1.32	0.7	0.38	0.15
GMED	0.69	0.35	1.71	0.96	1.67	0.46
IL	0.18	0.13	0.04	-0.2	-0.06	0.05
RF	-0.01	-0.01	-0.09	-0.04	0.03	-0.01
HAM	-0.01	0.03	0.15	0.1	0.12	-0.03
Subtotal	**0.54**	**0.33**	**3.25**	**1.9**	**2.29**	**0.67**
Non-hip-spanning muscles						
GAS	-0.03	---	0.5	---	0.07	---
SOL	< 0.01	---	-0.25	---	0.03	---
VAS	0.08	---	0.7	---	0.11	---
Subtotal	**0.05**	**---**	**0.95**	**---**	**0.21**	**---**
Others	**0.4**	**0.5**	**-1.08**	**0.96**	**-0.82**	**0.27**
Total	**0.99**	**0.82**	**3.12**	**2.86**	**1.67**	**0.94**

Table 5.6. Individual muscle contribution to the peak hip contact forces during CHS for the OI users (n=4).

	Anterior(+)/ Posterior(-)		Superior(+)/ Inferior(-)		Medial(+)/ Lateral(-)	
	Intact	Residual	Intact	Residual	Intact	Residual
hip-spanning muscles						
ALAM	-0.08	-0.04	0.42	0.21	0.04	0.07
GMAX	-0.83	-0.1	0.47	0.15	0.26	0.07
GMED	0.05	0.24	0.94	0.74	1.09	0.27
IL	0.82	-0.04	1.07	0.25	0.5	0.13
RF	0.09	0.01	0.56	-0.07	-0.01	< 0.01
HAM	0.13	0.15	0.52	0.33	-0.05	0.02
Subtotal	**0.18**	**0.23**	**3.98**	**1.6**	**1.82**	**0.57**
Non-hip-spanning muscles						
GAS	0.04	---	0.22	---	0.01	---
SOL	0.09	---	0.23	---	-0.01	---
VAS	0.14	---	0.43	---	-0.04	---
Subtotal	**0.27**	**---**	**0.89**	**---**	**-0.04**	**---**
Others	**0.48**	**0.4**	**-1.58**	**0.67**	**-0.04**	**-0.29**
Total	**0.93**	**0.63**	**3.29**	**2.27**	**1.73**	**0.28**

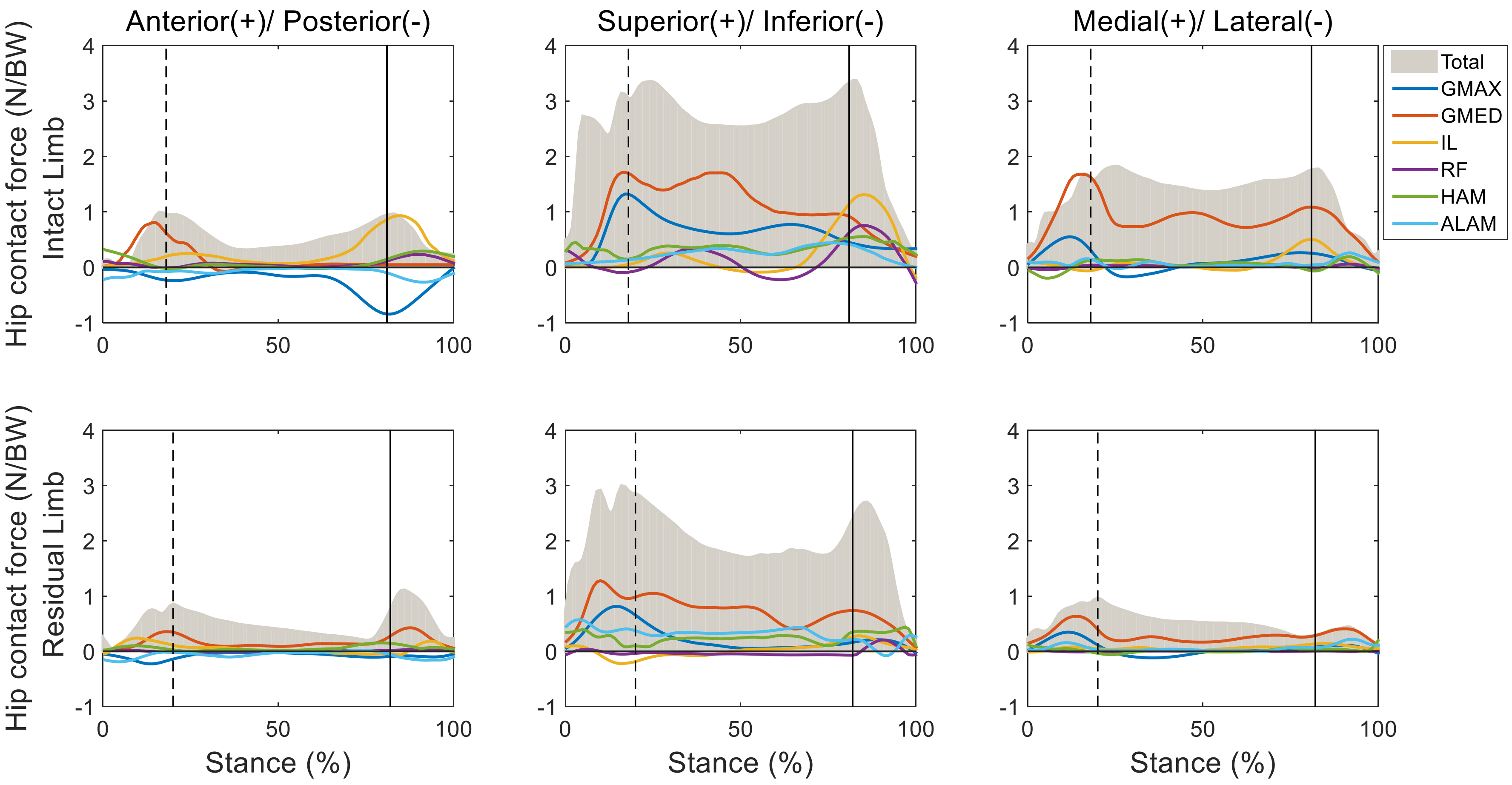

Figure 5.8. Individual hip-spanning muscles to the three components of the hip contact forces for the OI users (n=4). The vertical dashed and solid lines indicate contralateral toe-off and contralateral heel-strike, respectively. The shaded area represents the total hip contact forces acting along the three coordinate directions.

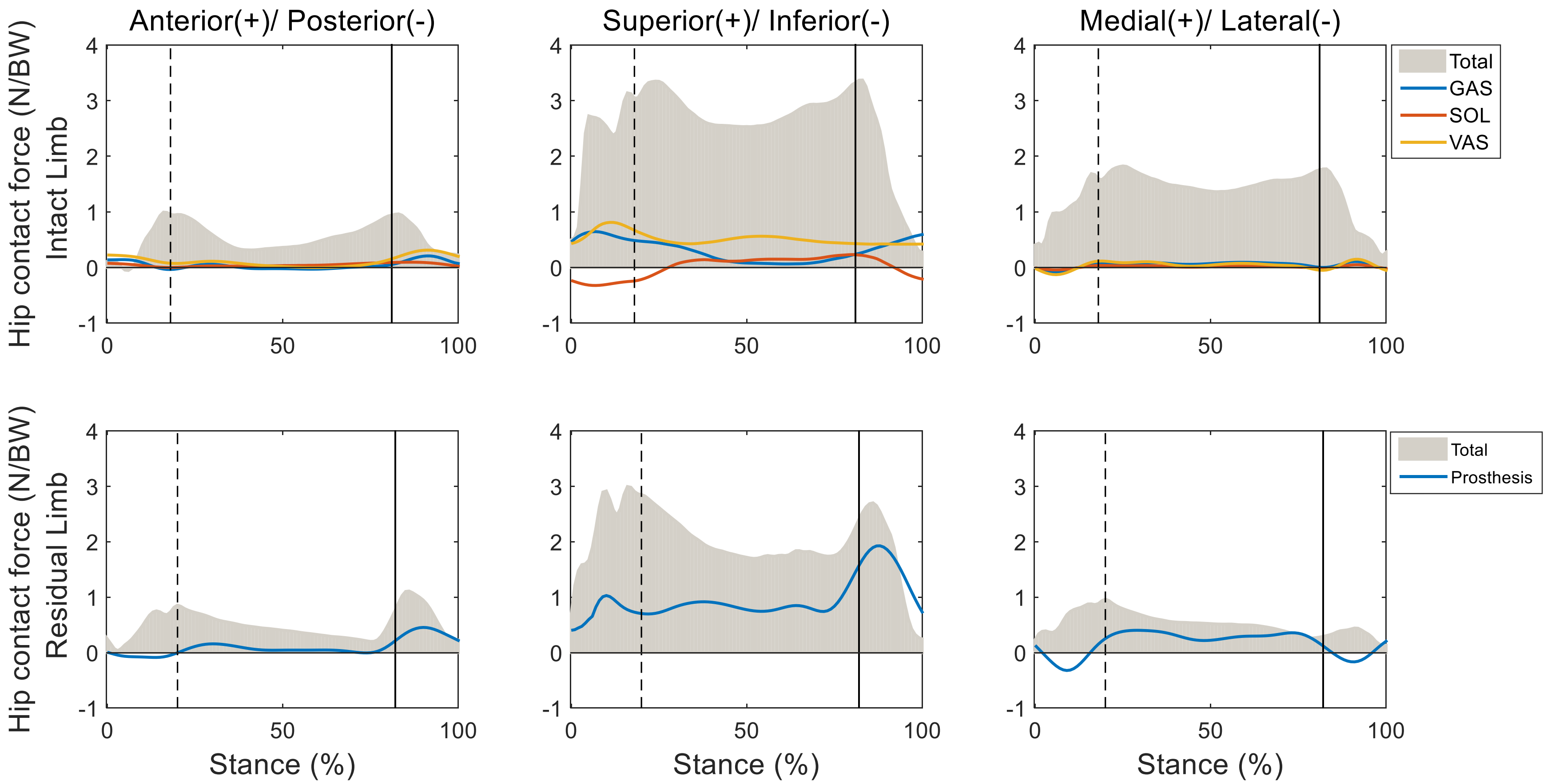

Figure 5.9. Individual non-hip-spanning muscles to the three components of the hip contact forces for the OI (n=4). The vertical dashed and solid lines indicate contralateral toe-off and contralateral heel-strike, respectively. The shaded area represents the total hip contact forces acting along the three coordinate directions.

5.4 Discussion

This study aimed to employ three-dimensional musculoskeletal modelling to analyze the individual muscle contribution to the hip contact forces in unilateral transfemoral amputees fitted with socket (passive and active knee prosthesis) and osseointegration prosthesis. The anterior-posterior, axial and medial-lateral hip contact forces were mostly generated by GMED and GMAX in the intact and residual limb among the SP and OI users; however, the magnitudes were greater in the intact limb than the residual limb.

The intact and residual limb resultant hip contact forces were in agreement with previous studies in terms of shape and number of peaks (Bergmann et al., 2001, Correa et al., 2010). For example, the model predicted two peaks in anterior-posterior, superior-inferior and mediolateral hip contact forces during stance. The resultant peak hip contact forces of the intact and residual limb were 3.83 and 2.92 N/BW for the SP users with passive knee, 3.30 and 2.75 N/BW for the SP users with active knee and 4.45 and 3.92 N/BW for the OI users, respectively. This result may be due to the greater GRF on the intact limb than the residual limb, which is consistent with previous studies (Silverman and Neptune, 2014). It might also be related to a gait adaptation of the amputees in which a reduction in hip extension has been reported to lead to decreased hip contact forces (Bennett et al., 2008, Beaulieu et al., 2010). As this study showed, the hip extension of the residual limb was smaller than that in the intact limb for the both SP and OI groups (Table 4.2-Table 4.7). Increase in the hip extension of the intact limb relative to the residual limb may be related to an increase in the hip extension moment which is consistent with previous studies (Sjödahl et al., 2003, Goujon-Pillet et al., 2008). This difference in hip extension angle and moment has been demonstrated to generate different hip contact forces (Wesseling et al., 2015).

The resultant peak hip contact forces in the intact limb of all the SP and OI users were greater than what measured (2.4 N/BW) on patients implanted with hip replacement, who walked at their normal speed (1.09 m/s); however, it was smaller than the peak hip contact forces (4.8 N/BW) in the same group walking at their fast speed of 1.46 m/s. The reason might be due to the relationship between the walking speed and joint contact forces. The hip contact forces may reduce when the walking speed decreases (Bergmann et al., 1993, Bergmann et al., 2001, Correa et al., 2010), which our results agreed with. The self-selected walking speed for SP users with passive knee, SP users with active knee and OI users was 1.19 m/s, 1.12 m/s and 1.29 m/s, respectively.

The predominant contribution to hip contact forces for the two SP-user groups and the OI users was mostly generated by the muscles crossing the hip joint in all three directions, specifically GMAX, GMED and IL, which have been shown in previous studies (Correa et al., 2010, Schache et al., 2018). GMED contributed anteriorly in both intact and residual limbs, while GMAX had a posterior contribution during stance. GMED and GMAX were the major contributors to the axial hip contact forces during the whole stance in the intact and the residual limb. In addition, GMED contributed more to the mediolateral hip contact forces throughout stance. Intact limb's GMAX contributed medially in the first half of stance, while it contributed to medial hip contact forces during the whole stance in the residual limb. Furthermore, IL contributed more superiorly to hip contact forces in late-stance. However, peak contribution of the hip muscles was higher in the intact limb than the residual limb. This increase might be pertained to the greater intact limb muscles forces than those in the residual limb, which resulted from higher intact limb's hip moments due to an increase in hip extension and adduction than that in the residual limb (Lenaerts et al., 2009, Lim et al., 2013, Valente et al., 2013, Lin et al., 2015, Wesseling et al., 2015). It has also been indicated that reduction in hip extension may be related to hip extensors weakness (Tranberg et al., 2011). In addition, increasing in hip contact forces has been influenced by increase in hip abductors (Valente et al., 2013, Wesseling et al., 2015). The increase in hip extension of the intact limb than the residual limb would thereby support the evidence of increase in hip joint loading which leads to anterior hip pain (Lewis et al., 2010). It also might be related to the longer stance phase of the intact limb, which led to the dependency of the body on the intact limb and was confirmed by greater GRFs of the intact limb to that of the residual limb (Nolan et al., 2003).

The muscles that did not cross the hip joint also had a considerable contribution to hip contact forces. VAS, SOL and GAS showed two peaks in the first and second half of stance, which is in contrast to previous healthy study showing one peak during stance (Correa et al., 2010). VAS contributed more to anterior and superior hip contact forces, while SOL had a greater contribution to anterior hip contact forces in mid-stance than the other two muscles. In addition, VAS and GAS contributed more to medial hip contact forces in the first half of stance. The contribution of ankle plantarflexors and knee extensors to hip contact forces is related to dynamic coupling. All lower limb muscles contribute to accelerate the joints and due to the relationship between angular acceleration of joints and joint contact forces, each muscle contributes to all joints contact forces (Zajac and Gordon, 1989, Pandy, 2001, Correa et al., 2010).

The prosthesis also contributed to the hip contact forces via coupling dynamic theory. It contributed to the posterior and anterior hip contact forces in the first and second half of stance, respectively for the three groups of the amputees (Figure 5.3, Figure 5.6, Figure 5.9). Furthermore, the prosthesis was the major contributor to the superior component of the hip contact forces during the whole stance. However, the prosthesis contribution to the medial-lateral hip contact forces was different between amputees. The amputees showed lateral, medial and lateral contribution of their prosthesis to hip contact forces during early-stance, mid-stance and late-stance, respectively. In general, its function was similar to the overall role of the VAS, SOL and GAS of the intact limb in superior and medial contribution to hip contact forces during the entire stance.

The first limitation is that averaging the results may not be a proper way to conclude further outcomes due to differences in knee types of the prostheses; however, the joints kinematics and moments of the amputees showed no significant difference (Figure 4.12, Figure 4.13). Further study is needed to individually consider different knee types in a broad range of amputees. Another potential limitation is that the intrinsic properties of the residual limb muscles such as atrophy and maximum isometric force were kept equal to what is in the intact limb's muscles, and this may affect the muscle forces calculation. Thirdly, neither muscles atrophy nor fatigue considered in the objective function used to calculate muscle forces, which was based on minimization of the sum of squared muscles activations. The fatigue-related cost functions may be more suitable for gait analysis in disabled population (Ackermann and Van den Bogert, 2010). Finally, the knee joint of the residual limb was modeled as a hinge joint, which may not be representative of an actual active knee joint of the prosthesis and may affect the muscle forces results of the reattached muscles.

The current study indicated greater hip muscles forces as well as muscle contributions to the hip contact forces of the intact than those in the residual limb of amputees. Increased hip extension of the intact limb was pertained to increase in the intact limb hip muscles forces and muscle contribution to hip contact forces. The overall trend of individual muscle contribution to hip contact forces in the intact and the residual limb was similar in the SP and OI users; however, the OI users showed less asymmetry in muscle contribution to hip contact forces between the two limbs than the SP users. Figure 5.10 depicted that there was significant difference ($P=0.028$) in hip contact impulse during stance phase between the intact and residual limb when considering the effect of socket. But we did not find any significant difference in hip contact impulse between the two limbs for the OI users ($P=0.068$). It should be mentioned that the power of data is too small to do statistical analysis between the intact and residual limb of the osseointegrated amputees. However, the outcome concludes that the osseointegration surgery might result less risk of osteoarthritis in the hip of the intact limb. As shown in section 4.3.2, the joint kinematics' magnitudes of the intact limb had a small difference compared to those of the residual limb. In addition, people with active knee demonstrated small differences in the hip angles between the two limbs if compared to the SP users with passive knee. The result may be useful to devise new rehabilitation training programs and new prostheses to improve their function.

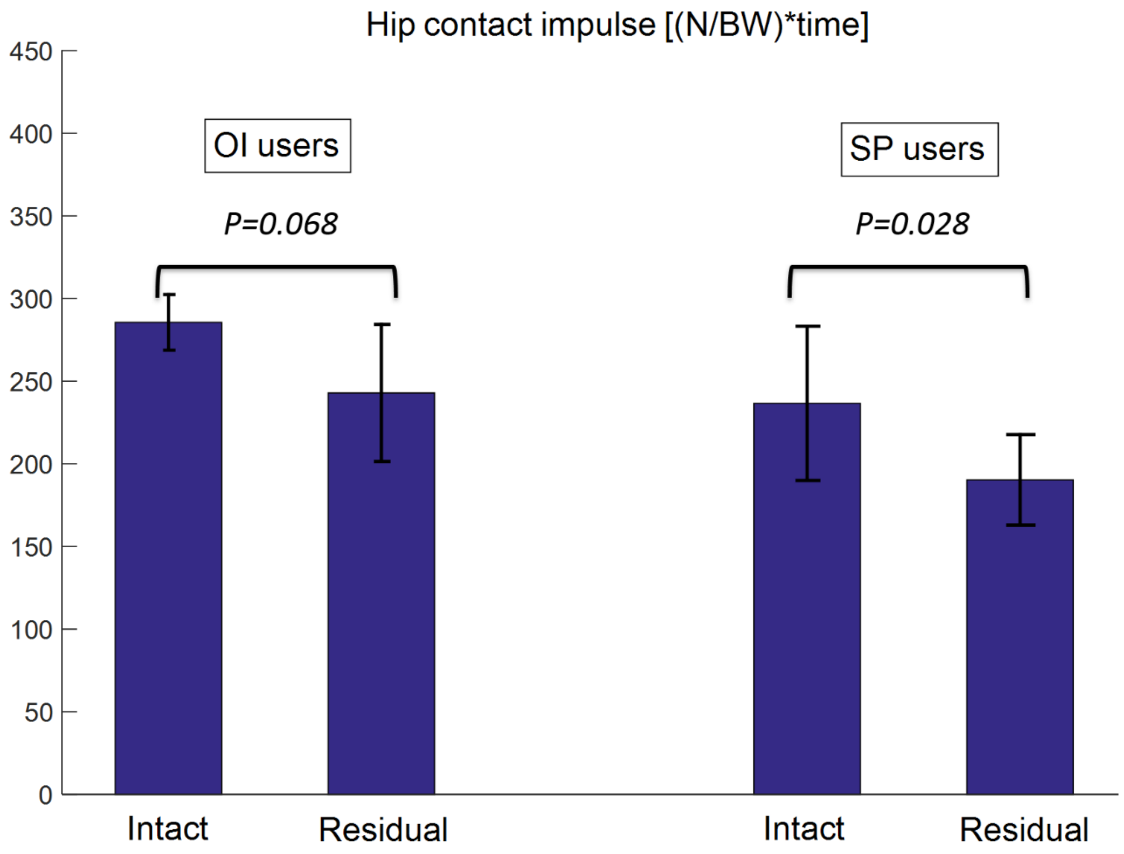

Figure 5.10. Hip contact impulse between the intact and residual limb for SP and OI user

Chapter 6. Summary and future work

The main focus of this thesis was to enhance understanding of the lower limb muscles during walking in unilateral transfemoral amputees with socket and osseointegration prosthesis. Firstly, a three-dimensional musculoskeletal modeling was developed in OpenSim for amputees. Secondly, a computational and dynamical framework was used to investigate the mechanism utilized by amputees. The results provided unique insight into the role of lower extremity muscles to forward propulsion, body support and mediolateral balance. In addition, the dynamic function of muscles to joint contact forces was investigated. This chapter outlines a brief summary of findings, associated implications and possible future advancements based on the limitations addressed in this thesis.

Computational and dynamical musculoskeletal frameworks have the potential to quantify individual muscle behavior which are impossible to be experimentally measured during walking such as muscle forces and muscle contribution. In Chapter 3, experimental data and an advanced developed computer-based modeling was used to find walking mechanism amongst transfemoral amputees. In this way, marker trajectories, ground reaction forces and EMG data were simultaneously collected for three amputees fitted with socket with passive knee joint, three amputees fitted with socket with active knee joint and four osseointegrated amputees during their self-selected over-ground walking. A generic model was developed in OpenSim for every single transfemoral amputee to individually simulate their walking and then calculate lower extremity joint angles and joint moments through inverse kinematics and inverse dynamics, respectively. The static optimization method was used to decompose joint moments into individual muscle to generate forces. These forces then applied to calculate muscle contribution to walking using induced acceleration analysis approach. Combined muscle forces and muscle contribution to center of mass acceleration, individual muscle contribution to joint contact forces were calculated for the amputees while walking.

Chapter 4 addressed the changes in lower limb spatiotemporal parameters, joint kinematics and kinetics, muscle forces and muscle contribution to walking between the intact and the residual limb for the three-group of amputees. The results showed that the intact limb hip muscles contributed more to propulsion, support and mediolateral balance compared to those of the residual limb. In general, the hip extension and abduction of the intact limb were greater than the residual limb, which might be associated with increase in anterior pelvis tilt when the residual limb was in stance compared to pelvis tilt when the intact limb was in stance. The differences in hip movement between the intact and residual limb were found to relate to the greater intact limb step length than that of the residual limb. However, the OI users showed less asymmetry in joint kinematics between the two limbs, which might be pertained to the direct attachment of the femur to the implant. The results also showed that the prosthesis functioned as the major contributor to walking in the residual limb. VAS of the intact limb contributed more to the fore-aft and vertical body center of mass acceleration in the first half of stance than other intact limb's muscles. Of the hip muscles, gluteal muscles were the main contributors to the fore-aft and vertical body center of mass acceleration in early to mid-stance. In addition, RF contributed more posterior and IL contributed more anterior than those of the residual limb. One of the key findings of this study was differences in contribution of VAS, SOL and GAS in the intact limb to mediolateral center of mass acceleration. The SP users demonstrated medial contribution of these muscle which contrasted with their lateral contribution in non-amputees from previous studies; however, SOL and GAS of the OI users generated lateral contribution which was similar to non-amputees. This might be associated with the greater step width and hip abduction in the intact limb compared to the residual limb.

Chapter 5 investigated individual muscle contribution to hip contact forces between the intact and residual limb in the SP and OI users. Overall, the hip contact forces of the intact limb were greater than the residual limb in all amputees. The resultant hip contact forces agreed with previous studies in terms of shape and number of peaks. The resultant peak of the hip contact forces of the intact limb was larger than that of the residual limb, which might be due to the greater ground reaction forces of the intact limb compared to the residual limb. It also might be due to walking mechanism of the amputees to reduce hip extension of the residual limb which is relative to reduction in hip contact forces. *Gluteal* and *iliopsoas* muscles were found major contributors to hip contact forces in both limbs. *Gluteus maximus* contributed to posterior hip contact forces, while *gluteus medius* contributed anteriorly throughout stance phase. The non-hip-spanning muscles and prosthesis also contributed to hip contact forces through dynamic coupling approach.

There are several limitations of the present study. Firstly, since three amputees had passive knee and the other three had active knee in their prosthesis, and different types of knee may affect joint kinematics and kinetics, averaging the results for all the participants may not be a proper way forward to show the muscle behaviors during walking. For example, amputees with mechanical passive knee are required to lock their prosthetic knee in full extension for stability during stance. It also requires to applying full body weight from stance stabilities feature. While microprocessor-controlled knee prostheses are designed to reduce the need for compensation of the intact limb's muscles. This might lead to differences in muscle recruitment. To address this limitation, the muscle contributions for participants with active and passive knee joints were also analyzed separately. Secondly, there was a lack of participants' experience information. For example, the level of participant's satisfaction with their socket were not scored, which may affect the results of gait asymmetries. Thirdly, the cost function used in the static optimization problem minimized the sum of squares of muscle activations, and this did not consider musculoskeletal conditions that are known to adversely affect joint function in these subjects. For example, muscle fatigue frequently occurs in atrophied muscles of lower limb amputees, and this may influence gait compensation strategies. Fourthly, residual limb muscle-tendon parameters such as maximum isometric force as well as atrophy were not considered in the musculoskeletal model, and this may ultimately result in larger muscle force predictions. In addition, a rigid connection was assumed between the residual limb and the socket due to the negligible deformation between the socket and stump, which need to be considered in further studies. Furthermore, the use of inverse dynamics may be challenging to calculate joint forces and moments. Further study is needed to consider direct measurement of joint moments in prosthesis components. Finally, the low number of subjects recruited may not be representative of the average data for a broad population of amputees and may affect statistically the results. Although, the sample size was sufficient to detect significant differences in spatiotemporal parameters and joint angles and joint moments between limbs, it did not allow to consider difference in age and gender of participants.

Chapter 7. References

ACKERMANN, M. & VAN DEN BOGERT, A. J. 2010. Optimality principles for model-based prediction of human gait. *Journal of biomechanics,* 43**,** 1055-1060.

ACKLAND, D. C., LIN, Y.-C. & PANDY, M. G. 2012. Sensitivity of model predictions of muscle function to changes in moment arms and muscle–tendon properties: a Monte-Carlo analysis. *Journal of biomechanics,* 45**,** 1463-1471.

AIHWB 2014. Cardiovascular disease, diabetes and chronic kidney disease: Australian facts: morbidity hospital care. *Cardiovascular, diabetes and chronic kidney disease series no. 3. Cat. no. CDK 3. Canberra: AIHW*.

AIT-HADDOU, R., BINDING, P. & HERZOG, W. 2000. Theoretical considerations on cocontraction of sets of agonistic and antagonistic muscles. *Journal of biomechanics,* 33**,** 1105-1111.

AL MUDERIS, M. M., LU, W. Y., LI, J. J., KAUFMAN, K., ORENDURFF, M., HIGHSMITH, M. J., LUNSETH, P. A. & KAHLE, J. T. 2018. Clinically relevant outcome measures following limb osseointegration; systematic review of the literature. *Journal of orthopaedic trauma,* 32**,** e64-e75.

ALLEN, J. L. & NEPTUNE, R. R. 2012. Three-dimensional modular control of human walking. *Journal of biomechanics,* 45**,** 2157-2163.

AMARO, A., AMADO, F., DUARTE, J. & APPELL, H.-J. 2007. Gluteus medius muscle atrophy is related to contralateral and ipsilateral hip joint osteoarthritis. *International Journal of Sports Medicine,* 28**,** 1035-1039.

ANDERSON, F. C. & PANDY, M. G. 1999. A dynamic optimization solution for vertical jumping in three dimensions. *Computer methods in biomechanics and biomedical engineering,* 2**,** 201-231.

ANDERSON, F. C. & PANDY, M. G. 2001a. Dynamic optimization of human walking. *Journal of biomechanical engineering,* 123**,** 381-390.

ANDERSON, F. C. & PANDY, M. G. 2001b. Static and dynamic optimization solutions for gait are practically equivalent. *Journal of biomechanics,* 34**,** 153-161.

ANDERSON, F. C. & PANDY, M. G. 2003. Individual muscle contributions to support in normal walking. *Gait & posture,* 17**,** 159-169.

BAE, T., CHOI, K. & MUN, M. 2009. Level walking and stair climbing gait in above-knee amputees. *Journal of medical engineering & technology,* 33**,** 130-135.

BAE, T. S., CHOI, K., HONG, D. & MUN, M. 2007. Dynamic analysis of above-knee amputee gait. *Clinical Biomechanics,* 22**,** 557-566.

BAHLER, A. S. 1968. Modeling of mammalian skeletal muscle. *IEEE Transactions on Biomedical Engineering***,** 249-257.

BEAULIEU, M. L., LAMONTAGNE, M. & BEAULÉ, P. E. 2010. Lower limb biomechanics during gait do not return to normal following total hip arthroplasty. *Gait & posture,* 32**,** 269-273.

BENNETT, D., HUMPHREYS, L., O'BRIEN, S., KELLY, C., ORR, J. & BEVERLAND, D. 2008. Gait kinematics of age-stratified hip replacement patients—a large scale, long-term follow-up study. *Gait & posture,* 28**,** 194-200.

BERGMANN, G., DEURETZBACHER, G., HELLER, M., GRAICHEN, F., ROHLMANN, A., STRAUSS, J. & DUDA, G. 2001. Hip contact forces and gait patterns from routine activities. *Journal of biomechanics,* 34**,** 859-871.

BERGMANN, G., GRAICHEN, F. & ROHLMANN, A. 1993. Hip joint loading during walking and running, measured in two patients. *Journal of biomechanics,* 26**,** 969-990.

BERKE, G., BUELL, N., FERGASON, J., GAILEY, R., HAFNER, B., HUBBARD, S. & WILLINGHAM, L. 2008. Transfemoral Amputation: The Basics and Beyond. *Prosthetics Research Study*.

BOGEY, R., PERRY, J. & GITTER, A. 2005. An EMG-to-force processing approach for determining ankle muscle forces during normal human gait. *IEEE Transactions on Neural Systems and Rehabilitation Engineering,* 13**,** 302-310.

BONATO, P., ROY, S. H., KNAFLITZ, M. & DE LUCA, C. J. 2001. Time-frequency parameters of the surface myoelectric signal for assessing muscle fatigue during cyclic dynamic contractions. *IEEE Transactions on Biomedical Engineering,* 48**,** 745-753.

BOONSTRA, A., SCHRAMA, J., EISMA, W., HOF, A. & FIDLER, V. 1996. Gait analysis of transfemoral amputee patients using prostheses with two different knee joints. *Archives of physical medicine and rehabilitation,* 77**,** 515-520.

BRAND, R. A., PEDERSEN, D. R., DAVY, D. T., KOTZAR, G. M., HEIPLE, K. G. & GOLDBERG, V. M. 1994. Comparison of hip force calculations and measurements in the same patient. *The Journal of arthroplasty,* 9**,** 45-51.

BRÅNEMARK, R., BERLIN, Ö., HAGBERG, K., BERGH, P., GUNTERBERG, B. & RYDEVIK, B. 2014. A novel osseointegrated percutaneous prosthetic system for the treatment of patients with transfemoral amputation: A prospective study of 51 patients. *The bone & joint journal,* 96**,** 106-113.

BRANEMARK, R., BRANEMARK, P., RYDEVIK, B. & MYERS, R. R. 2001. Osseointegration in skeletal reconstruction and rehabilitation: a review. *Journal of rehabilitation research and development,* 38**,** 175-182.

BUCHANAN, T. S., LLOYD, D. G., MANAL, K. & BESIER, T. F. 2004. Neuromusculoskeletal modeling: estimation of muscle forces and joint moments and movements from measurements of neural command. *Journal of applied biomechanics,* 20**,** 367-395.

BUCHANAN, T. S., LLOYD, D. G., MANAL, K. & BESIER, T. F. 2005. Estimation of muscle forces and joint moments using a forward-inverse dynamics model. *Medicine & Science in Sports & Exercise,* 37**,** 1911-1916.

BURKETT, B., SMEATHERS, J. & BARKER, T. M. 2004. A computer model to simulate the swing phase of a transfemoral prosthesis. *Journal of Applied Biomechanics,* 20**,** 25-37.

BUTLER, K., BOWEN, C., HUGHES, A.-M., TORAH, R., AYALA, I., TUDOR, J. & METCALF, C. D. 2014. A systematic review of the key factors affecting tissue viability and rehabilitation outcomes of the residual limb in lower extremity traumatic amputees. *Journal of Tissue Viability,* 23**,** 81-93.

CAPPOZZO, A., FIGURA, F., GAZZANI, F., LEO, T. & MARCHETTI, M. 1982. Angular displacements in the upper body of AK amputees during level walking. *Prosthetics and orthotics international,* 6**,** 131-138.

CHUMANOV, E. S., HEIDERSCHEIT, B. C. & THELEN, D. G. 2011. Hamstring musculotendon dynamics during stance and swing phases of high speed running. *Medicine and science in sports and exercise,* 43**,** 525.

CLEATHER, D. J. & BULL, A. M. 2011. An optimization-based simultaneous approach to the determination of muscular, ligamentous, and joint contact forces provides insight into musculoligamentous interaction. *Annals of biomedical engineering,* 39**,** 1925-1934.

COLLINS, J. 1995. The redundant nature of locomotor optimization laws. *Journal of biomechanics,* 28**,** 251-267.

CORREA, T. A., CROSSLEY, K. M., KIM, H. J. & PANDY, M. G. 2010. Contributions of individual muscles to hip joint contact force in normal walking. *Journal of biomechanics,* 43**,** 1618-1622.

CROWINSHIELD, R. D., BRAND, R. A. & JOHNSTON, R. 1978. The effects of walking velocity and age on hip kinematics and kinetics. *Clinical Orthopaedics and Related Research***,** 140-144.

CROWNINSHIELD, R., JOHNSTON, R., ANDREWS, J. & BRAND, R. 1978. A biomechanical investigation of the human hip. *Journal of biomechanics,* 11**,** 75-85.

CROWNINSHIELD, R. D. & BRAND, R. A. 1981. A physiologically based criterion of muscle force prediction in locomotion. *Journal of biomechanics,* 14**,** 793-801.

DAMM, P., SCHWACHMEYER, V., DYMKE, J., BENDER, A. & BERGMANN, G. 2013. In vivo hip joint loads during three methods of walking with forearm crutches. *Clinical Biomechanics,* 28**,** 530-535.

DAVY, D. & AUDU, M. 1987. A dynamic optimization technique for predicting muscle forces in the swing phase of gait. *Journal of biomechanics,* 20**,** 187-201.

DAVY, D., KOTZAR, G., BROWN, R., HEIPLE, K., GOLDBERG, V., HEIPLE, J. K., BERILLA, J. & BURSTEIN, A. 1988. Telemetric force measurements across the hip after total arthroplasty. *The Journal of bone and joint surgery. American volume,* 70**,** 45-50.

DE CERQUEIRA, A. S. O., YAMAGUTI, E. Y., MOCHIZUKI, L., AMADIO, A. C. & SERRÃO, J. C. 2013. Ground reaction force and electromyographic activity of transfemoral amputee gait: a case series. *Brazilian Journal of Kinanthropometry and Human Performance,* 15**,** 16-26.

DE LUCA, C. J. 1997. The use of surface electromyography in biomechanics. *Journal of applied biomechanics,* 13**,** 135-163.

DEBAERE, S., DELECLUSE, C., AERENHOUTS, D., HAGMAN, F. & JONKERS, I. 2015. Control of propulsion and body lift during the first two stances of sprint running: a simulation study. *Journal of sports sciences,* 33**,** 2016-2024.

DELP, S. L., ANDERSON, F. C., ARNOLD, A. S., LOAN, P., HABIB, A., JOHN, C. T., GUENDELMAN, E. & THELEN, D. G. 2007. OpenSim: open-source software to create and analyze dynamic simulations of movement. *IEEE transactions on biomedical engineering,* 54**,** 1940-1950.

DELP, S. L. & LOAN, J. P. 1995. A graphics-based software system to develop and analyze models of musculoskeletal structures. *Computers in biology and medicine,* 25**,** 21-34.

DELP, S. L., LOAN, J. P., HOY, M. G., ZAJAC, F. E., TOPP, E. L. & ROSEN, J. M. 1990. An interactive graphics-based model of the lower extremity to study orthopaedic surgical procedures. *Biomedical Engineering, IEEE Transactions on,* 37**,** 757-767.

DEMET, K., MARTINET, N., GUILLEMIN, F., PAYSANT, J. & ANDRE, J.-M. 2003. Health related quality of life and related factors in 539 persons with amputation of upper and lower limb. *Disability and rehabilitation,* 25**,** 480-486.

DEVAN, H., HENDRICK, P., RIBEIRO, D. C., HALE, L. A. & CARMAN, A. 2014. Asymmetrical movements of the lumbopelvic region: is this a potential mechanism for low back pain in people with lower limb amputation? *Medical hypotheses,* 82**,** 77-85.

DILLINGHAM, T. R., PEZZIN, L. E. & SHORE, A. D. 2005. Reamputation, mortality, and health care costs among persons with dysvascular lower-limb amputations. *Archives of physical medicine and rehabilitation,* 86**,** 480-486.

DILLON, M. P., FORTINGTON, L. V., AKRAM, M., ERBAS, B. & KOHLER, F. 2017. Geographic variation of the incidence rate of lower limb amputation in Australia from 2007-12. *PloS one,* 12**,** e0170705.

DORN, T. W. 2011. *Computational modelling of lower-limb muscle function in human running.*

DORN, T. W., LIN, Y.-C. & PANDY, M. G. 2012a. Estimates of muscle function in human gait depend on how foot-ground contact is modelled. *Computer methods in biomechanics and biomedical engineering,* 15**,** 657-668.

DORN, T. W., SCHACHE, A. G. & PANDY, M. G. 2012b. Muscular strategy shift in human running: dependence of running speed on hip and ankle muscle performance. *Journal of Experimental Biology,* 215**,** 1944-1956.

DUDEK, N. L., MARKS, M. B., MARSHALL, S. C. & CHARDON, J. P. 2005. Dermatologic conditions associated with use of a lower-extremity prosthesis. *Archives of physical medicine and rehabilitation,* 86**,** 659-663.

DUMAS, R., BRÅNEMARK, R. & FROSSARD, L. 2016. Gait analysis of transfemoral amputees: errors in inverse dynamics are substantial and depend on prosthetic design. *IEEE transactions on neural systems and rehabilitation engineering,* 25**,** 679-685.

DUMAS, R., CHEZE, L. & FROSSARD, L. A. 2009. Load during prosthetic gait: Is direct measurement better than inverse dynamics?

EDWARDS, W. B., TAYLOR, D., RUDOLPHI, T. J., GILLETTE, J. C. & DERRICK, T. R. 2010. Effects of running speed on a probabilistic stress fracture model. *Clinical Biomechanics,* 25**,** 372-377.

ERDEMIR, A., MCLEAN, S., HERZOG, W. & VAN DEN BOGERT, A. J. 2007. Model-based estimation of muscle forces exerted during movements. *Clinical biomechanics,* 22**,** 131-154.

EWING, K. A., FERNANDEZ, J. W., BEGG, R. K., GALEA, M. P. & LEE, P. V. 2016. Prophylactic knee bracing alters lower-limb muscle forces during a double-leg drop landing. *Journal of biomechanics,* 49**,** 3347-3354.

FELSON, D. T. 2004. Obesity and vocational and avocational overload of the joint as risk factors for osteoarthritis. *The Journal of Rheumatology Supplement,* 70**,** 2-5.

FELSON, D. T., ZHANG, Y., ANTHONY, J. M., NAIMARK, A. & ANDERSON, J. J. 1992. Weight loss reduces the risk for symptomatic knee osteoarthritis in women: the Framingham Study. *Annals of internal medicine,* 116**,** 535-539.

FERRIS, A. E., SMITH, J. D., HEISE, G. D., HINRICHS, R. N. & MARTIN, P. E. 2017. A general model for estimating lower extremity inertial properties of individuals with transtibial amputation. *Journal of Biomechanics,* 54**,** 44-48.

FOUCHER, K. C., HURWITZ, D. E. & WIMMER, M. A. 2009. Relative importance of gait vs. joint positioning on hip contact forces after total hip replacement. *Journal of Orthopaedic Research,* 27**,** 1576-1582.

FREGLY, B. J., BESIER, T. F., LLOYD, D. G., DELP, S. L., BANKS, S. A., PANDY, M. G. & D'LIMA, D. D. 2012. Grand challenge competition to predict in vivo knee loads. *Journal of Orthopaedic Research,* 30**,** 503-513.

FRIEDERICH, J. A. & BRAND, R. A. 1990. Muscle fiber architecture in the human lower limb. *Journal of biomechanics,* 23**,** 91-95.

FROSSARD, L. 2019. Loading characteristics data applied on osseointegrated implant by transfemoral bone-anchored prostheses fitted with basic components during daily activities. *Data in brief,* 26**,** 104492.

FROSSARD, L., CHEZE, L. & DUMAS, R. 2011. Dynamic input to determine hip joint moments, power and work on the prosthetic limb of transfemoral amputees: ground reaction vs knee reaction. *Prosthetics and Orthotics International,* 35**,** 140-149.

FROSSARD, L., HAGBERG, K., HÄGGSTRÖM, E., GOW, D. L., BRÅNEMARK, R. & PEARCY, M. 2010. Functional outcome of transfemoral amputees fitted with an osseointegrated fixation: temporal gait characteristics. *JPO: Journal of Prosthetics and Orthotics,* 22**,** 11-20.

FROSSARD, L., LEECH, B. & PITKIN, M. 2019. Automated characterization of anthropomorphicity of prosthetic feet fitted to bone-anchored transtibial prosthesis. *IEEE Transactions on Biomedical Engineering,* 66**,** 3402-3410.

FROSSARD, L. A., HAGGSTROM, E., HAGBERG, K. & BRANEMARK, R. 2013. Load applied on a bone-anchored transfemoral prosthesis: Characterisation of a prosthesis: A pilot study. *Journal of rehabilitation research and development,* 50**,** 619-634.

FUKASHIRO, S., ROB, M., ICHINOSE, Y., KAWAKAMI, Y. & FUKUNAGA, T. 1995. Ultrasonography gives directly but noninvasively elastic characteristic of human tendon in vivo. *European journal of applied physiology and occupational physiology,* 71**,** 555-557.

GARD, S. A. 2006. Use of quantitative gait analysis for the evaluation of prosthetic walking performance. *JPO: Journal of Prosthetics and Orthotics,* 18**,** P93-P104.

GENIN, J. J., BASTIEN, G. J., FRANCK, B., DETREMBLEUR, C. & WILLEMS, P. A. 2008. Effect of speed on the energy cost of walking in unilateral traumatic lower limb amputees. *European journal of applied physiology,* 103**,** 655.

GIARMATZIS, G., JONKERS, I., WESSELING, M., VAN ROSSOM, S. & VERSCHUEREN, S. 2015. Loading of hip measured by hip contact forces at different speeds of walking and running. *Journal of Bone and Mineral Research,* 30**,** 1431-1440.

GOTTSCHALK, F. 1999. Transfemoral amputation: biomechanics and surgery. *Clinical Orthopaedics and Related Research®,* 361**,** 15-22.

GOTTSCHALK, F. 2004. Transfemoral amputation: surgical management. *Atlas of amputations and limb deficiencies: surgical, prosthetic, and rehabilitation principles. 3rd ed. Rosemont, IL: American Academy of Orthopaedic Surgeons***,** 533-40.

GOUJON-PILLET, H., SAPIN, E., FODÉ, P. & LAVASTE, F. 2008. Three-dimensional motions of trunk and pelvis during transfemoral amputee gait. *Archives of physical medicine and rehabilitation,* 89**,** 87-94.

HAGBERG, K. & BRÅNEMARK, R. 2001a. Consequences of non-vascular trans-femoral amputation: a survey of quality of life, prosthetic use and problems. *Prosthetics and orthotics international,* 25**,** 186-194.

HAGBERG, K. & BRÅNEMARK, R. 2001b. Consequences of non-vascular trans-femoral amputation: A survey of quality of life, prosthetic use and problems. *Prosthetics and orthotics international,* 25**,** 186-194.

HAGBERG, K., BRÅNEMARK, R. & HÄGG, O. 2004. Questionnaire for Persons with a Transfemoral Amputation (Q-TFA): Initial validity and reliability of a new outcome measure. *Journal of Rehabilitation Research & Development,* 41.

HAGBERG, K., HÄGGSTRÖM, E., UDEN, M. & BRÅNEMARK, R. 2005. Socket versus bone-anchored trans-femoral prostheses: hip range of motion and sitting comfort. *Prosthetics and orthotics international,* 29**,** 153-163.

HAGBERG, K., HANSSON, E. & BRÅNEMARK, R. 2014. Outcome of percutaneous osseointegrated prostheses for patients with unilateral transfemoral amputation at two-year follow-up. *Archives of physical medicine and rehabilitation,* 95**,** 2120-2127.

HAGGSTROM, E., HAGBERG, K., RYDEVIK, B. & BRANEMARK, R. 2013. Vibrotactile evaluation: osseointegrated versus socket-suspended transfemoral prostheses. *Journal of Rehabilitation Research & Development,* 50**,** 1423-1436.

HALL, A. L., PETERSON, C. L., KAUTZ, S. A. & NEPTUNE, R. R. 2011. Relationships between muscle contributions to walking subtasks and functional walking status in persons with post-stroke hemiparesis. *Clinical biomechanics,* 26**,** 509-515.

HAMMARLUND, C. S., CARLSTRÖM, M., MELCHIOR, R. & PERSSON, B. M. 2011. Prevalence of back pain, its effect on functional ability and health-related quality of life in lower limb amputees secondary to trauma or tumour: a comparison across three levels of amputation. *Prosthetics and orthotics international,* 35**,** 97-105.

HAMNER, S. R. & DELP, S. L. 2013. Muscle contributions to fore-aft and vertical body mass center accelerations over a range of running speeds. *Journal of biomechanics,* 46**,** 780-787.

HAMNER, S. R., SETH, A. & DELP, S. L. 2010. Muscle contributions to propulsion and support during running. *Journal of biomechanics,* 43**,** 2709-2716.

HARANDI, V. J., ACKLAND, D. C., HADDARA, R., LIZAMA, L. E. C., GRAF, M., GALEA, M. P. & LEE, P. V. S. 2020. Gait compensatory mechanisms in unilateral transfemoral amputees. *Medical Engineering & Physics*.

HEINTZ, S. & GUTIERREZ-FAREWIK, E. M. 2007. Static optimization of muscle forces during gait in comparison to EMG-to-force processing approach. *Gait & posture,* 26**,** 279-288.

HELLER, M., BERGMANN, G., DEURETZBACHER, G., DÜRSELEN, L., POHL, M., CLAES, L., HAAS, N. & DUDA, G. 2001. Musculo-skeletal loading conditions at the hip during walking and stair climbing. *Journal of biomechanics,* 34**,** 883-893.

HERMENS, H. J., FRERIKS, B., DISSELHORST-KLUG, C. & RAU, G. 2000. Development of recommendations for SEMG sensors and sensor placement procedures. *Journal of electromyography and Kinesiology,* 10**,** 361-374.

HERMENS, H. J., FRERIKS, B., MERLETTI, R., STEGEMAN, D., BLOK, J., RAU, G., DISSELHORST-KLUG, C. & HÄGG, G. 1999. European recommendations for surface electromyography. *Roessingh research and development,* 8**,** 13-54.

HERZOG, W., LONGINO, D. & CLARK, A. 2003. The role of muscles in joint adaptation and degeneration. *Langenbeck's Archives of Surgery,* 388**,** 305-315.

HIGHSMITH, M. J., SCHULZ, B. W., HART-HUGHES, S., LATLIEF, G. A. & PHILLIPS, S. L. 2010. Differences in the spatiotemporal parameters of transtibial and transfemoral amputee gait. *JPO: Journal of Prosthetics and Orthotics,* 22**,** 26-30.

HILL, A. V. 1938. The heat of shortening and the dynamic constants of muscle. *Proceedings of the Royal Society of London. Series B-Biological Sciences,* 126**,** 136-195.

HILL, A. V. 1953. The mechanics of active muscle. *Proceedings of the Royal Society of London. Series B-Biological Sciences,* 141**,** 104-117.

HOF, A. L., VAN BOCKEL, R. M., SCHOPPEN, T. & POSTEMA, K. 2007. Control of lateral balance in walking: experimental findings in normal subjects and above-knee amputees. *Gait & posture,* 25**,** 250-258.

HOF, A. L. & VAN DEN BERG, J. 1981. EMG to force processing I: an electrical analogue of the Hill muscle model. *Journal of biomechanics,* 14**,** 747-758.

HONG, J. H. & MUN, M. S. 2005. Relationship between socket pressure and EMG of two muscles in trans-femoral stumps during gait. *Prosthetics and orthotics international,* 29**,** 59-72.

HUCH, K., KUETTNER, K. E. & DIEPPE, P. Osteoarthritis in ankle and knee joints. Seminars in arthritis and rheumatism, 1997. Elsevier, 667-674.

HUNGERFORD, D. & COCKIN, J. 1975. Fate of the retained lower limb joints in Second World War amputees. *J Bone Joint Surg,* 57**,** 111.

JACOBS, R., BRÅNEMARK, R., OLMARKER, K., RYDEVIK, B., STEENBERGHE, D. V. & BRÅNEMARK, P. I. 2000. Evaluation of the psychophysical detection threshold level for vibrotactile and pressure stimulation of prosthetic limbs using bone anchorage or soft tissue support. *Prosthetics and orthotics international,* 24**,** 133-142.

JAEGERS, S. M., ARENDZEN, J. H. & DE JONGH, H. J. 1995a. Changes in hip muscles after above-knee amputation. *Clinical orthopaedics and related research,* 319**,** 276-284.

JAEGERS, S. M., ARENDZEN, J. H. & DE JONGH, H. J. 1995b. Prosthetic gait of unilateral transfemoral amputees: a kinematic study. *Archives of physical medicine and rehabilitation,* 76**,** 736-743.

JAEGERS, S. M., ARENDZEN, J. H. & DE JONGH, H. J. 1996. An electromyographic study of the hip muscles of transfemoral amputees in walking. *Clinical orthopaedics and related research,* 328**,** 119-128.

JINHA, A., AIT-HADDOU, R., BINDING, P. & HERZOG, W. 2006. Antagonistic activity of one-joint muscles in three-dimensions using non-linear optimisation. *Mathematical biosciences,* 202**,** 57-70.

KAUFMAN, K. R., FRITTOLI, S. & FRIGO, C. A. 2012. Gait asymmetry of transfemoral amputees using mechanical and microprocessor-controlled prosthetic knees. *Clinical Biomechanics,* 27**,** 460-465.

KAUFMAN, K. R., LEVINE, J. A., BREY, R., IVERSON, B., MCCRADY, S., PADGETT, D. & JOYNER, M. J. 2007. Gait and balance of transfemoral amputees using passive mechanical and microprocessor-controlled prosthetic knees. *Gait & posture,* 26**,** 489-493.

KENNON, C. R. http://www.jisrf.org/osteointegration-implant-for-transfemoral-amputation.html.

KERRIGAN, D. C., TODD, M. K., DELLA CROCE, U., LIPSITZ, L. A. & COLLINS, J. J. 1998. Biomechanical gait alterations independent of speed in the healthy elderly: evidence for specific limiting impairments. *Archives of physical medicine and rehabilitation,* 79**,** 317-322.

KOMI, P., BELLI, A., HUTTUNEN, V., BONNEFOY, R., GEYSSANT, A. & LACOUR, J. 1996. Optic fibre as a transducer of tendomuscular forces. *European journal of applied physiology and occupational physiology,* 72**,** 278-280.

KOMI, P., SALONEN, M., JÄRVINEN, M. & KOKKO, O. 1987. In vivo registration of Achilles tendon forces in man. *International journal of sports medicine,* 8**,** S3-S8.

KOMI, P. V. 2000. Stretch-shortening cycle: a powerful model to study normal and fatigued muscle. *Journal of biomechanics,* 33**,** 1197-1206.

KOTZAR, G., DAVY, D., GOLDBERG, V., HEIPLE, K., BERILLA, J., HEIPLE JR, K., BROWN, R. & BURSTEIN, A. 1991. Telemeterized in vivo hip joint force data: a report on two patients after total hip surgery. *Journal of Orthopaedic Research,* 9**,** 621-633.

KRISTIANSLUND, E., KROSSHAUG, T. & VAN DEN BOGERT, A. J. 2012. Effect of low pass filtering on joint moments from inverse dynamics: implications for injury prevention. *Journal of biomechanics,* 45**,** 666-671.

KRISTIANSLUND, E., KROSSHAUG, T. & VAN DEN BOGERT, A. J. 2013. Artefacts in measuring joint moments may lead to incorrect clinical conclusions: the nexus between science (biomechanics) and sports injury prevention! : BMJ Publishing Group Ltd and British Association of Sport and Exercise Medicine.

KULKARNI, J., ADAMS, J., THOMAS, E. & SILMAN, A. 1998. Association between amputation, arthritis and osteopenia in British male war veterans with major lower limb amputations. *Clinical Rehabilitation,* 12**,** 348-353.

KULKARNI, J., GAINE, W., BUCKLEY, J., RANKINE, J. & ADAMS, J. 2005. Chronic low back pain in traumatic lower limb amputees. *Clinical rehabilitation,* 19**,** 81-86.

KUO, A. D. 1998. A least-squares estimation approach to improving the precision of inverse dynamics computations. *Journal of biomechanical engineering,* 120**,** 148-159.

LAFEBER, F. P., INTEMA, F., VAN ROERMUND, P. M. & MARIJNISSEN, A. C. 2006. Unloading joints to treat osteoarthritis, including joint distraction. *Current opinion in rheumatology,* 18**,** 519-525.

LEIJENDEKKERS, R. A., VAN HINTE, G., FRÖLKE, J. P., VAN DE MEENT, H., NIJHUIS-VAN DER SANDEN, M. W. & STAAL, J. B. 2017. Comparison of bone-anchored prostheses and socket prostheses for patients with a lower extremity amputation: a systematic review. *Disability and rehabilitation,* 39**,** 1045-1058.

LEMAIRE, E. D. & FISHER, F. R. 1994. Osteoarthritis and elderly amputee gait. *Archives of physical medicine and rehabilitation,* 75**,** 1094-1099.

LENAERTS, G., MULIER, M., SPAEPEN, A., VAN DER PERRE, G. & JONKERS, I. 2009. Aberrant pelvis and hip kinematics impair hip loading before and after total hip replacement. *Gait & posture,* 30**,** 296-302.

LEWIS, C. L., SAHRMANN, S. A. & MORAN, D. W. 2007. Anterior hip joint force increases with hip extension, decreased gluteal force, or decreased iliopsoas force. *Journal of biomechanics,* 40**,** 3725-3731.

LEWIS, C. L., SAHRMANN, S. A. & MORAN, D. W. 2010. Effect of hip angle on anterior hip joint force during gait. *Gait & posture,* 32**,** 603-607.

LI, K., ACKLAND, D. C., MCCLELLAND, J. A., WEBSTER, K. E., FELLER, J. A., DE STEIGER, R. & PANDY, M. G. 2013. Trunk muscle action compensates for reduced quadriceps force during walking after total knee arthroplasty. *Gait & posture,* 38**,** 79-85.

LIM, Y. P., LIN, Y.-C. & PANDY, M. G. 2013. Muscle function during gait is invariant to age when walking speed is controlled. *Gait & posture,* 38**,** 253-259.

LIN, Y.-C., DORN, T. W., SCHACHE, A. G. & PANDY, M. G. 2012. Comparison of different methods for estimating muscle forces in human movement. *Proceedings of the Institution of Mechanical Engineers, Part H: Journal of Engineering in Medicine,* 226**,** 103-112.

LIN, Y.-C., FOK, L. A., SCHACHE, A. G. & PANDY, M. G. 2015. Muscle coordination of support, progression and balance during stair ambulation. *Journal of biomechanics,* 48**,** 340-347.

LIN, Y. C., KIM, H. J. & PANDY, M. G. 2011. A computationally efficient method for assessing muscle function during human locomotion. *International Journal for Numerical Methods in Biomedical Engineering,* 27**,** 436-449.

LIU, M. Q., ANDERSON, F. C., PANDY, M. G. & DELP, S. L. 2006. Muscles that support the body also modulate forward progression during walking. *Journal of biomechanics,* 39**,** 2623-2630.

LIU, M. Q., ANDERSON, F. C., SCHWARTZ, M. H. & DELP, S. L. 2008. Muscle contributions to support and progression over a range of walking speeds. *Journal of biomechanics,* 41**,** 3243-3252.

LLOYD, D. G. & BESIER, T. F. 2003. An EMG-driven musculoskeletal model to estimate muscle forces and knee joint moments in vivo. *Journal of biomechanics,* 36**,** 765-776.

LU, T.-W. & O'CONNOR, J. 1999. Bone position estimation from skin marker co-ordinates using global optimisation with joint constraints. *Journal of biomechanics,* 32**,** 129-134.

MADSEN, M. S., RITTER, M. A., MORRIS, H. H., MEDING, J. B., BEREND, M. E., FARIS, P. M. & VARDAXIS, V. G. 2004. The effect of total hip arthroplasty surgical approach on gait. *Journal of orthopaedic research,* 22**,** 44-50.

MATSUMOTO, M. E., CZERNIECKI, J. M., SHAKIR, A., SURI, P., ORENDURFF, M. & MORGENROTH, D. C. 2018. The relationship between lumbar lordosis angle and low back pain in individuals with transfemoral amputation. *Prosthetics and orthotics international***,** 0309364618792746.

MATTES, S. J., MARTIN, P. E. & ROYER, T. D. 2000. Walking symmetry and energy cost in persons with unilateral transtibial amputations: matching prosthetic and intact limb inertial properties. *Archives of physical medicine and rehabilitation,* 81**,** 561-568.

MCGOWAN, C., KRAM, R. & NEPTUNE, R. 2009. Modulation of leg muscle function in response to altered demand for body support and forward propulsion during walking. *Journal of biomechanics,* 42**,** 850-856.

MELZER, I., YEKUTIEL, M. & SUKENIK, S. 2001. Comparative study of osteoarthritis of the contralateral knee joint of male amputees who do and do not play volleyball. *The Journal of rheumatology,* 28**,** 169-172.

MESSIER, S. P., GUTEKUNST, D. J., DAVIS, C. & DEVITA, P. 2005. Weight loss reduces knee-joint loads in overweight and obese older adults with knee osteoarthritis. *Arthritis & Rheumatism,* 52**,** 2026-2032.

MEULENBELT, H. E., GEERTZEN, J. H., JONKMAN, M. F. & DIJKSTRA, P. U. 2009. Determinants of skin problems of the stump in lower-limb amputees. *Archives of physical medicine and rehabilitation,* 90**,** 74-81.

MEULENBELT, H. E., GEERTZEN, J. H., JONKMAN, M. F. & DIJKSTRA, P. U. 2011. Skin problems of the stump in lower limb amputees: 1. A clinical study. *Acta dermato-venereologica,* 91**,** 173-177.

MOIRENFELD, I., AYALON, M., BEN-SIRA, D. & ISAKOV, E. 2000. Isokinetic strength and endurance of the knee extensors and flexors in trans-tibial amputees. *Prosthetics and orthotics international,* 24**,** 221-225.

MOKHTARZADEH, H., PERRATON, L., FOK, L., MUÑOZ, M. A., CLARK, R., PIVONKA, P. & BRYANT, A. L. 2014. A comparison of optimisation methods and knee joint degrees of freedom on muscle force predictions during single-leg hop landings. *Journal of biomechanics,* 47**,** 2863-2868.

MOKHTARZADEH, H., YEOW, C. H., GOH, J. C. H., OETOMO, D., MALEKIPOUR, F. & LEE, P. V.-S. 2013. Contributions of the soleus and gastrocnemius muscles to the anterior cruciate ligament loading during single-leg landing. *Journal of biomechanics,* 46**,** 1913-1920.

MORGENROTH, D. C., GELLHORN, A. C. & SURI, P. 2012. Osteoarthritis in the disabled population: a mechanical perspective. *PM&R,* 4**,** S20-S27.

MORGENROTH, D. C., ORENDURFF, M. S., SHAKIR, A., SEGAL, A., SHOFER, J. & CZERNIECKI, J. M. 2010. The relationship between lumbar spine kinematics during gait and low-back pain in transfemoral amputees. *American Journal of Physical Medicine & Rehabilitation,* 89**,** 635-643.

MORGENROTH, D. C., SHAKIR, A., ORENDURFF, M. S. & CZERNIECKI, J. M. 2009. Low-back pain in transfemoral amputees: is there a correlation with static or dynamic leg-length discrepancy? *American journal of physical medicine & rehabilitation,* 88**,** 108-113.

MOVEFORWARDDPT http://www.jisrf.org/osteointegration-implant-for-transfemoral-amputation.

MOXEY, P., HOFMAN, D., HINCHLIFFE, R., JONES, K., THOMPSON, M. & HOLT, P. 2010. Epidemiological study of lower limb amputation in England between 2003 and 2008. *British journal of surgery,* 97**,** 1348-1353.

MPHTY, H. D. 2012. Physical activity and lower-back pain in persons with traumatic transfemoral amputation: a national cross-sectional survey. *Journal of rehabilitation research and development,* 49**,** 1457.

MUNGIOLE, M. & MARTIN, P. E. 1990. Estimating segment inertial properties: comparison of magnetic resonance imaging with existing methods. *Journal of Biomechanics,* 23**,** 1039-1046.

NARANG, Y. S., ARELEKATTI, V. M. & WINTER, A. G. 2015. The effects of prosthesis inertial properties on prosthetic knee moment and hip energetics required to achieve able-bodied kinematics. *IEEE Transactions on Neural Systems and Rehabilitation Engineering,* 24**,** 754-763.

NELSON, R. G., GOHDES, D. M., EVERHART, J. E., HARTNER, J. A., ZWEMER, F. L., PETTITT, D. J. & KNOWLER, W. C. 1988. Lower-extremity amputations in NIDDM: 12-yr follow-up study in Pima Indians. *Diabetes care,* 11**,** 8-16.

NEPTUNE, R. & HULL, M. 1998. Evaluation of performance criteria for simulation of submaximal steady-state cycling using a forward dynamic model. *Journal of Biomechanical Engineering,* 120**,** 334-341.

NEPTUNE, R., KAUTZ, S. & ZAJAC, F. 2001. Contributions of the individual ankle plantar flexors to support, forward progression and swing initiation during walking. *Journal of biomechanics,* 34**,** 1387-1398.

NEPTUNE, R., ZAJAC, F. & KAUTZ, S. 2004. Muscle force redistributes segmental power for body progression during walking. *Gait & posture,* 19**,** 194-205.

NOLAN, L. & LEES, A. 2000. The functional demands on the intact limb during walking for active trans-femoral and trans-tibial amputees. *Prosthetics and orthotics international,* 24**,** 117-125.

NOLAN, L., WIT, A., DUDZIÑSKI, K., LEES, A., LAKE, M. & WYCHOWAÑSKI, M. 2003. Adjustments in gait symmetry with walking speed in trans-femoral and trans-tibial amputees. *Gait & posture,* 17**,** 142-151.

NORVELL, D. C., CZERNIECKI, J. M., REIBER, G. E., MAYNARD, C., PECORARO, J. A. & WEISS, N. S. 2005. The prevalence of knee pain and symptomatic knee osteoarthritis among veteran traumatic amputees and nonamputees. *Archives of physical medicine and rehabilitation,* 86**,** 487-493.

OKITA, Y., YAMASAKI, N., NAKAMURA, T., KUBO, T., MITSUMOTO, A. & AKUNE, T. 2018. Kinetic differences between level walking and ramp descent in individuals with unilateral transfemoral amputation using a prosthetic knee without a stance control mechanism. *Gait & Posture,* 63**,** 80-85.

OTTOBOCK https://www.ottobock.in/prosthetics/information-for-amputees.

PANDY, M., GARNER, B. & ANDERSON, F. 1995. Optimal control of non-ballistic muscular movements: a constraint-based performance criterion for rising from a chair. *Journal of biomechanical engineering,* 117**,** 15-26.

PANDY, M. G. 2001. Computer modeling and simulation of human movement. *Annual review of biomedical engineering,* 3**,** 245-273.

PANDY, M. G. & ANDRIACCHI, T. P. 2010. Muscle and joint function in human locomotion. *Annual review of biomedical engineering,* 12**,** 401-433.

PANDY, M. G., LIN, Y.-C. & KIM, H. J. 2010. Muscle coordination of mediolateral balance in normal walking. *Journal of biomechanics,* 43**,** 2055-2064.

PANTALL, A. & EWINS, D. 2013. Muscle activity during stance phase of walking: Comparison of males with transfemoral amputation with osseointegrated fixations to nondisabled male volunteers. *J Rehabil Res Dev,* 50**,** 499-514.

PEJHAN, S., FARAHMAND, F. & PARNIANPOUR, M. Design optimization of an above-knee prosthesis based on the kinematics of gait. 2008 30th Annual International Conference of the IEEE Engineering in Medicine and Biology Society, 2008. IEEE, 4274-4277.

PETERSON, C. L., HALL, A. L., KAUTZ, S. A. & NEPTUNE, R. R. 2010. Pre-swing deficits in forward propulsion, swing initiation and power generation by individual muscles during hemiparetic walking. *Journal of biomechanics,* 43**,** 2348-2355.

PEZZIN, L. E., DILLINGHAM, T. R. & MACKENZIE, E. J. 2000. Rehabilitation and the long-term outcomes of persons with trauma-related amputations. *Archives of physical medicine and rehabilitation,* 81**,** 292-300.

PEZZIN, L. E., DILLINGHAM, T. R., MACKENZIE, E. J., EPHRAIM, P. & ROSSBACH, P. 2004a. Use and satisfaction with prosthetic limb devices and related services. *Archives of physical medicine and rehabilitation,* 85**,** 723-729.

PEZZIN, L. E., DILLINGHAM, T. R., MACKENZIE, E. J., EPHRAIM, P. & ROSSBACH, P. 2004b. Use and satisfaction with prosthetic limb devices and related services 1. *Archives of physical medicine and rehabilitation,* 85**,** 723-729.

PICKLE, N. T., GRABOWSKI, A. M., AUYANG, A. G. & SILVERMAN, A. K. 2016. The functional roles of muscles during sloped walking. *Journal of biomechanics,* 49**,** 3244-3251.

PINARD, V. & FROSSARD, L. 2012. Spatio-temporal characteristics of locomotion and functional outcomes of individuals with transfemoral amputation fitted with OPRA fixation.

PRINSEN, E. C., NEDERHAND, M. J. & RIETMAN, J. S. 2011. Adaptation strategies of the lower extremities of patients with a transtibial or transfemoral amputation during level walking: a systematic review. *Archives of physical medicine and rehabilitation,* 92**,** 1311-1325.

RABUFFETTI, M., RECALCATI, M. & FERRARIN, M. 2005. Trans-femoral amputee gait: Socket–pelvis constraints and compensation strategies. *Prosthetics and orthotics international,* 29**,** 183-192.

RADIN, E., BURR, D., CATERSON, B., FYHRIE, D., BROWN, T. & BOYD, R. Mechanical determinants of osteoarthrosis. Seminars in arthritis and rheumatism, 1991. Elsevier, 12-21.

RANZ, E. C. 2016. *Mobility in individuals with traumatic lower-limb injuries: implications for device design, surgical intervention and rehabilitation therapies.*

RANZ, E. C., WILKEN, J. M., GAJEWSKI, D. A. & NEPTUNE, R. R. 2017. The influence of limb alignment and transfemoral amputation technique on muscle capacity during gait. *Computer methods in BiomeChaniCs and BiomediCal engineering,* 20**,** 1167-1174.

RASMUSSEN, J., DAMSGAARD, M. & VOIGT, M. 2001. Muscle recruitment by the min/max criterion—a comparative numerical study. *Journal of biomechanics,* 34**,** 409-415.

READ, L. & NIGG, B. 1999. An analysis of hip joint loading during walking, running, and skiing. *Medicine and science in sports and exercise,* 31**,** 131-142.

REMY, C. D. & THELEN, D. G. 2009. Optimal estimation of dynamically consistent kinematics and kinetics for forward dynamic simulation of gait. *Journal of biomechanical engineering,* 131**,** 031005.

RENSTRÖM, P., GRIMBY, G. & LARSSON, E. 1983. Thigh muscle strength in below-knee amputees. *Scandinavian journal of rehabilitation medicine. Supplement,* 9**,** 163-173.

ROBBINS, S., WAKED, E. & KROUGLICOF, N. 2001. Vertical impact increase in middle age may explain idiopathic weight-bearing joint osteoarthritis. *Archives of physical medicine and rehabilitation,* 82**,** 1673-1677.

ROBINSON, D. L., SAFAI, L., HARANDI, V. J., GRAF, M., LIZAMA, L. E. C., LEE, P., GALEA, M. P., KHAN, F., TSE, K. M. & ACKLAND, D. C. 2020. Load response of an osseointegrated implant used in the treatment of unilateral transfemoral amputation: An early implant loosening case study. *Clinical Biomechanics,* 73**,** 201-212.

RÖHRLE, H., SCHOLTEN, R., SIGOLOTTO, C., SOLLBACH, W. & KELLNER, H. 1984. Joint forces in the human pelvis-leg skeleton during walking. *Journal of biomechanics,* 17**,** 409-424.

ROMMERS, G., VOS, L., GROOTHOFF, J. & EISMA, W. 1996. Clinical rehabilitation of the amputee: a retrospective study. *Prosthetics and orthotics international,* 20**,** 72-78.

RYDELL, N. W. 1966. Forces acting on the femoral head-prosthesis: a study on strain gauge supplied prostheses in living persons. *Acta Orthopaedica Scandinavica,* 37**,** 1-132.

SARTORI, M., REGGIANI, M., FARINA, D. & LLOYD, D. G. 2012. EMG-driven forward-dynamic estimation of muscle force and joint moment about multiple degrees of freedom in the human lower extremity. *PloS one,* 7**,** e52618.

SASAKI, K. & NEPTUNE, R. R. 2010. Individual muscle contributions to the axial knee joint contact force during normal walking. *Journal of biomechanics,* 43**,** 2780-2784.

SAWICKI, G. S. & FERRIS, D. P. 2009. Powered ankle exoskeletons reveal the metabolic cost of plantar flexor mechanical work during walking with longer steps at constant step frequency. *Journal of Experimental Biology,* 212**,** 21-31.

SCHAARSCHMIDT, M., LIPFERT, S. W., MEIER-GRATZ, C., SCHOLLE, H.-C. & SEYFARTH, A. 2012. Functional gait asymmetry of unilateral transfemoral amputees. *Human movement science,* 31**,** 907-917.

SCHACHE, A. G., BLANCH, P. D., DORN, T. W., BROWN, N. A., ROSEMOND, D. & PANDY, M. G. 2011. Effect of running speed on lower limb joint kinetics. *Medicine & Science in Sports & Exercise,* 43**,** 1260-1271.

SCHACHE, A. G., LIN, Y.-C., CROSSLEY, K. M. & PANDY, M. G. 2018. Is Running Better than Walking for Reducing Hip Joint Loads? *Medicine and science in sports and exercise,* 50**,** 2301-2310.

SEGAL, A. D., ORENDURFF, M. S., KLUTE, G. K. & MCDOWELL, M. L. 2006. Kinematic and kinetic comparisons of transfemoral amputee gait using C-Leg® and Mauch SNS® prosthetic knees. *Journal of rehabilitation research and development,* 43**,** 857.

SEROUSSI, R. E., GITTER, A., CZERNIECKI, J. M. & WEAVER, K. 1996. Mechanical work adaptations of above-knee amputee ambulation. *Archives of physical medicine and rehabilitation,* 77**,** 1209-1214.

SETH, A. & PANDY, M. G. 2007. A neuromusculoskeletal tracking method for estimating individual muscle forces in human movement. *Journal of biomechanics,* 40**,** 356-366.

SHANDIZ, M. A., FARAHMAND, F., OSMAN, N. A. A. & ZOHOOR, H. 2013. A robotic model of transfemoral amputee locomotion for design optimization of knee controllers. *International Journal of Advanced Robotic Systems,* 10**,** 161.

SHAO, Q., BASSETT, D. N., MANAL, K. & BUCHANAN, T. S. 2009. An EMG-driven model to estimate muscle forces and joint moments in stroke patients. *Computers in biology and medicine,* 39**,** 1083-1088.

SILVERMAN, A. K. & NEPTUNE, R. R. Individual muscle function in below Knee amputee walking. Conference Proceedings of the Annual Meeting of the American Society, 2010. 166.

SILVERMAN, A. K. & NEPTUNE, R. R. 2012. Muscle and prosthesis contributions to amputee walking mechanics: a modeling study. *Journal of biomechanics,* 45**,** 2271-2278.

SILVERMAN, A. K. & NEPTUNE, R. R. 2014. Three-dimensional knee joint contact forces during walking in unilateral transtibial amputees. *Journal of biomechanics,* 47**,** 2556-2562.

SJÖDAHL, C., JARNLO, G.-B., SÖDERBERG, B. & PERSSON, B. 2002. Kinematic and kinetic gait analysis in the sagittal plane of trans-femoral amputees before and after special gait re-education. *Prosthetics and orthotics international,* 26**,** 101-112.

SJÖDAHL, C., JARNLO, G. B., SÖDERBERG, B. & PERSSON, B. 2003. Pelvic motion in trans-femoral amputees in the frontal and transverse plane before and after special gait re-education. *Prosthetics and orthotics international,* 27**,** 227-237.

SMITH, J. D., FERRIS, A. E., HEISE, G. D., HINRICHS, R. N. & MARTIN, P. E. 2014. Oscillation and reaction board techniques for estimating inertial properties of a below-knee prosthesis. *Journal of visualized experiments: JoVE*.

STANSFIELD, B. & NICOL, A. 2002. Hip joint contact forces in normal subjects and subjects with total hip prostheses: walking and stair and ramp negotiation. *Clinical Biomechanics,* 17**,** 130-139.

STANSFIELD, B., NICOL, A., PAUL, J., KELLY, I., GRAICHEN, F. & BERGMANN, G. 2003. Direct comparison of calculated hip joint contact forces with those measured using instrumented implants. An evaluation of a three-dimensional mathematical model of the lower limb. *Journal of biomechanics,* 36**,** 929-936.

STEELE, K. M., DEMERS, M. S., SCHWARTZ, M. H. & DELP, S. L. 2012a. Compressive tibiofemoral force during crouch gait. *Gait & posture,* 35**,** 556-560.

STEELE, K. M., SETH, A., HICKS, J. L., SCHWARTZ, M. S. & DELP, S. L. 2010. Muscle contributions to support and progression during single-limb stance in crouch gait. *Journal of biomechanics,* 43**,** 2099-2105.

STEELE, K. M., VAN DER KROGT, M. M., SCHWARTZ, M. H. & DELP, S. L. 2012b. How much muscle strength is required to walk in a crouch gait? *Journal of biomechanics,* 45**,** 2564-2569.

STRUYF, P. A., VAN HEUGTEN, C. M., HITTERS, M. W. & SMEETS, R. J. 2009. The prevalence of osteoarthritis of the intact hip and knee among traumatic leg amputees. *Archives of physical medicine and rehabilitation,* 90**,** 440-446.

SUZUKI, Y. 2010. Dynamic optimization of transfemoral prosthesis during swing phase with residual limb model. *Prosthetics and Orthotics International,* 34**,** 428-438.

THELEN, D. G. 2003. Adjustment of muscle mechanics model parameters to simulate dynamic contractions in older adults. *Journal of biomechanical engineering,* 125**,** 70-77.

THELEN, D. G. & ANDERSON, F. C. 2006. Using computed muscle control to generate forward dynamic simulations of human walking from experimental data. *Journal of biomechanics,* 39**,** 1107-1115.

THELEN, D. G., ANDERSON, F. C. & DELP, S. L. 2003. Generating dynamic simulations of movement using computed muscle control. *Journal of biomechanics,* 36**,** 321-328.

TINTLE, S. M., AGNER FORSBERG, J., KEELING, J. J., SHAWEN, S. B. & KYLE POTTER, B. 2010. Lower extremity combat-related amputations. *Journal of surgical orthopaedic advances,* 19**,** 35.

TRANBERG, R., ZÜGNER, R. & KÄRRHOLM, J. 2011. Improvements in hip-and pelvic motion for patients with osseointegrated trans-femoral prostheses. *Gait & posture,* 33**,** 165-168.

TSAOPOULOS, D. E., MAGANARIS, C. N. & BALTZOPOULOS, V. 2007. Can the patellar tendon moment arm be predicted from anthropometric measurements? *Journal of Biomechanics,* 40**,** 645-651.

VALENTE, G., TADDEI, F. & JONKERS, I. 2013. Influence of weak hip abductor muscles on joint contact forces during normal walking: probabilistic modeling analysis. *Journal of biomechanics,* 46**,** 2186-2193.

VAN DE MEENT, H., HOPMAN, M. T. & FRÖLKE, J. P. 2013. Walking ability and quality of life in subjects with transfemoral amputation: a comparison of osseointegration with socket prostheses. *Archives of physical medicine and rehabilitation,* 94**,** 2174-2178.

VAUGHAN, C. L., DAVIS, B. L. & O'CONNOR, J. C. 1992. *Dynamics of human gait,* Human Kinetics Publishers Champaign, Illinois.

VENTURA, J. D., KLUTE, G. K. & NEPTUNE, R. R. 2015. Individual muscle contributions to circular turning mechanics. *Journal of biomechanics,* 48**,** 1067-1074.

WARD, S. R., ENG, C. M., SMALLWOOD, L. H. & LIEBER, R. L. 2009. Are current measurements of lower extremity muscle architecture accurate? *Clinical orthopaedics and related research,* 467**,** 1074-1082.

WELKE, B., JAKUBOWITZ, E., SEEHAUS, F., DANIILIDIS, K., TIMPNER, M., TREMER, N., HURSCHLER, C. & SCHWARZE, M. 2019. The prevalence of osteoarthritis: Higher risk after transfemoral amputation?—A database analysis with 1,569 amputees and matched controls. *PloS one,* 14**,** e0210868.

WENTINK, E. C., PRINSEN, E. C., RIETMAN, J. S. & VELTINK, P. H. 2013. Comparison of muscle activity patterns of transfemoral amputees and control subjects during walking. *Journal of neuroengineering and rehabilitation,* 10**,** 1.

WESSELING, M., DE GROOTE, F., MEYER, C., CORTEN, K., SIMON, J. P., DESLOOVERE, K. & JONKERS, I. 2015. Gait alterations to effectively reduce hip contact forces. *Journal of Orthopaedic Research,* 33**,** 1094-1102.

WICKIEWICZ, T. L., ROY, R. R., POWELL, P. L. & EDGERTON, V. R. 1983. Muscle architecture of the human lower limb. *Clinical orthopaedics and related research***,** 275-283.

WINTER, D. A. 2009. *Biomechanics and motor control of human movement*, John Wiley & Sons.

WRETENBERG, P., NÉMETH, G., LAMONTAGNE, M. & LUNDIN, B. 1996. Passive knee muscle moment arms measured in vivo with MRI. *Clinical Biomechanics,* 11**,** 439-446.

ZAJAC, F. E. 1989. Muscle and tendon Properties models scaling and application to biomechanics and motor. *Critical reviews in biomedical engineering,* 17**,** 359-411.

ZAJAC, F. E. 2002. Understanding muscle coordination of the human leg with dynamical simulations. *Journal of biomechanics,* 35**,** 1011-1018.

ZAJAC, F. E. & GORDON, M. E. 1989. Determining muscle's force and action in multi-articular movement. *Exercise and sport sciences reviews,* 17**,** 187-230.

ZAJAC, F. E., NEPTUNE, R. R. & KAUTZ, S. A. 2002. Biomechanics and muscle coordination of human walking: Part I: Introduction to concepts, power transfer, dynamics and simulations. *Gait & posture,* 16**,** 215-232.

ZAJAC, F. E., NEPTUNE, R. R. & KAUTZ, S. A. 2003. Biomechanics and muscle coordination of human walking: part II: lessons from dynamical simulations and clinical implications. *Gait & posture,* 17**,** 1-17.

ZIEGLER-GRAHAM, K., MACKENZIE, E. J., EPHRAIM, P. L., TRAVISON, T. G. & BROOKMEYER, R. 2008. Estimating the prevalence of limb loss in the United States: 2005 to 2050. *Archives of physical medicine and rehabilitation,* 89**,** 422-429.